Master's thesis

NTNU
Norwegian University of Science and Technology
Faculty of Engineering
Department of Mechanical and Industrial Engineering

Birk Hveding Ersdal

Investigating NIR Illumination for Nighttime Bird Tracking with RGB Cameras

The development of a NIR illumination system with the use of the wayfaring method, aiming to enable nighttime monitoring of bird activity around offshore wind turbines with common RGB cameras

Master's thesis in Mechanical Engineering
Supervisor: Håkon Jarand Dugstad Johnsen
July 2023

NTNU
Norwegian University of
Science and Technology

Birk Hveding Ersdal

Investigating NIR Illumination for Nighttime Bird Tracking with RGB Cameras

The development of a NIR illumination system with the use of the wayfaring method, aiming to enable nighttime monitoring of bird activity around offshore wind turbines with common RGB cameras

Master's thesis in Mechanical Engineering
Supervisor: Håkon Jarand Dugstad Johnsen
July 2023

Norwegian University of Science and Technology
Faculty of Engineering
Department of Mechanical and Industrial Engineering

NTNU
Norwegian University of
Science and Technology

Investigating NIR Illumination for Nighttime Bird Tracking with RGB Cameras

The development of a NIR illumination system with the use of the wayfaring method, aiming to enable nighttime monitoring of bird activity around offshore wind turbines with common RGB cameras.

Birk Hveding Ersdal

2023-07-12

Preface

This thesis results from the course TPK4969 - Robotics and Automation during the spring of 2023 at the Department of Engineering Design and Materials, Norwegian University and Technology (NTNU) in Trondheim. The thesis is a continuation of my pre-master project: *Technology for Biodiversity: A Prestudy for the Development of Autonomous Measurement of Collisions Between Birds and Offshore Wind Turbines* carried out in the fall of 2022.

I want to thank my supervisors in the prestudy, Amund Skavhaug, and during this thesis, Håkon Jarand Dugstad Johnsen, for guiding me through this journey. Thank you for giving me valuable advice and the freedom to pursue this topic. While the freedom to pursue matters out of interest might not result in the most detailed of solutions, it will most definitely challenge a student and plant the seed of confidence needed for pursuing challenges by themselves. In an age where we as a society need to move away from the safety of traditional industries, the opportunity to innovate in the safe environment of the university should be encouraged.

Further, I want to thank Bjørn Iuell for taking the time to introduce me to this topic and sharing his experiences, initializing the work leading to this thesis. Furthermore, I want to thank Roel May for sharing his experiences and giving advice through the prestudy and this thesis. Without your help, the execution of this work would not have been possible.

At last, I should thank all my peers and professors for helping me through these two semesters, it has been a blast. I hope you know that even though I have used my fair share of "call a friend" options, I did so because I value your opinion[1].

For any reader who might want to continue this work, or have any questions, feel free to contact me[2].

[1] Mostly, except the "just shoot the birds before they reach the turbine"-part

[2] Email: Birk.ersdal@gmail.com

Summary

This thesis has used the wayfaring approach in an attempt to develop a method that uses commercially available RGB cameras for monitoring bird activity around offshore wind turbines at a low cost. Due to the increased focus on offshore wind turbines as a way of battling rapid climate change, the potential loss of biodiversity caused by renewable energies has been a source of debate. To increase the knowledge about the impact, it is necessary to develop methods allowing scientists to get fast and accurate data on how wildlife is influenced to gain better grounds for decision-makers. The work of this thesis is a continuation of the previous work of the author, investigating autonomous methods for obtaining collision rates between birds and turbines.

In the first concept-investigating process, referred to as a probe, it was investigated if commercially available cameras can detect birds with the available ambient light at night. This would allow existing camera systems or cheap cameras to be modified and remove the need for other, more expensive solutions. By removing the infrared (IR) cutoff filter, the light outside of the visible spectrum is allowed into the image sensor of the camera, consequently giving it better night vision capabilities. However, the ambient night light by itself is considered insufficient, and the use of a near infrared (NIR) light source was investigated.

In the second probe, a NIR light source in combination with the modified camera was investigated, trying to find the minimum required amount of light. Results from experiments indicated that a 20W light source with a horizontal and vertical FOV of 40° is likely sufficient for videos with a high frame rate to detect the presence of birds at short distances. However, due to uncertainties in the equipment and methodology, no minimum value for the required illumination was obtained. Yet, valuable information regarding the setup of further experiments was obtained. Further, is considered likely that a single lamp is insufficient for confident detection and recognition of birds at long distances. Thus, it was decided to develop a method for increasing the light intensity.

Extensive use of lamps was undesirable, as it is assumed to reduce the likelihood of implementation. Therefore, a method for increasing the light intensity by focusing the lamp is investigated. Thus, the last probe investigates whether a single narrow

lamp can illuminate the desired area in a reasonable amount of time. A proposal to design and function is outlined, with a narrowed light beam to increase the radiant intensity of a single lamp and swipe it over the desired area. Further, limitations regarding safety and practicality were gathered to function as guidelines for further development. A proof of concept was developed and presented, illustrating that a sufficiently illuminated video stream should be possible to obtain.

It is thus concluded that modified RGB cameras should be suitable for some degree of nighttime surveillance if a NIR source is present. Further, the solution presented in the third probe is promising, but further work is needed. This includes how to focus the required light beam, how it can be steered, and how small-scale models should be developed. A lens system, possibly in combination with some rotation of the lamp itself, is suggested for further investigations. For the small-scale test setup, it is recommended that a proper termination criterion is developed based on the end-user and that the small-scale bird models should mimic the details of an actual bird. At last, a method for comparing the NIR sensitivity of the camera should be developed to make it easier for companies and others interested in utilizing the solution to find suitable cameras.

Sammendrag

Denne masteroppgaven har brukt en wayfaring-tilnærmingen inspirert av Steinert & Leifer [1] i et forsøk på å utvikle en konstandseffektiv metode som bruker kommersielt tilgjengelige RGB-kameraer for å overvåke fugleaktivitet rundt havgående vindturbiner. På grunn av økt fokus rundt havvind som en del-løsning for å bekjempe klimaendringene har det oppstått en debatt rundt innvirkning de har på det biologisk mangfoldet. For å forbedre kunnskapsgrunnlaget for beslutningstagere er det nødvendig å utvikle metoder som tillater forskere å få rask og nøyaktig data om hvordan dyrelivet påvirkes. Arbeidet i denne masteroppgaven er en fortsettelse av forfatterens tidligere arbeid innen dette temaet, og undersøker autonome metoder for å skaffe kollisjonsrater mellom fugler og turbiner.

I den første konseptundersøkelsen, her referert til som en sondering, ble det undersøkt om kommersielt tilgjengelige kameraer kan oppdage fugler med det tilgjengelige bakgrunnslyset om natten. Dette ville tillatt eksisterende kamerasystemer eller rimelige kameraer å bli modifisert, og dermed fjerne behovet for andre, dyrere løsninger. Ved å fjerne det infrarøde (IR) båndpassfilteret tillates lyset utenfor det synlige spekteret å komme inn til bildebrikken i kameraet, noe som gir det bedre nattsynsegenskaper. Undersøkelser antyder på at det tilgjengelige nattlyset for seg selv ikke er tilstrekkelig, så bruken av en nær infrarød (NIR) lyskilde ble undersøkt videre.

I den andre sonderingen ble en NIR lyskilde undersøkt i kombinasjon med det modifiserte kameraet, med mål om å finne det nødvendige lysnivået. Resultatene fra eksperimenter indikerer at en 20W lyskilde med et horisontalt og vertikalt synsfelt på 40° sannsynligvis er tilstrekkelig for videoopptak med kort lukketid å oppdage tilstedeværelsen av fugler på korte avstander. Imidlertid ble det på grunn av usikkerheter i utstyret og metodene ikke funnet et nødvendig lysnivå. Likevel ble verdifull informasjon angående oppsettet for videre eksperimentering oppnådd. Det ansees også som usannsynlig at en enkelt lampe 20W, 40° lampe vil være tilstrekkelig for kvaliteten som kreves for at en observasjon og gjenkjennelse skal oppnås for fugler på lengere avstander. Derfor ble det besluttet å utvikle en metode for å øke lysintensiteten.

En omfattende bruk av lamper er vurdert som uønsket, da det antas å redusere

sannsynligheten for at løsningen blir implementert. Derfor ble en metode for å øke lysintensiteten til en enkelt lampe undersøkt. I den siste sonderingen ble det dermed undersøkt om en smal lampe kan belyse det ønskede området i løpet av en rimelig tidsperiode. Et forslag til design og funksjon blir skissert, hvor lysstrålen til en enkelt lampe blir fokusert for å øke strålings intensiteten. For å dekke det nødvendige området er det foreslått å sveipe lyskjeglen over det ønskede området. Videre ble det samlet begrensninger angående sikkerhet og praktisk gjennomføring som retningslinjer for videre utvikling. Et konseptbevis ble utviklet, som illustrerer at det bør være mulig å oppnå en tilstrekkelig opplyst video.

Konklusjonen er dermed at et modifiserte RGB-kameraer bør være egnet for nattovervåkning til en viss grad. Videre er løsningen presentert i den tredje sonderingen lovende, men ytterligere arbeid er nødvendig. Dette inkluderer hvordan man kan fokusere lysstrålen, hvordan den kan styres, og hvordan småskalamodeller skal utvikles. Et linsesystem, muligens kombinert med noe rotasjon av lampen selv, blir foreslått for videre undersøkelser fro å styre lyskjeglen. For småskala testoppsettet anbefales det å utvikle en passende termineringskriterium basert på sluttbrukeren for å kunne avgjøre når en løsning er tilstrekkelig. I tillegg burde småskalamodellene av fugler gjenspeile detaljene til en faktisk fugl. Til slutt bør en metode for å sammenligne kameraers følsomhet ovenfor NIR lys bli utviklet, slik at det blir enklere for bedrifter og andre som kan være interessert i å utnytte løsningen å finne passende kameraer.

Contents

Preface i

Summary iii

Sammendrag v

Acronyms xvii

1. Introduction 1
- 1.1. Motivation . . . 1
- 1.2. Goal of this report . . . 2
- 1.3. Approach . . . 2
- 1.4. Structure . . . 4

2. Theory 7
- 2.1. Camera model . . . 7
  - 2.1.1. Pinhole model . . . 7
  - 2.1.2. Image sensor . . . 7
  - 2.1.3. Camera lens . . . 12
  - 2.1.4. Pixels per meter, PPM . . . 12
- 2.2. Radiometry . . . 12
  - 2.2.1. Irradiance: E . . . 13
  - 2.2.2. Solid angle: Ω . . . 13
  - 2.2.3. Radiant intensity: I . . . 13
  - 2.2.4. Radiance: L . . . 13
  - 2.2.5. Inverse-square law . . . 14
  - 2.2.6. Conservation of Radiance . . . 15
  - 2.2.7. Principle of reversibly . . . 15
- 2.3. IEC standard . . . 16
- 2.4. Offshore Wind Turbine . . . 18

3. Previous work **21**
3.1. State of the art . . . 21
3.1.1. Bird monitoring among offshore wind turbines . . . 21
3.1.2. NIR illumination . . . 21
3.1.3. Comparative evaluation . . . 22
3.2. Preliminary work . . . 23
3.2.1. Sensors in the turbine blades . . . 23
3.2.2. Radars . . . 24

4. No IR filter and ambient light **25**
4.1. Motivation . . . 25
4.2. Method . . . 26
4.2.1. Iteration 1. . . . 26
4.2.2. Iteration 2. . . . 27
4.3. Results . . . 30
4.4. Discussion . . . 32
4.5. Conclusion . . . 33

5. Required illumination **35**
5.1. Iteration 1: Small scale rig . . . 36
5.1.1. Motivation . . . 36
5.1.2. Method . . . 36
5.1.3. Result . . . 43
5.1.4. Discussion . . . 44
5.1.5. Conclusion . . . 44
5.2. Iteration 2: Testing with Stuffed Birds . . . 45
5.2.1. Motivation . . . 45
5.2.2. Method . . . 47
5.2.3. Result . . . 51
5.2.4. Discussion . . . 60
5.2.5. Conclusion . . . 64
5.3. Iteration 3: Small scale in spacious room . . . 65
5.3.1. Motivation and Method . . . 65
5.3.2. Results . . . 71
5.3.3. Discussion . . . 75
5.3.4. Conclusion . . . 77

6. Narrow swiping lamp **79**
6.1. Motivation . . . 79
6.1.1. Functional limits . . . 84
6.1.2. Swiping motion . . . 87
6.1.3. Radiometric exposure limits . . . 87

6.1.4. Reducing the distance . . . 92
6.2. Method . . . 92
6.3. Results . . . 97
6.4. Discussion . . . 101
6.5. Conclusion . . . 102

7. Summary discussion **103**
7.1. Further work . . . 105

8. Summary conclusion **107**

A. Test results **115**
A.1. Required irradiance . . . 116
A.2. Small-scale test rig . . . 118

B. Background **125**
B.1. Requirement specifications . . . 125

C. File naming **127**

List of Figures

1.1. Principle representation of the wayfaring journey and the probing cycle. . . . 3
1.2. The wayfaring journey of this thesis . . . 4

2.1. Illustration of Bayer filter . . . 9
2.2. Removing the IR cutoff filter . . . 10
2.3. Spectral sensitivity characteristic of the IMX 477 image sensor . . . 11
2.4. Inverse square law . . . 15
2.5. Solid angle of a lamp's light cone . . . 18
2.6. Size of the hypothetical offshore wind turbine evaluated in this report. . . . 19

4.1. Location of experiment . . . 28
4.2. The equipment used in the experiment . . . 28
4.3. No IR cutoff filter - Night sky . . . 30
4.4. No IR cutoff filter - Moon . . . 31
4.5. Default exposure time of FPS:5, 15, and 30 in the dark. . . . 32

5.1. Principal representation of real and model setup . . . 37
5.2. Box isolated with MDF plates in the test location. . . . 38
5.3. Illustration of how the model bird represents birds of various sizes 39
5.4. First iteration model birds on levers. . . . 40
5.5. Mounting of LED_{12} relative to the camera. . . . 41
5.6. Assembly of small-scale test rig . . . 42
5.7. Box interior after being lined with cloth. . . . 42
5.8. Benchmark image form inside the box, illustrating the successful isolation against external light sources. . . . 43
5.9. $8mA$ LED_{12} NIR illumination . . . 43
5.10. The lamps used in the experiments. . . . 47
5.11. Stuffed birds for testing visibility. . . . 48
5.12. Setup for camera and 20W visual light source in the storage room where the experiments were performed. . . . 50
5.13. NIR reflection comparison with plates - Northern Fulmar . . . 51

5.14. NIR reflection comparison with plates - Cormorant 52
5.15. LED flickering in 60 FPS video. 53
5.16. Aliasing in 40 FPS video. 54
5.17. Aliasing in 1 FPS video. 55
5.18. Exposure time of FPS:40 for varying configurations 56
5.19. Aliasing in 1 FPS video. 56
5.20. Gradient over the fulmar curvature 59
5.21. Bird models and the setup 66
5.22. Setup for testing the suitability of a 20W lamp with LED_{12} - Storage room. 66
5.23. Radiant intensity behavior for LED_{12} for varying input current I_F 68
5.24. Plot of the actual velocity of a bird at various distances from the camera, corresponding to the velocity of the model bird. 71
5.25. Gradient at I_F 28mA over sharp-edged bird models 72
5.26. Gradient over sharp-edged bird models 73
5.27. Gradient over round-edged bird models 73
5.28. Motion blur for FPS:20, shutter: 1/20s 74
5.29. Motion blur for FPS:60, shutter: 1/60s 75
5.30. Gradient over moving, round black bird model with I_F:12mA, fps:60, shutter:1/60s, gain:16. 75

6.1. Focused FOV of a lamp to increase radiant intensity 79
6.2. Comparison of irradiance reduction for a single lamp with P:20W, symmetrical FOV:10°, 20°, and 40°. In addition, a lamp with power P:80W and symmetrical FOV:40°. 80
6.3. The projected area of a point source at a distance 0-200m away when the FOV of the lamp's FOV is 40° and 20° 81
6.4. **(a)** A stationary lamp illuminating the whole projected area of the camera. **(b)** A rotating lamp covering one-third of the camera's projected area, illuminating each section one-third of a second. Both lamps cover the full area in the same amount of time. 82
6.5. The swiping motion of the lamp's light beam illuminates different areas of the camera's FOV 84
6.6. Illustration of channels 86
6.7. The radiance limit for light sources with low stimuli, L_{IR}, for various apparent source sizes, α 89
6.8. The minimum area for the apparent source to satisfy the irradiance limit, given various power outputs. 91
6.9. Minimum solid angle and symmetrical FOV for a lamp 92
6.10. Slider crank mechanism for concentrating and directing source light. 93
6.11. Schematic figure of the crankshaft mechanism with dimensions and variable names 94

6.12. Placement of the lens moving mechanism on the camera rig. The lens moved within the FOV of the LED_{12}. 95
6.13. Illustration of the light intensity with and without the focusing lens. 96
6.14. 9 frames of lens swipe from video with configuration: FPS:60, shutter:1/60s, gain:16 97
6.15. Measured swiping cycles over 1 second from video with FPS:60, shutter:1/60s, gain:16. Each frame is presented as red dots with their corresponding frame number in the plot. 98
6.16. Fourier transform of the sample, illustrating a swiping frequency of the light beam is $4Hz$. 98
6.17. Theoretical position (blue line) of the lens over a $1s$ sequence, together with the camera frame rate (red dots) of 60 FPS. Following the lens path for one cycle, moving from one side to the other and back. 99
6.18. Total illumination over the first half cycle (Top), the second half (Middle), and the combined illumination over one cycle (Bottom) . 100

A.1. Finding required irradiance. 116
A.1. Finding required irradiance. 117
A.2. Finding required irradiance. 118
A.3. 20W small scale test with rounded bird model, I_F:3mA 118
A.4. 20W small scale test with rounded bird model, I_F:4mA 119
A.5. 20W small scale test with rounded bird model, I_F:5mA 119
A.6. Gradient over moving round black bird model with I_F:3mA, fps:40, Shutter:1/40s, gain:16. 120
A.7. Gradient over moving round black bird model with I_F:3mA, fps:60, Shutter:Default, gain:16. 120
A.8. Gradient over moving round black bird model with I_F:3mA, fps:60, shutter:1/60s, gain:16. 121
A.9. Motion blur 40 FPS, default shutter 121
A.10. Motion blur 40 FPS, 1/40s shutter 121
A.11. Motion blur 60 FPS, default shutter 122
A.12. Gradient over moving round black bird model with I_F:3mA, fps:40, Shutter:Default, gain:16. 122
A.13. Gradient over moving round black bird model with I_F:3mA, fps:60, shutter:1/60s, gain:16. 123
A.14. Approximate 14W test, for comparison with the results obtained by Verhoef et al.[3] 123

List of Tables

1. Acronyms used in this report. xvii

2.1. Some common camera resolutions for CCTV cameras, obtained from [5] 8

5.1. LED Radiant Intensity at $I_F = 20mA$ for LED_{12}. 41
5.2. Minimum irradiance for detection and identification - Google Images. 57
5.3. Minimum irradiance for detection and identification - Artsorakelet. 58
5.4. Maximum values for the gradient of the sharp edge image in Figure 5.26, higher in absolute value than the round edge image in 5.27. 74

6.1. Dimensions of slider-crank mechanism. 94

C.1. Bash script and video filename variables. 128

Acronyms

AI	Artificial intelligence
CMOS	Complementary Metal-Oxide Semiconductor, a camera sensor technology.
FOV	Field of View
IEC	International Electrotechnical Commission
IR	Infra Red
MDF	Medium Density Fibreboard
NINA	The Norwegian Institute of Nature Research
NIR	Near Infra Red
ORJIP	Offshore Renewable Joint Industry Program
OWT	Offshore Windt Turbine
RPi	Raspberry Pi
RPi HQ camera	Raspberry Pi High Quality camera
RGB	Red-Green-Blue, the configuration of a Bayer filter found in consumer cameras.

Table 1.: Acronyms used in this report.

Chapter 1.

Introduction

1.1. Motivation

To battle rapid climate change and conflicts associated with onshore wind energy, the possibility of offshore wind turbines (OWT) as a potential solution has been subject to increased focus. However, in recent years, attention has come to the human impact on biodiversity, highlighting how anthropocentric activity is threatening populations of wild animals and in turn whole ecosystems. In light of the planned development of new offshore wind farms and the concern about the cumulative effect of human activities, attempts have been made to monitor the impact of OWTs on native and migrating marine birds. There is, however, a lack of knowledge about their migration paths, numbers, and their behavior when flying among OWTs. This, in turn, is causing the current estimations of collision rates to be uncertain. This has led to an investigation, performed by the Offshore Renewable Joint Industry Program (ORJIP), on how the current, statistical model can be validated[2]. In their latest report on biodiversity, it is concluded that a method for obtaining empirical collision rates is needed and that there is no system currently capable of delivering this service.

In a previous study performed by the author of this thesis, the technologies considered in the ORJIP report and a selection considered by The Norwegian Institute of Nature Research (NINA) were evaluated. Additionally, a set of requirement specifications was obtained to which the technologies were evaluated. There it was found that a shortcoming of the existing systems is the lack of nighttime tracking. Several companies delivering bird surveillance systems offer methods for detecting birds with radar or thermal cameras, but these technologies do not allow for species recognition. Additionally, such systems are costly, making surveillance of large wind turbine parks expensive. High costs can have a negative effect on the number of installments, and methods for reducing costs should be subject to research. Consequently, investigations into how relatively cheap RGB cameras

can be used is interesting. They can be found in most of the evaluated technologies, but are mainly used for daytime monitoring. Verhoef et al. took the use of commercially available low-light digital cameras further, investigating if they can be used for low-cost nighttime surveillance with NIR illumination[3]. Their results indicate that the approach might be applicable, but it was not entirely successful, and thus more research is required. Additionally, there is reason to believe that the solution might be more reliable today than it was in 2003, when they performed their experiment, due to advances in camera technology.

1.2. Goal of this report

The aim of this report is to develop a method for bird detection at night, allowing for species recognition, with the use of RGB cameras. The design shall be guided by the requirement specifications obtained in the prestudy of the thesis presented in Appendix B.

1.3. Approach

To approach the task at hand, the *Waifaring method*, described by Steiner & Leifer, has been utilized. They suggest an iterative learning-based approach for finding the "next big idea"[1]. The method is further elaborated by Garstenberg et al., arguing that the use of the wayfaring approach to complex, early-phase problems allows for the detection of *unknown unknowns*[4]. That is, *solutions that are part of your solution/problem that you are neither aware of nor do you know their value*[4]. They further argue that the model is suitable for the development of products with a high degree of uncertainty.

The wayfaring model is designed for the investigation of early phase product development. As there exists several solutions for monitoring bird activity, the overall problem cannot be considered to be in an early phase. However, none of the available solutions has proven to be the *next big idea*, as the number of implementations are still low. The available technologies can be considered different islands of probing cycles in the solution space, not necessarily connected to each other. Thus, this work takes the baton from the existing probing cycles in an attempt to find the next big idea by initiating new probing ideas.

The approach makes use only of a vision of the solution; a cheap and reliable method for monitoring bird species. A series of requirement specifications for the technology considered in this thesis is already obtained, presented in Appendix B. However, there is a wide range of possible solutions within the requirements, and arguably still room for many unknown unknowns. For this reason, it was decided

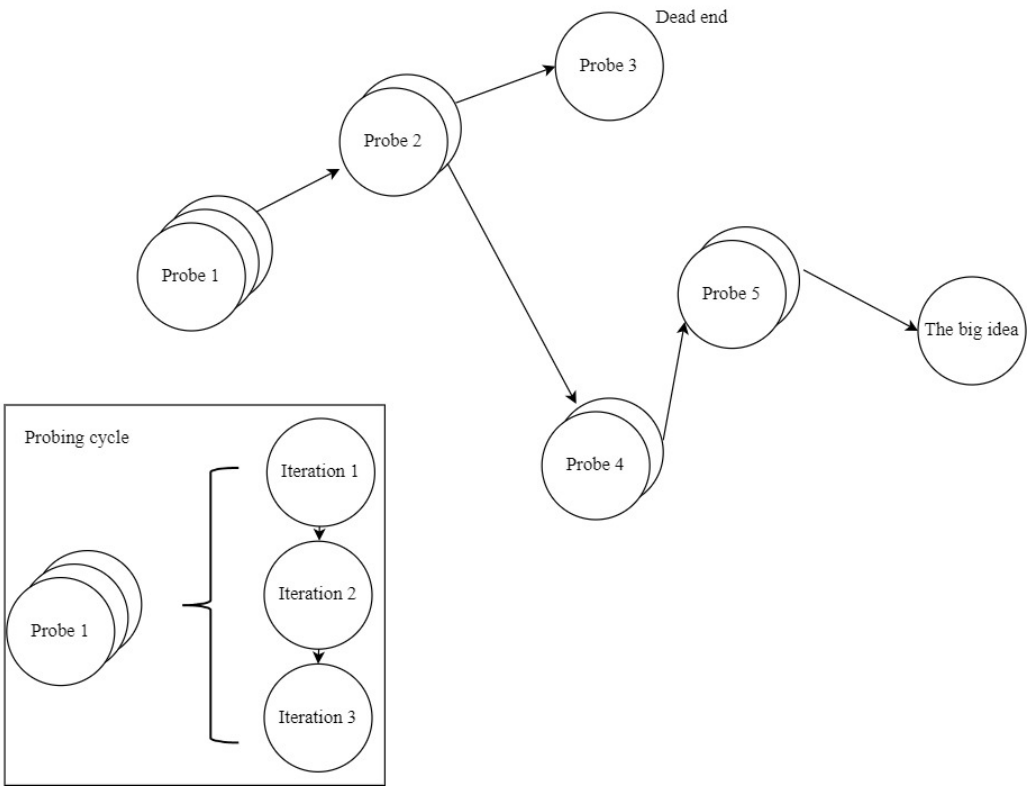

Figure 1.1.: Principle representation of the wayfaring journey and the probing cycle.

to make use of what Grastenberg et al. describe as *low resolution prototyping*. That is, prototypes reduced to the critical properties only, which require little time and cost. This allows for fast iterations through solutions and choosing the most promising one, a procedure referred to as *probing*. To avoid time-consuming work on dead-end solutions, the solutions have been opportunistically chosen, where a solution that proves sufficient for the task at hand is chosen for further investigations.

The wayfaring method can be illustrated as Figure 1.1, where each group of circles represents the probing ideas investigated. Each circle in a probing group represents the *iterations* of low resolution prototypes, obtaining knowledge through abductive learning. With new knowledge, new ideas are investigated until the final solution is discovered.

1.4. Structure

This thesis is structured in the chronological journey of the wayfaring approach, presented in Figure 1.2. Each chapter will consider a probe, where a new concept is investigated. Each chapter is divided into the probing cycles or *iterations*, in which the prototypes are built and tested.

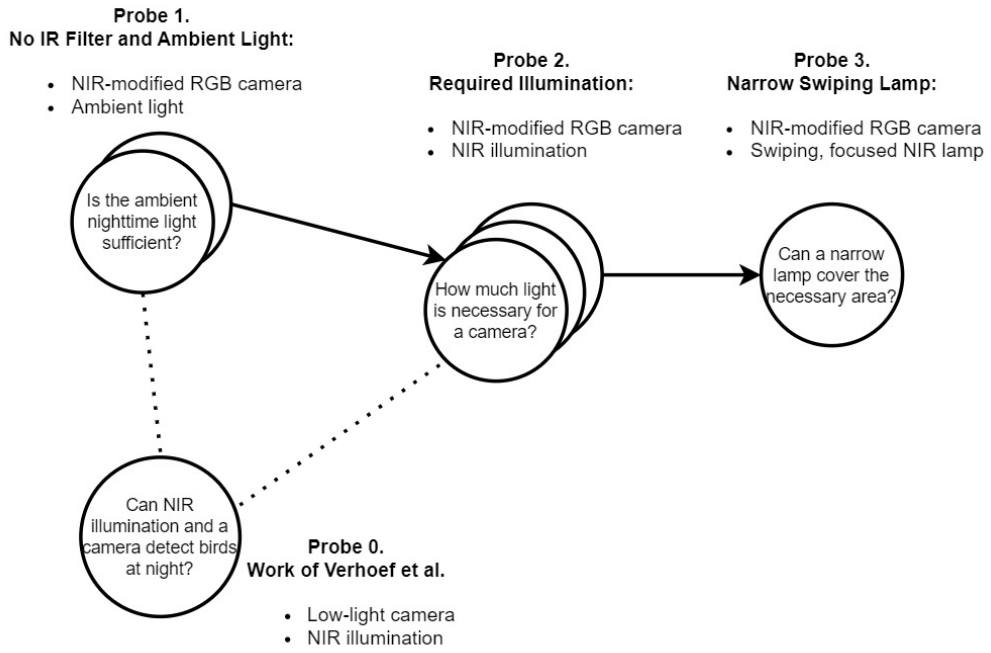

Figure 1.2.: The wayfaring journey of this thesis. The circles illustrate the probing ideas, and the number of circles in a group indicates the number of iterations performed in each. The arrows represent what direction was chosen based on the accumulated knowledge. The dotted line from **Probe 0.** to **1.** and **2.** illustrates the theoretical knowledge obtained from their report, which motivated their initialization. The list presented over each probe illustrates the key components of the idea. The question inside each probe outlines the critical function investigated, where the answer determines the next move.

Each iteration consists of a motivation based on the accumulated knowledge from the previous iterations, followed by an experiment. Thus, each iteration is presented with an IMRAD structure, where motivation and some background knowledge function as the introduction.

Chapter 2: Theory

This chapter introduces some of the background knowledge of the topics presented in this thesis. In addition, the circumstances in which the technology is meant to be implemented are presented.

Chapter 3: Previous Work
This chapter presents state of the art within bird tracking in offshore wind turbine plants, and some preliminary work is presented.

Chapter 4: No IR Filter and Ambient Light
This is the first probe, where the use of a consumer camera without its IR cutoff filter is investigated. The critical function investigated is the camera's ability to detect an object with the available ambient light at night. Two iterations were completed:

- **Iteration 1:** Small scale testing in a dark box.
- **Iteration 2:** Outside testing at night.

Chapter 5: Required Illumination
This is the second probe. Based on the findings from probe 1, an investigation of combining a NIR light source with the modified camera is performed. The critical function investigated is the required illumination for a camera to detect and recognize the bird. Three iterations were completed:

- **Iteration 1:** Small scale rig with a NIR LED, model birds, and camera placed in a box.
- **Iteration 2:** Visual light source with stuffed birds in a storage room.
- **Iteration 3:** Small-scale rig with NIR LED, model birds, and camera placed in a large room. Modifications to the setup are performed based on the knowledge obtained from the previous iterations.

Chapter 6: Narrow Swiping Lamp
This is the third and last probe. The critical function investigated is the ability to illuminate the camera's FOV sufficiently with a swiping lamp. Here, one iteration is performed:

- **Iteration 1:** Swiping light cone with a lens.

Summary Discussion
The findings of the probing cycles are discussed, and further work is presented.

Summary Conclusion
The conclusion of the overall work is presented.

Appendix A
Attachment with results from the experiments. A large number of image frames

and figures illustrate trends but would require too much space in the result sections of their corresponding experiment.

Appendix B
A table describing the variables used in the video files.

Appendix C
The requirement specifications guiding this thesis, obtained from the previous work of the author.

Chapter 2.

Theory

2.1. Camera model

2.1.1. Pinhole model

The pinhole model describes the mathematical relationship between a 3D object and its projected 2D image. The model assumes that light emitted from a source, such as the light reflected from a point on a tree, is spread uniformly in all directions. When several light sources are present, like the light reflected from other points on the same tree, the light is mixed, and one cannot obtain an image of it. If the light is only allowed to pass through a small entrance, then unwanted light is not allowed to pass through, and only the light with a direct path through the entrance can pass. The entrance is what is referred to as the pinhole, and when a wall is placed behind it, a 2D projection, or image, of the tree is generated. A large pinhole allows for more light to pass through, and the projected image becomes blurry, and reducing the size of the pinhole results in a crisper image. Now, using geometry, any point on the image can be mapped to its corresponding light-reflecting source on the real-world tree.

2.1.2. Image sensor

To obtain the tree image, digital RGB cameras utilize a surface of tightly packed photodiodes, pixels, a surface to which the image is projected. The amount of pixels in an image sensor is referred to as the sensor resolution and common resolutions for consumer cameras can be found in Table 2.1.

Resolution	Pixels (W x H)
D1	720 x 480
720p	1280 x 720
1080p	1920 x 1080
3MP	2048 x 1536
4K	4000 x 3000

Table 2.1.: Some common camera resolutions for CCTV cameras, obtained from [5]

Each photodiode consists of a silicon crystal that releases electrons when subjected to *electromagnetic radiation* (EMR) in the range 400nm to about 1000nm [6]. Visible light is EMR in the range of 400nm to 750nm, while near infrared (NIR) light lies between 750nm to 1400nm. This means that photodiodes can convert both visible and NIR light into digital signals. The intensity of the light can be measured by the energy released by each crystal over a unit of time, which is referred to as the *shutter speed* or *exposure time* of digital cameras. The electrons released by the crystal are accumulated in the duration of the shutter sequence and measured. This is again calculated as the brightness observed by the pixel. A low shutter speed allows more light to be absorbed by the pixels and is ideal for dark environments. However, this can cause the pixels to be over-saturated such that no more electrons can be released. This is what happens when one tries to depict a clear sky, where the image turns all white and contours are removed. Another issue with using a low shutter speed is that fast-moving objects can move over several pixels. This causes the image to depict the path of the object, and is referred to as *motion blur*. A high shutter speed can thus be used to reduce the amount of light accumulated in each pixel and generate a crisper image.

Higher numbers of photons result in a higher voltage readout and each pixel value can be stored and used when displaying the image on a digital screen. However, the pixels cannot determine what wavelengths of light are present. This is solved by placing color filters on top of the crystals so that one can know which wavelength is measured and only the intensity is needed. In RGB cameras, this is resolved by using the Bayer filter and an IR-cutoff filter.

Bayer filter

The *Bayer filter* is a grid of colored glass placed on top of the photodiodes, such that each diode is covered by either a red, green, or blue filter. This way, only EMR with a wavelength similar to the filter is allowed to pass, and one can determine how much of the given spectrum was present in the image. The color grid is

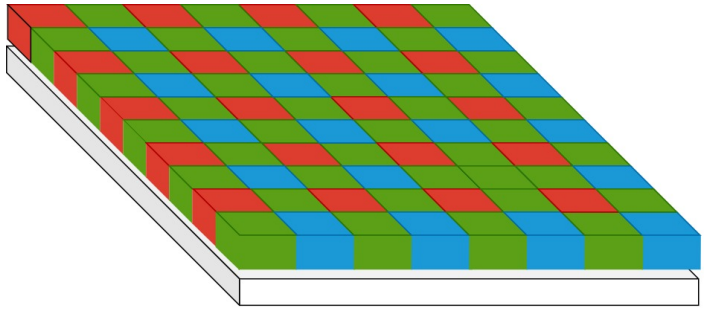

Figure 2.1.: Illustration of a Bayer filter, with the filter laying above the image sensor.

referred to as a *mosaic*, and the grid code of the Bayer filter is red-green-green-blue (RGGB), referring to the relative amount of filters and their order. The RGGB configuration, depicted inn Figure 2.1, consists of twice as many green filters compared to either the red or blue filters to mimic the human eye, which is more sensitive to green light.

IR cutoff filter

The *IR cutoff filter* is a band pass filter allowing visible light to pass through while blocking IR and UV light, and is usually in the form of a glass plate placed above the image sensor. If removed, the sensor can absorb more light and thus improves its ability to observe in low-light conditions. However, the contamination of additional light exposes the pixels to more light than the human eye can perceive, as seen in Figure 2.2, which can cause unnatural colors in the images. For instance, this causes red pixels exposed to both visible and NIR light to appear unnaturally bright.

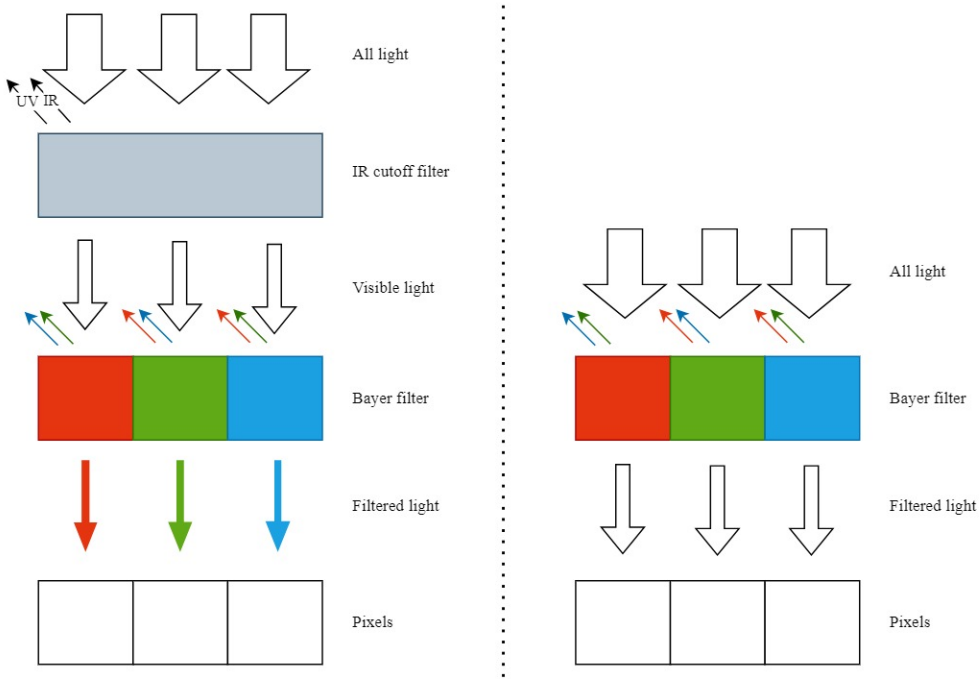

Figure 2.2.: Left: The IR cutoff filter blocks infrared (IR) and ultraviolet (UV) from reaching the image sensor. Next, the Bayer filter filters the red, green, and blue light such that each pixel is illuminated mainly by one color. **Right:** IR cutoff filter removed, and both UV and IR light are allowed through, including NIR. This allows more light to the image sensor.

In Figure 2.3, one can see the relative spectral response of a Sony IMX477 image sensor designed for consumer products. The spectral response can be considered as the image sensor's sensitivity to the different wavelengths. Note that the response is relative and not absolute, so the sensor is 11% more sensitive to green light at 540nm than it is to red light at 610nm. This is a design choice made by the manufacturer which causes the image to look natural to human eyes and can differ between camera models.

The relative spectral response to NIR light in consumer cameras is usually significantly lower than visible light. In the sensitivity obtained by Wang et al. one can see the spectral response decreases approximately linearly towards 1000nm [8]. Thus, it is desirable to utilize high-frequency NIR rather than low, as it is more likely the camera will detect it.

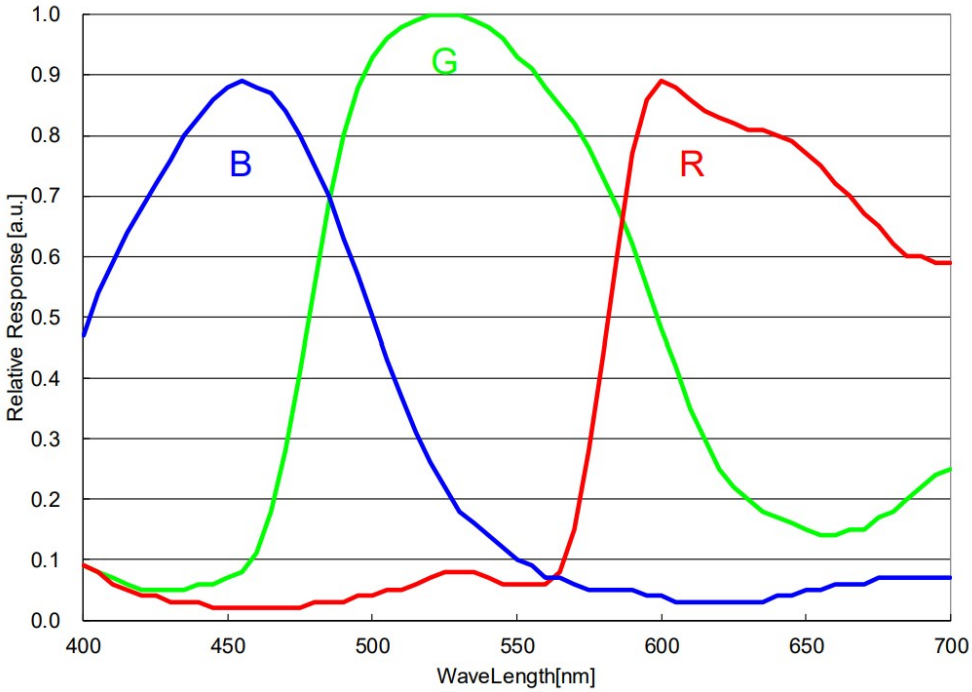

Figure 2.3.: Spectral sensitivity characteristic of the IMX 477 image sensor. The graph does not include lens characteristics or light source characteristics. Retrieved from the IMX 477 data sheet [7].

2.1.3. Camera lens

The camera lens allows for a desired amount of light to pass through. Similar to the pinhole of the pinhole model, only rays of light headed directly to the lens are allowed through. Light is then bent to be projected in a desirable angle to generate a 2D image on the camera sensor. Advanced lens systems make use of a series of lenses to allow for better image quality in various conditions. The lens determines the camera's *field of view* (FOV), determining how much of the scenery is captured in the image. Consumer lenses usually range from super-telephoto with a 4° FOV, to fish-eye with a 180° FOV, where a low FOV captures less of the scenery than a lens with a high FOV. However, a high FOV is generally ill-suited for long-distance imagery, due to the low pixel density generating details in the image.

2.1.4. Pixels per meter, PPM

The pixel density is a measure of the detail obtainable with the camera at a given distance, commonly known as pixels per meter, *PPM*. It is calculated by dividing the number of the horizontal or vertical pixels, N_{pixels}, by the projected width or height of the image sensor, $l_{projected}$ at a distance, d, away from the camera. Knowing the FOV of the camera and the distance to the target, we obtain Equation 2.1 and can calculate the PPM with Equation 2.2.

$$l = 2 * \tan(\frac{FOV}{2}) * d \tag{2.1}$$

$$PPM = \frac{N_{pixels}}{l_{projected}} \tag{2.2}$$

A low PPM will result in an unsharp image with little detail relative to an image with a high PPM. The full video resolution obtainable for the RPi HQ camera is 1920x1080, and an $A_{projected}$ of $230m$ at $200m$ with a 60° lens. This gives a horizontal PPM of 8.3 pixels per meter.

2.2. Radiometry

Irradiance, radiant intensity, and radiance are fundamental concepts in the field of optics and radiometry. They are crucial for understanding and manipulating light and its interactions with various surfaces. This section presents their definitions.

2.2.1. Irradiance: E

The *irradiance*, E, is the amount of light incident on a surface per unit area in a specific surface[9]. It quantifies the intensity of the light hitting a surface from all directions. The irradiance, E, resulting from a single light source can be calculated by dividing the power, P, of the source by the area, A, to which the light falls upon.

$$E = \frac{P}{A} \tag{2.3}$$

2.2.2. Solid angle: Ω

An important unit for interpreting radiation in three dimensions is the *solid angle* Ω. The solid angle describes the spatial spread of radiation and has the SI unit steradians $[sr]$, and is defined as 2.4. A_n is an area perpendicular to the cone axis described by Ω and r its distance from the source [10]. Its magnitude is the projected area of the surface A_n onto a sphere with unit radius. That is, the projection of all points on a closed curve, onto a point from which the solid angle is measured [9].

$$\Omega = \frac{A_n}{r^2} \tag{2.4}$$

2.2.3. Radiant intensity: I

The *radiant intensity*, I, is the amount of light energy in a particular direction per unit of solid angle per unit of time[9]. It quantifies the concentration of radiant energy with a specific angular range. I can be calculated by dividing the power, P, of the source by its solid angle, Ω. We here consider the source as a point source, which can be applied to lamps if considerable distances are evaluated.

$$I = \frac{P}{\Omega} \tag{2.5}$$

2.2.4. Radiance: L

The *radiance*, L, is the amount of light energy emitted, transmitted, or reflected from a surface in a particular direction per unit of solid angle, per unit projected area, and per unit of time[9]. It is a comprehensive measure of light's power in a given direction. Radiance describes the amount of light emitted by a source and its spatial distribution.

$$L = \frac{P}{\Omega * A} = \frac{E}{\Omega} = \frac{I}{A} \tag{2.6}$$

In radiometry, the SI unit for radiance is [W m^{-1} sr^{-1}]. However, in photometry, a subset of radiometry focusing on visible light, radiance is annotated with [cd m^{-2}]. The latter makes use of the SI base unit for light, *candela* [9].

2.2.5. Inverse-square law

The inverse-square law, Equation 2.7, states that a physical quantity is inversely proportional to the square of the distance from the source of that physical quantity[9, 11]

$$I \propto \frac{1}{d^2} \tag{2.7}$$

For a point source of light with homogeneous distribution, the light will continue in a straight path unless directed. As the distance increases, the distance between rays of light will increase, and thus, the density of light per unit area will decrease as illustrated in Figure 2.4. It is important to note, however, that this considers a point source, which for a lamp can be obtained at large distances. McCluney suggests that a source with lateral dimension, x, should be less than 10% of the distance d can serve as an approximate criterion for when a source can be considered a point source[9].

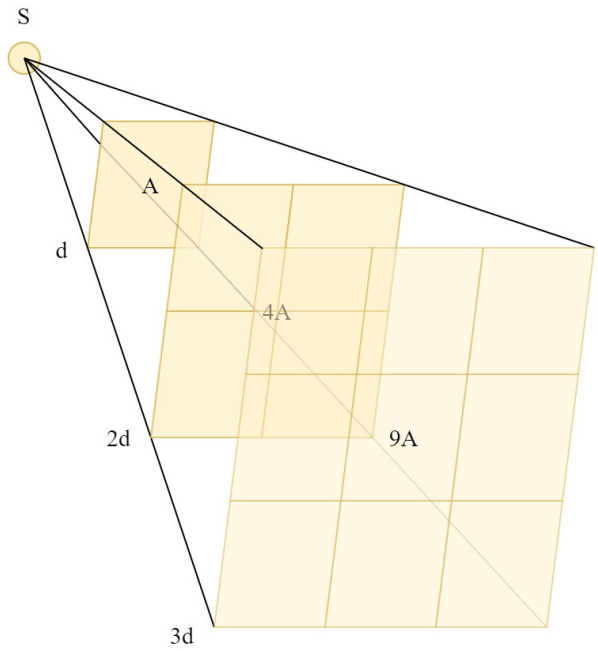

Figure 2.4.: As the distance increase, the area A at a distance d from the source S increase inverse proportionally to d^2.

2.2.6. Conservation of Radiance

The radiance divided by the index of refraction squared is invariant in ideal geometric optics. This means that the output radiance for an ideal optical system is identical or less to the input radiance [9, 12]. This is referred to as the conservation of radiance. This is due to radiance's dependence on solid angles. If a lens concentrates the light of a source onto a small area, the irradiance increase, but the incident light fills a larges solid angle, and the radiance stays the same.

2.2.7. Principle of reversibly

The principle of reversibility states that the light will follow the same path if its direction is reversed. This can be understood as if one places a point source of light in the focal point of an antenna or a lens, the light will follow the same path as it would if an external source was shining onto the antenna or lens[13].

2.3. IEC standard

The *near infrared spectrum* (NIR) will, in this report, refer to EMR with wavelengths in the range 780nm - 1400nm. That is, EMR with longer wavelengths than visible light and shorter than infrared light. NIR light is invisible to mammals [14, 15], and is thus often used for night surveillance with trail cameras and other wildlife cameras. Although NIR light is invisible, it can potentially damage the eye. A strong light source can damage the retina and the cornea, and lamps emitting NIR are thus regulated.

In this report, the use and design of lamp systems will follow the IEC standards for lamps (NEK IEC 62471:2006)[16] and projectors (NEK IEC 62471-5:2015)[17]. The IEC 62471-5 standard is based on the IEC 62471 standard but designed for manufacturers to determine the risk group and the belonging safety precautions needed projectors.

In IEC-62471, two exposure limits are significant to NIR lamps:

- 4.3.6 Retinal thermal hazard exposure limit - weak visual stimulus
- 4.3.7 Infrared radiation hazard exposure limits for the eye

The remaining limits are either:

- Considering the exposure to UV and blue light, which is not considered in this report where it is assumed that the light source is only radiating in the NIR spectrum.
- Concerning the same limits, but is less strict than the limits evaluated in this report.

$$E_{IR} \leq 18000 * t^{-0.75} \qquad t < 1000s \tag{2.8}$$

$$E_{IR} \leq 100 \qquad t > 1000s \tag{2.9}$$

$$L_R \leq \frac{28000}{\alpha} \qquad t < 10s \tag{2.10}$$

$$L_{IR} \leq \frac{6000}{\alpha} \qquad t < 1000s \tag{2.11}$$

Requirement 4.3.7 states that the maximum radiation flux cannot exceed 100 W/m^2 for exposure times longer than 1000 seconds. This requirement is then used as a limit for the *exempt group* of projectors in the 62471-5 standard. The exempt group is considered to have no risk of injury.

Req. 4.3.6 is a modification to 4.3.5 which consider all light with wavelengths of

$380nm - 3000nm$ and exposure times below $10s$. In req. 4.3.6 the invisibility of NIR to the human eye is considered and is applicable for exposure times longer than 10s. This suggests that as long as req. 4.3.6 is satisfied, req. 4.3.5 is too. For calculating the retinal thermal hazard exposure limit, L_R, the size of the apparent source is important. Smaller sources are less damaging than large ones. To standardize the measurement of the source size, it is determined by its *angular substance*, α, for an observer placed $l = 1m$ away from the source. The angular subtense is the angle of the projected image of an object on the retina. In projectors, it is no longer the size of the light source but the *apparent source* which is considered. The apparent source is the exit pupil of the projector where light is limited to a contained area. Additionally, the distance for measuring the angular subtense is modified to include the distance, l_b, between the apparent source and the lens front such that the total distance is $l = 1m + l_b$.

For strong visible light, the aversion response of humans exposed to strong light hinders damage to the eye. The risk group requirements of IEC-6247-5 are based on the damage obtained between exposure and total avoidance, which is set to be $0.25s$. This does not, however, apply to a low visual stimulus where the observer can have strong radiation directly into the eyes without reaction. Thus, a NIR projector should not be evaluated only under the IEC-62471-5 standards, but the procedure for measuring the exposure limits should be considered.

Solid angle, Ω, in IEC 62471

In the IEC 62471 standard, the solid angle for small angles can be calculated with Equation 2.12, where α is the visual angle subtended by the source at the eye of an observer at a distance r away from the source.

$$\Omega = \frac{\pi * \alpha^2}{4} \tag{2.12}$$

For a oblong source, alpha is calculated with Equation 2.13, where Z is an averaged width of the source, calculated with Equation 2.14

$$\alpha = \frac{Z}{r} \tag{2.13}$$

$$Z = \frac{height + width}{2} \tag{2.14}$$

When considering the source size and the eye's exposure to radiation, α has a maximum and minimum limit: α_{max} of $0.1rad$ and a α_{min} of $0.0017rad$. The

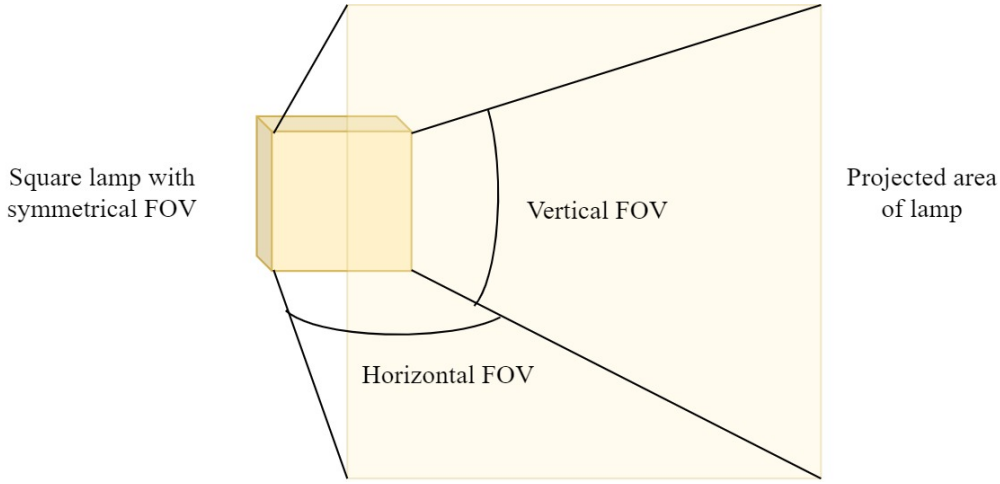

Figure 2.5.: Solid angle of a square lamp's light cone, here with a symmetrical FOV creating a square projected area.

minimum value α_{min} is due to limitations of human vision, where objects generating a subtended angle less than α_{min} will be perceived as being the same size as α_{min}. α_{max} results from the small source being spread over the retina due to task-determined eye movements over an extended period of time.

In the IEC 62471-5 standard, the solid angle of a projector is calculated with the horizontal and vertical FOV as presented in Equation 2.15 and illustrated in Figure 2.5.

$$\Omega = FOV_{vertical} * FOV_{horizontal} \tag{2.15}$$

2.4. Offshore Wind Turbine

An outline of the fictive offshore wind turbine used for guiding the development process in this thesis is presented in this section. The following text is obtained from the previous work of the author[18].

The size of the offshore wind turbine that will be considered in this report, Figure 2.6, is set to be $107m$ in height from the water surface to the center of the retort and $170m$ in diameter. The bottom reach of the rotor blades is assumed to be 22m above the water surface, while the landing platform for the maintenance crew is assumed to be 13m below the bottom reach of the rotor blades. This is inspired by the turbines in Haywind Tampen, but the goal of the system is to be

applicable to a wide range of sizes. The tribunes are installed on spar bouys.

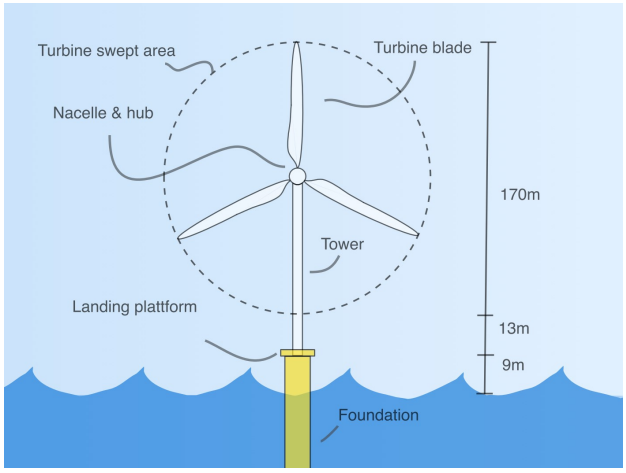

Figure 2.6.: Size of the hypothetical offshore wind turbine evaluated in this report.

The landing platform is a plateau for personnel to access the turbine entrance and a base for mounting equipment. The platform is assumed to have a circular shape, and a protruding section with additional space. A rail circumference is the platform to which it is assumed that equipment can be mounted. On the top of the nacelle, there is a platform for instrumentation. It is, however, not readily accessible due to the being in the height.

The top reach of the wind turbine is $192m$ above sea level. The range, or distance to which an object can be detected by the camera will, in this work, be considered satisfactory if it is at 200m. This range will then allow for detecting birds flying slightly above the top reach of the rotors.

Chapter 3.

Previous work

In this chapter, the previous work related to the topics of this thesis is presented. Further, some preliminary work is presented to give the reader the motivation for the choice of direction covered by this thesis.

3.1. State of the art

3.1.1. Bird monitoring among offshore wind turbines

The Offshore Renewables Joint Industry Programme (ORJIP)(2022) presented an extensive review of seabird monitoring technologies for offshore wind farms[1]. Here, solutions proposed by previous research and companies are presented, describing the systems in detail. The study concludes that further research on camera systems is necessary for obtaining species-specific collision rates and bird flight behaviors at different scales under different conditions. Camera solutions are evaluated as necessary for the capability to determine species and birds at risk, and other technologies should be added for aiding identification in low-light conditions[2].

3.1.2. NIR illumination

Verhoef et al.(2003) attempted to develop a low-cost solution for detecting bird collisions. As part of their study, they investigated the possibility of using a low-light camera combined with a 14W 940nm light source for capturing video of birds and bats flying past the turbine at night. Testing both with and without the light source, they conclude that the illuminator is necessary. However, they state that their setup was insufficient, as the exposure time was too long, causing

[1] https://www.carbontrust.com/our-work-and-impact/guides-reports-and-tools/review-of-seabird-monitoring-technologies-for-offshore-wind-farms

too low sampling frequencies. It is unclear whether the camera's autofocus caused the issue of long exposure times or if the light conditions required long exposure times for obtaining any footage of the animals. They found that the added NIR light source improved footage up to $40m$, but not at larger distances due to the limited capacity of the source. Further, they recommend more research where it is probable that more light is needed. It is also noted that special attention should be given to the wavelength of the NIR light, as it is unclear to what extent birds are sensitive to it[3].

3.1.3. Comparative evaluation

As part of the pre-study of this thesis, an evaluation of 19 solutions for automated bird detection was performed, including all the solutions presented in the ORJIP, in addition to some presented by NINA. The current state-of-the-art makes use of the following technologies some or all of the following technologies:

- Radarad
- RGB camera
- Near Infrared and Infrared camera
- Microphone
- Accelerometer on the turbine blades

The technologies are both used by themselves and in different combinations. The technologies were evaluated against the requirement specifications presented in Appendix A, obtained from in-person conversations with institutes of science and companies associated with wind turbines. The pre-study focused on technologies for obtaining collision rates in specific. It was found that automated methods for registration are necessary due to the scale of the task, and considered probable that machine learning can determine collision rates based on the trajectory of a bird before and after passing the turbine-swept area[18].

Radars could be suitable but require a large area on the turbines and cannot be placed onto old installations as adaptations are needed. The MUSE system[2] was implemented in a study performed by Vattenfall. While a radar was present, it mainly provided information flight track and not species, which was performed by the camera[19]. A thermal camera was included in the system for night observation, but night-time observations were not included in the report.

Microphones can determine species based on bird calls, but if no calls are present, it is blind. To detect collisions, they also require that the sound of a collision

[2] https://www.dhigroup.com/business-applications/dhi-muse/

between the bird and the turbine is distinguishable from the background noise.

Detecting a collision using sensors would provide sound evidence on the collision rates. However, a suitable method is currently unavailable. This is both due to the behavior of the turbine blade, which will be discussed further in section 3.2, and due to violating the warranty of the wind turbine blades.

A method for detecting birds with RGB cameras at night is currently unavailable, where near-infrared or thermal cameras are the only options. However, these technologies are expensive compared to RGB cameras and require extensive investments if several are applied to every turbine in a plant. Thus, it was concluded that a low-cost solution should be investigated. 11 out of the 19 investigated solutions make use of RGB cameras for daytime monitoring, and a method of using these for night-time monitoring would reduce costs.

3.2. Preliminary work

Several technologies were investigated as alternatives to camera solutions after the pre-study and before the initialization of this thesis. For the benefit of future work on this topic, the findings of this work will be presented here.

3.2.1. Sensors in the turbine blades

The use of sensors in wind turbine blades for predictive maintenance is an exciting topic, and the possibility of utilizing various sensor technologies for detecting the collision between a bird and a blade was investigated. While this does not allow for direct species recognition, it would give valuable information about collision rates. Further, it could be coupled with other systems to find what species were in the area at the time of the collision and, from this, determine the probable species. However, existing vibration measuring sensors are placed in the nacelle and not the blades, in addition to capturing readings in intervals and not continuously. Thus, these sensors are unlikely to detect a collision. Further, the use of optical-fiber sensors was considered, as they can be placed along the inside of the turbine blade and are highly sensitive. Its ability to detect discrepancies in the blade would also function as an incentive for the companies to implement the solution. However, a wind turbine blade will likely function as a low-pass filter, smoothing out the impact of a collision. It could thus be difficult to distinguish the collision from regular vibration noise. Even if a machine learning algorithm could distinguish the collisions, training data was not available, and a method for creating the training data was required, ideally with a wind turbine blade. As this was not available, and as the sufficiency of the solution seemed unlikely, the solution was discarded.

3.2.2. Radars

Radars are commonly used for detecting objects in spacious environments. Some of the solutions presented in the ORJIP report claim their solution is able to determine species based on flight patterns and was thus investigated further. The radars are used for monitoring several wind turbines and could thus be efficient for detecting bird collisions. However, due to noise cluttering caused by radio waves reflecting off the turbines, radars covering large areas were considered unreliable for collision detection, as they will struggle with detecting objects close to the turbine. However, a radar facing away from the tribune tower could monitor the trajectory of a bird passing by. By evaluating the expected trajectory to the actual trajectory, a deviation could be counted as a probable collision event. However, the two types of radars considered, continuous pulse modulated wave and pulse radar, were considered to be insufficient. Pules radars have a physical limitation to the minimum range, which was found to be too large and would generate a sizable blind zone. The pulse-modulated wave radar has a low field of view and would not be able to cover the volume of interest. An interesting solution can, however, be the development of phased array radars in the desired wave band. They are, in theory, able to scan large areas by directing the radar beam without moving the antenna. However, no suitable radar was found, and the development of one would require a large amount of digital to analog-to-digital converters and the authors background knowledge on the field is low, and it was thus discarded for further work in this thesis.

Chapter 4.

No IR filter and ambient light

This is the first of the probing ideas investigated in this thesis. Based on the knowledge gained from the previous work, it was decided to investigate the capabilities of RGB cameras without IR cutoff filters. Thus, in this chapter, it is investigated if a cheap, commercially available camera can detect an object in the night sky by utilizing the entire range of light the image sensor can detect by removing the IR cutoff filter.

4.1. Motivation

All computer vision relies on enough light for the pixels to obtain a value. In daylight video surveillance, it is the ambient light reflecting off the target which is captured by the camera. At night, the available ambient light is reduced, with the main sources being the moon, stars, light pollution, and sky glow [20, 21, 22]. It is thus interesting to investigate if the accumulation of night-time light sources will be enough to generate any pixel value, and if so, how high.

Cameras do not need as much light as the human eye to detect an object, where slight contrasts can be enough for an algorithm to detect the same object. Important tools for object detection and tracking are edge, line, and feature detection[23]. Edge and line detection relies on the change in intensity values between neighboring pixels to mark edges, the *gradient*[23]. Threshold values can be set to determine how large and sharp changes in pixel values are needed for the transition to be an edge, allowing for edge detection in low-light conditions. However, low thresholds make for a noisy image, and a minimum of light is still required for the pixels to distinguish between the object and its background. Feature extraction relies on the identification of reliable and unique features of an object, where high detail in the image allows for good tracking and recognition of objects.

Inspecting the World Atlas for Artificial Sky Brightness, it indicates that areas

close to existing offshore installations are subject to light pollution [20]. In rural areas, the light available is set to be sub 0.176 mcd/m^2, while close to offshore installations and the coast of Norway, the light pollution ranges between 0.176-0.619 mcd/m^2.

Sky glow emits mainly near-infrared light[24]. However, consumer cameras remove the non-visible light by filtering it out before it reaches the image sensor to mimic the vision of humans. Thus, it removes available information from the image. Vollmerhausen et al. suggests that silicon-based cameras designed in low light conditions and open to the NIR spectrum are beneficial for nighttime surveillance from planes compared to IR cameras due to the ability to see contrasts in the image and the abundance of NIR light[24].

4.2. Method

4.2.1. Iteration 1.

To obtain an idea of the effects of removing the IR cutoff filter, an available web camera was dismantled, and the IR cutoff filter was removed. The modification enabled the camera to detect the NIR light used by smartphones for face recognition. It was evident that the modification allowed some degree of NIR light detection, the first minimum critical function. However, the camera provided only a live stream video and offered no ability to manipulate the camera settings such as shutter speed and frame rate. As these functions allow for improvement to the footage, a Raspberry Pi HQ camera was bought for further investigation.

The HQ camera uses the 12.3-megapixel Sony IMX477 sensor, which is the largest of the RPi cameras. The HQ camera allows for the removal of the IR cutoff filter, another key reason for choosing the camera. The HQ camera comes without a lens, so a 60° lens with a 6mm focal length from a third party was attached[1]. 60° is considered to be a wide lens for cameras and can be expected as a surveillance camera. To enable all detectable light access to the image sensor, the IR cutoff filter was removed according to the description in the instruction manual [25].

The NIR-modified RPI HQ camera was placed in the largest available cardboard box to investigate its performance in low-light conditions. The cardboard walls were corrugated, and the box had a base area of 60x60 cm^2 and 78 cm in height. The box was thick enough to remove all visible light in frame rates above five FPS before removing the filter. However, after removing the filter, the box was dimly illuminated by the NIR light.

The RPi cameras are designed to be compatible with Raspberry Pi (RPi), a

[1] https://docs.rs-online.com/4798/A700000006829447.pdf

single-board computer that is a popular choice for hardware prototyping. This allows for software modifications to the camera settings, enabling a wide variety of configurations. Additionally, due to RPi cameras being a popular choice for hobby purposes, there are many resources on how to solve or avoid limitations and issues with either hardware or software. A Raspberry Pi 4 model B was used with a 16GB memory card to communicate with the camera. The default Raspberry Pi OS was chosen as the software. The Pi's main goal was to communicate with the camera, while all image or video processing was performed on a secondary computer except for some initial attempts. For shooting video and images, the RPi camera application *libcamera* for complex camera systems was used.

4.2.2. Iteration 2.

As the camera obtained illustrated a considerable improvement for recording in low light conditions, it was decided to investigate the performance in more realistic circumstances. The camera was brought to a harbor in Trondheim at night in March with a clear sky. The camera was held against the sky, directed away from the nearby light sources presented in Figure 4.1.

Power outlets were not available, so the RPi was controlled over a computer through a secure shell connection (SSH). The full setup is illustrated in Figure 4.2.

(a) Light pollution from nearby harbor

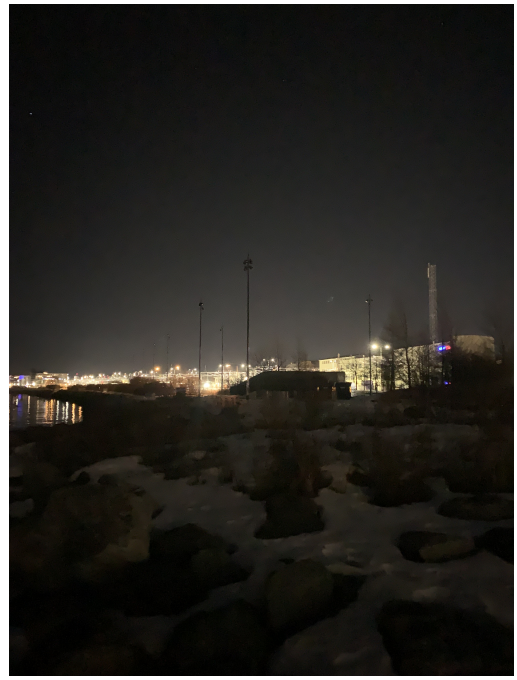

(b) Light pollution from the city

Figure 4.1.: Location of experiment

Figure 4.2.: The equipment used in the experiment

4.3. Results

(a) Night sky image - 5 FPS

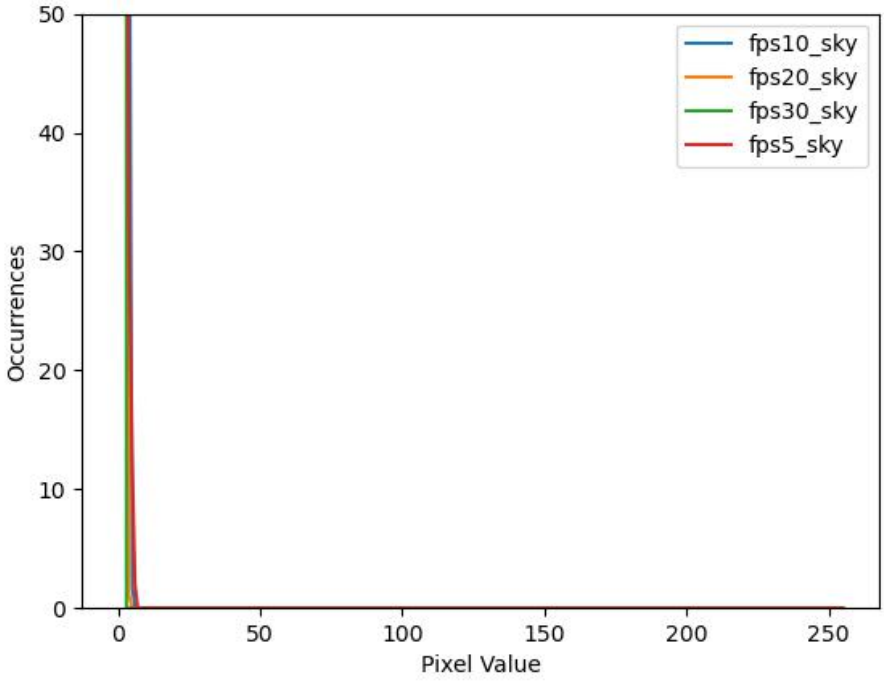

(b) Night sky image - Histogram

Figure 4.3.: (a) Frame 5 from video *5fps_sky* of a clear night sky taken in the winter at the harbor of Trondheim. **(b)** Histogram of night sky image without IR cutoff filter. The histogram of frame 5 from videos with FPS set to 30, 20, 10, and 5. Plots illustrate the number of pixels on the Y-axis and their values on the X-axis. Due to the large lack of values below 10, Y-axis is cropped to 50 occurrences to illustrate that close to no high values were present.

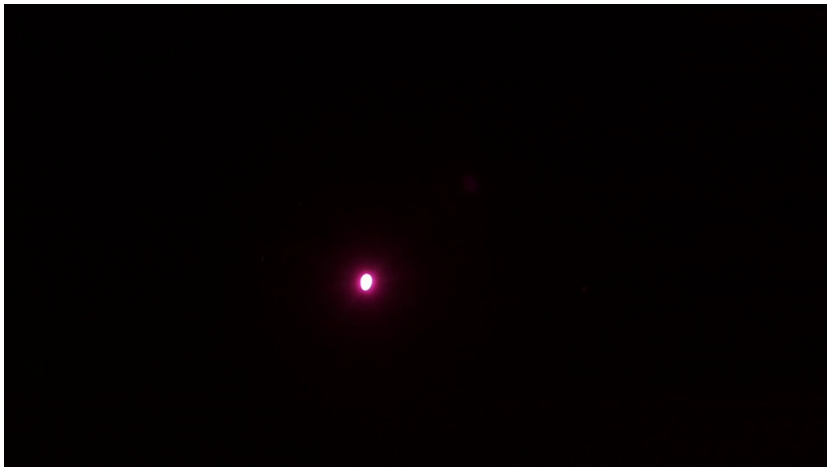

(a) Moon image - 5 FPS

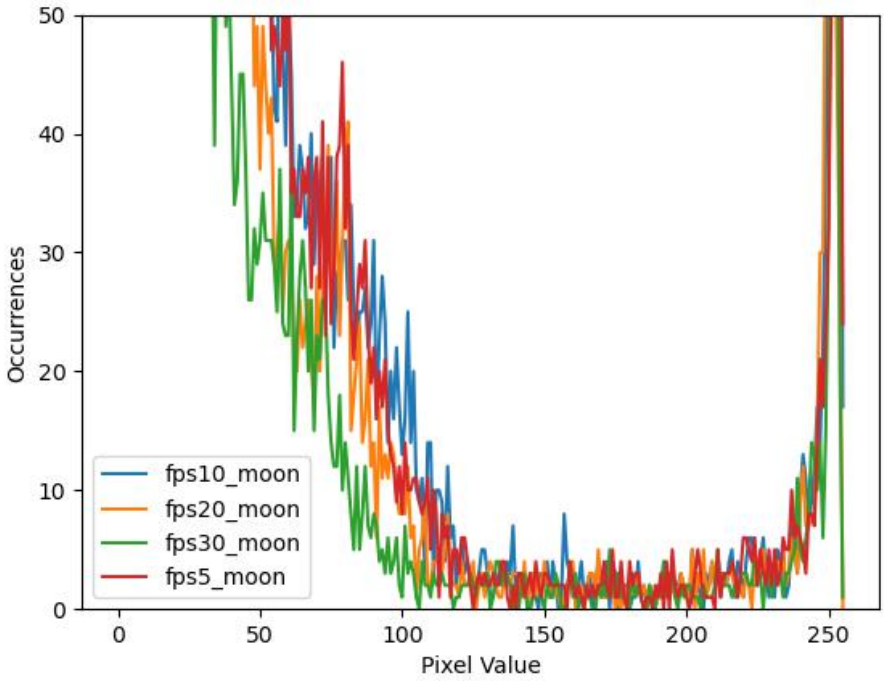

(b) Night sky image - Histogram

Figure 4.4.: (a) Frame 5 from video *5fps_moon* of a clear night sky taken in the winter at the harbor of Trondheim. **(b)** Histogram of night sky image without IR cutoff filter. The histogram of frame 5 from videos with FPS set to 30, 20, 10, and 5. Plots illustrate the number of pixels on the Y-axis and their values on the X-axis. Due to the large number of pixel values below 10, Y-axis is cropped to 50 occurrences to illustrate the remaining values better.

```
#1 (5.00 fps) exp 66657.00 ag 16.00 dg 1.00
#2 (5.00 fps) exp 66657.00 ag 16.00 dg 1.00
```

(a) FPS:5, exposure time:1/15s

```
#1 (15.00 fps) exp 66323.00 ag 16.00 dg 1.00
#2 (15.00 fps) exp 66323.00 ag 16.00 dg 1.00
```

(b) FPS:15, exposure time:1/15s

```
#1 (30.01 fps) exp 32987.00 ag 8.00 dg 1.00
#2 (30.01 fps) exp 32987.00 ag 8.00 dg 1.00
```

(c) FPS:30, exposure time:1/30s

Figure 4.5.: Default exposure time of frame rates 5, 15, and 30 when no light is available. The **exp** value represents the exposure time and is presented in μs, where the exposure time is capped at 1/15s for frame rates below 15 FPS.

It was later noticed that the exposure time of the camera is dynamic at default, where an algorithm tries to balance out the colors in the image. It was, however, assumed that the exposure time was equivalent to the frame rate. Thus, an experiment was performed to identify the most likely exposure times utilized in the night-time experiment. Placing a lid on the camera enabled total light isolation, and the results are presented in Figure 4.5. One can see that the frame rate of 1 and 15 FPS have the same exposure time, or shutter speed, while for 30 FPS, the exposure time is identical to the frame rate.

4.4. Discussion

The values of Figure 4.3b clearly show that the available ambient light is insufficient for a pixel to generate a base value. The results indicate that the NIR illumination in the box was likely due to the material penetrating properties of NIR, a property widely used in medical and plant health research [8, 26].

Figure 4.4b show that the light provided by the moon is not sufficient for illuminating the whole image. The right spike around 250 in pixel value is the center of the moon, while the slope to the right on the graph is caused by the glow surrounding the moon. As the total amount of pixels in this image is 1920x1080 pixels, the sum of pixels with higher values is minimal in comparison.

Note that it is the frame rate and not the exposure time, which is changed in this test. It was assumed that the frame rate and the exposure time were identical

unless manually changed. However, one would expect a larger difference in pixel values from the 5 FPS footage compared to the 10 FPS footage in Figure 4.4b. From Figure 4.5 one can see that the exposure time is capped at 1/15s, and consequently, the frame rates 5 and 10 FPS were probably using the same exposure times in the night-time experiment.

While uncertain, the results indicate that exposure times of 1/15 and higher are insufficient for detecting birds at night without additional light sources. For a configuration where the frame rate and exposure time are inversely proportional, these results show that a frame rate above 15 FPS is insufficient. For a bird traveling at 10m/s in a 25m/s wind, the bird will travel 10m in the duration of a frame, thus being depicted as a diffuse line in the image.

Thus, it is either necessary with a camera designed for low light conditions, such as a true NIR camera, or more light. The cost of NIR cameras is commonly cost several thousand NOK, while lamps can cost less than 1000NOK in addition to power costs. In addition, there is no easy way of testing the applicability of a NIR camera without a NIR camera, which is not available for testing in this project. Since the goal of this paper is to find a low-cost solution, a lamp system is considered to be the most interesting subject for further investigation.

The removal of the IR cutoff filter from the RPi camera is cumbersome and breaks its warranty, which is undesirable for a company with several cameras whose warranty is intact. However, it is possible to buy industrial cameras where the filter is optional, and investments in new cameras can be made with this in mind.

4.5. Conclusion

The available ambient light from the night sky is, in the winter, likely insufficient for the detection of birds with frame rates above 15 FPS. Consequently, it is also insufficient for recognizing species. Cameras designed to operate in the NIR spectrum might be suitable but are discarded for further work due to high costs and not being available for testing in this project. It is thus desirable to investigate a light source for increasing the bird's brightness in the footage. The removal of the IR cutoff filter is cumbersome and breaks the warranty of the RPi HQ camera, and is therefore not ideal for industrial usage. However, industrial cameras might be more compliant.

Chapter 5.

Required illumination

As it was concluded in chapter 4 that an external NIR source was required, it was decided to investigate the necessary amount of light. The goal of bird monitoring systems is to detect collision rates and monitor the behavior of the birds among offshore wind turbines. Thus, the system must not disturb the bird, as this can cause it to change behavior and invalidate the data, and, in the worst case, be the cause of collisions. As NIR light is invisible to mammals, they are commonly used for nighttime surveillance.

Verhoef et al. made use of a 14W 940nm lamp and a low-light camera [3]. However, the distance at which their observations were detected is not presented, and one cannot determine the irradiance at the distance the bird was detected. It is thus desirable to develop a method for obtaining the required irradiance on the bird for a camera to detect it and for a human or algorithm to recognize the species.

The required illumination can indicate the feasibility of using illumination, as it can be used to determine the order of magnitude required. For instance, if the required illumination only can be obtained with one hundred 20W lamps, another solution is preferable. Thus, delivering the required illumination is the *most critical function* of the lamp, which will be investigated in this chapter.

5.1. Iteration 1: Small scale rig

5.1.1. Motivation

Due to a lack of a spacious location, a powerful NIR source, and birds, a low-resolution small-scale rig was developed to investigate the required irradiance on a surface for the camera to obtain a readable signal. The development and findings of the setup will be presented in this section.

While Verhoef et al. used a 14W 940nm lamp[3], but 20W 850nm was found to be more accessible. Further, the camera sensor is likely to be more sensitive to EMR with higher frequencies, 850nm is preferable. Thus, the goal of this iteration is to investigate the suitability of a 20W lamp, assumed to have a symmetrical FOV of 40°.

5.1.2. Method

The experiment aimed to investigate how much light a 20W power source could provide. The choice fell on 20W, as it was found to be available and thus easy to obtain for both further experiments and potential users of the end product. To obtain a relationship between the model and a full-scale system, we can use the inverse square law. We know from Equation 2.7 that any physical quantity is inversely proportional to the distance from the source of the physical quantity. For irradiance, we obtain Equation 5.1. This can be used to determine the irradiance at any given distance away from the point source.

$$\begin{aligned} \frac{P_1}{d_1^2} &= \frac{P_2}{d_2^2} \\ P_1 &= P_2 \cdot \frac{d_1^2}{d_2^2} \end{aligned} \tag{5.1}$$

Further, we can require that the irradiance is the same at the position of the model bird in a small-scale experiment and at the position of a real bird in a full-scale scenario as presented in Figure 5.1. From this, we can insert Equation 2.3 and obtain an expression between the power output of the small-scale model and full-scale lamp:

$$\begin{aligned} E_{Bird,model} &= E_{Bird,real} \\ \frac{P_{model}}{d^2_{model}} &= \frac{P_{real}}{d^2_{model}} \\ P_{model} &= P_{source}\frac{d^2_{model}}{d^2_{source}} \end{aligned} \tag{5.2}$$

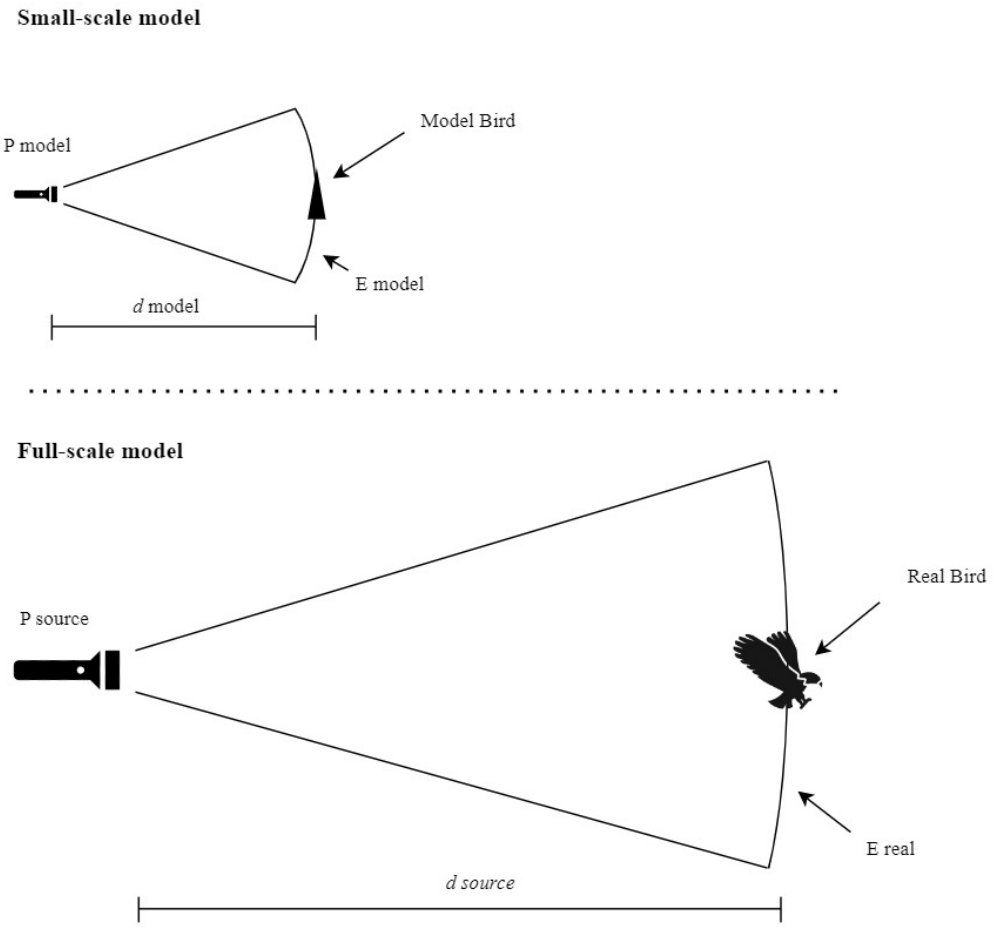

Figure 5.1.: Principal representation of real and model setup. Illustrative icons are provided by PowerPoint.

With this expression, any lamp can be used in a small-scale experiment to simulate the real system illumination, as long as a sufficient distance d_{model} is obtainable.

The required power could indicate if a single lamp was sufficient or if several were required, and whether they could be placed on the rig foundation or if they needed to be placed closer to the birds, mounted on the turbine. Due to a lack of available dark rooms, the box from subsection 4.2.1 was used further. To avoid NIR light leaking out and to block the external ambient light, the box was isolated with MDF plates on all sides as illustrated in Figure 5.2.

Figure 5.2.: Box isolated with MDF plates in the test location.

To function as a model for birds, a right triangle was cut out of a white and a black foamcore boards. Foamcore boards are sandwich structures with cardboard glued to each side of the foam. They can be cut out into various pieces shaped to desired geometries. This allows for rapid testing and adaptation of the model, which is ideal for rapid prototyping. The shape served two purposes: investigating the minimum width of the bird, and spatial resolution. Since there is no definitive size for the birds, a range of sizes was desirable. The triangle shape allowed for investigating the visibility of the larger width for large birds and the smaller width for small birds as presented in Figure 5.3. With the shape measurements known and the distance between the camera and the model, the widths could be calculated with trigonometry. For investigating the spatial resolution, the width of the smallest visible object could be determined by where the pixels could no longer generate a sharp image of the point of the triangle.

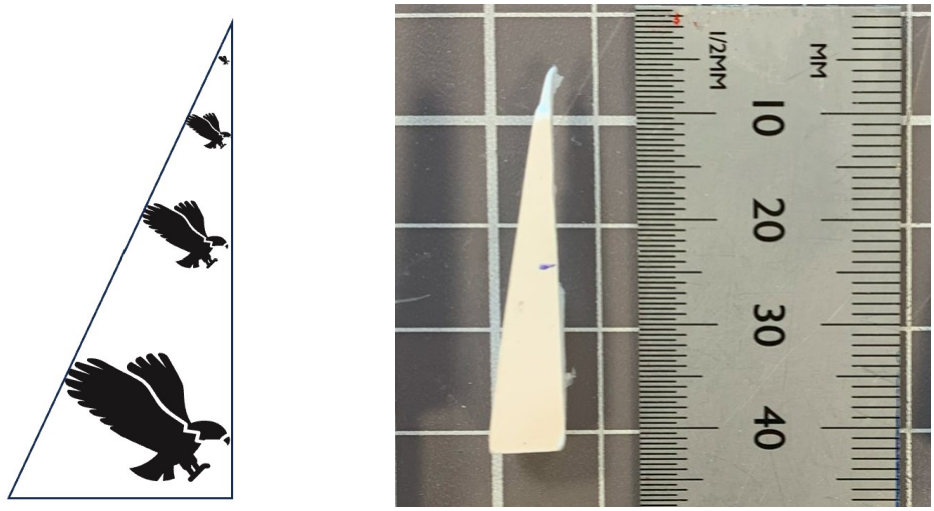

(a) Principle representation of the model **(b)** Actual model

Figure 5.3.: Illustration of how the model bird represents birds of various sizes. Illustrative icons are provided by PowerPoint.

To simulate the velocity of a real bird, the model bird was attached to a wooden lever, as illustrated in Figure 5.4 (a), driven by a DC motor to obtain translational movement. However, attempts to distinguish the model's outline with the histogram equalization and canny edge detection illustrated that the width of the lever diffused the outline of the triangle base. Thus, the wooden lever was replaced by a metallic lever covered with tape to reduce reflections, as illustrated in Figure 5.4 (b). The speed of the motor, and thus the velocity of the bird, was controlled by a variable DC power source. Due to the perceived speed of a bird's velocity being dependent on the distance between the camera and the bird, the main goal of the motion was not to have the same velocity as the real bird but to compare the presence of motion blur for various video frame rates. The model's velocity was measured by capturing a slow-motion video of its translational displacement and dividing it by the time.

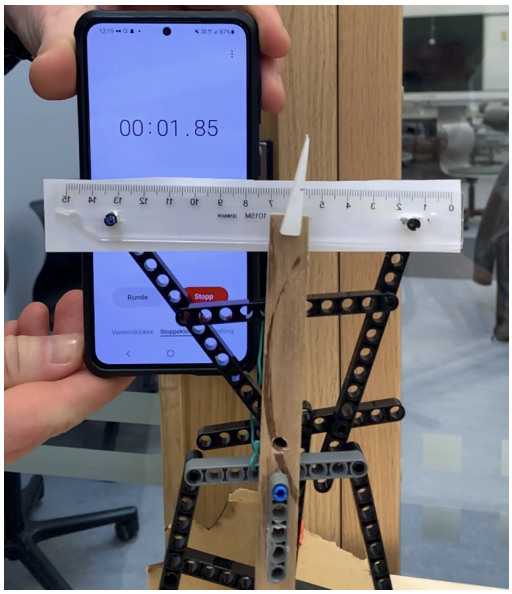

(a) Wooden lever with timer and ruler for velocity measurement

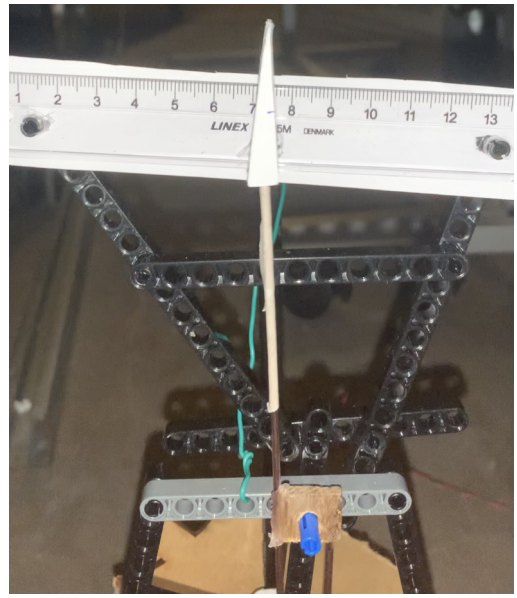

(b) Metal lever with ruler for velocity measurement

Figure 5.4.: First iteration model birds on levers.

The RPi HQ camera without NIR filter and the RPi 4b from 4 were used to capture images and video recordings. The camera was controlled directly from the RPi, presented on a screen on the outside of the box. All cables were pulled through a corner of the box, which was sealed to avoid any light leakage.

Two different 850nm LEDs were tested as light sources, differing in light intensity and FOV. The first had an angle of half intensity equal to ±40° along the center axis, corresponding to an 80° FOV, and will be referred to as LED_{40}. The other with ±12°, corresponds to a total of 24° FOV. The LED_{40} [1] has a minimum radiant intensity, $I_{40,min}$, of $350 \pm 75mW/sr$ when subjected to 0.35A, and a maximum radiant intensity, $I_{40,max}$ of $4100 \pm 1250mW/sr$ at 5A.

The LED_{12}[2] was thought to have a $I_{12,min}$ of $25mW/sr$ and $I_{12,max}$ of $50mW/sr$. However, an inspection of the documentation indicates that the manufacturer delivers the $LED_{12}s$ in batches, segmented based on their performance at 20mA. The groups are presented in Table 5.1, and the supplier could not confirm which of the four batches was delivered. Thus $I_{12,min}$ is set to $6.3mW/sr$ and $I_{12,max}$ in the range of $50mW/sr$ at $20mA$.

[1] https://docs.rs-online.com/7690/A700000008522136.pdf
[2] https://docs.rs-online.com/ddc9/0900766b808aed9c.pdf

LED group	Min	Max
Q	6.3	12.5
R	10	20
S	16	32
T	25	50

Table 5.1.: LED Radiant Intensity at $I_F = 20mA$ for LED_{12}.

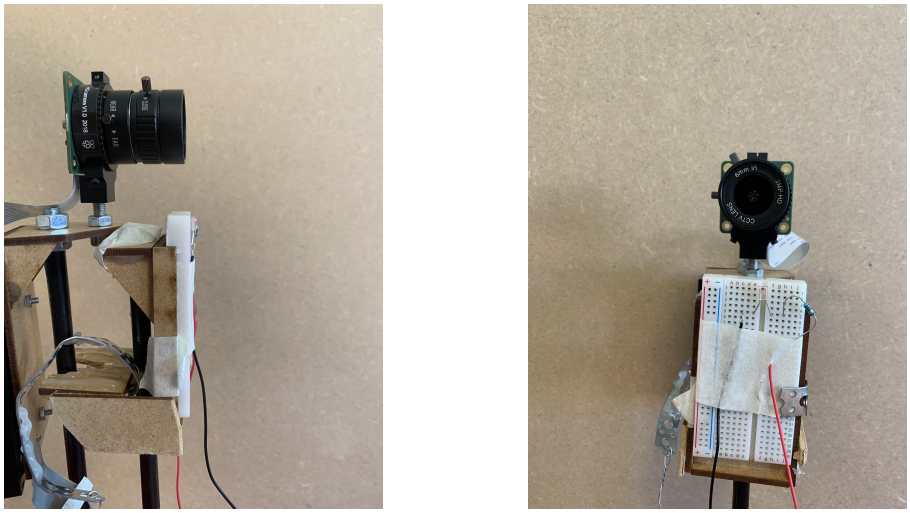

(a) Side view of LED mount relative to camera

(b) Front side view of LED mount relative to camera

Figure 5.5.: Mounting of LED_{12} relative to the camera.

The LED_{12} was mounted to a breadboard together with a resistance of 10 ohm, and powered by a variable power supply as illustrated in Figure 5.5. The LED was mounted below the camera and shielded such that no light could reflect back into the camera, avoiding saturation in the image.

The camera rig is presented in Figure 5.6. The rig's base was cut out of MDF plates, with a slit to allow the rods to be brought back and forth. The length of the rig was set to 65cm, so it could fit into the diagonal of the box, which allowed for a maximum of 50cm between the camera and the model bird. With a 1m ruler, the distance between the LED and the model bird could be adjusted, and the camera lens was aligned with the LED. An illustration of the rig setup inside the box is presented in Figure 5.7. Due to a concern about the reflectivity of the walls, the inside walls were lined with a dark cloth.

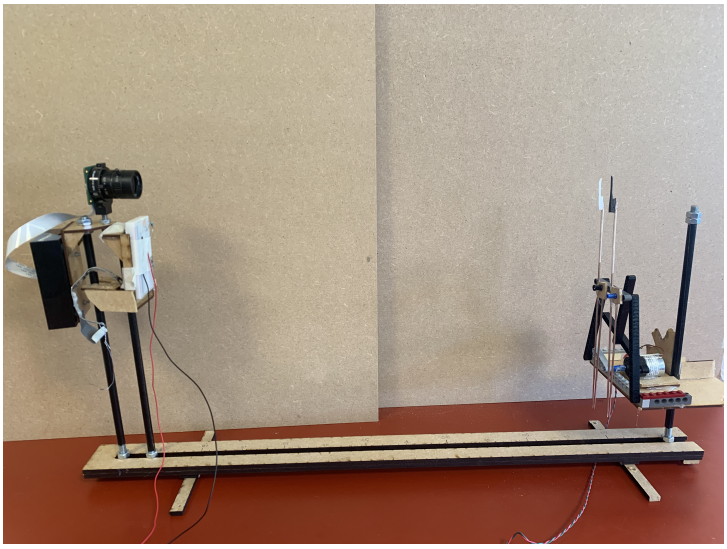

Figure 5.6.: Assembly of small-scale test rig

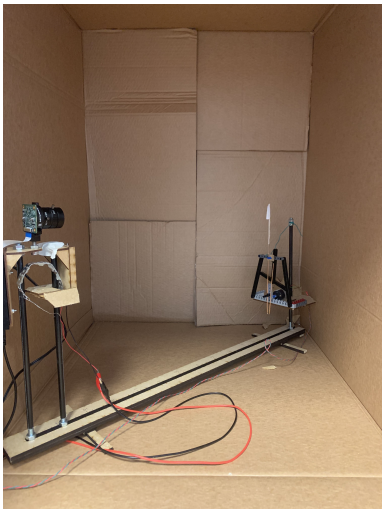

(a) Box interior before being lined with cloth.

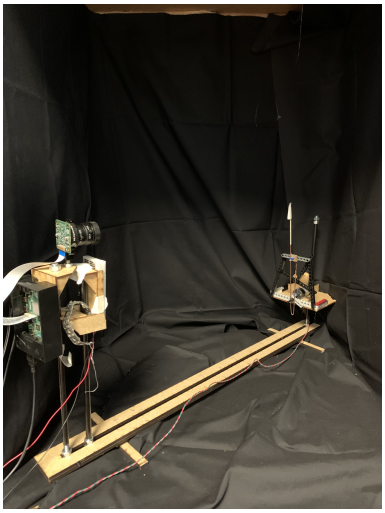

(b) Outside view of the box

Figure 5.7.: Box interior after being lined with cloth.

5.1.3. Result

Figure 5.8.: Benchmark image form inside the box, illustrating the successful isolation against external light sources.

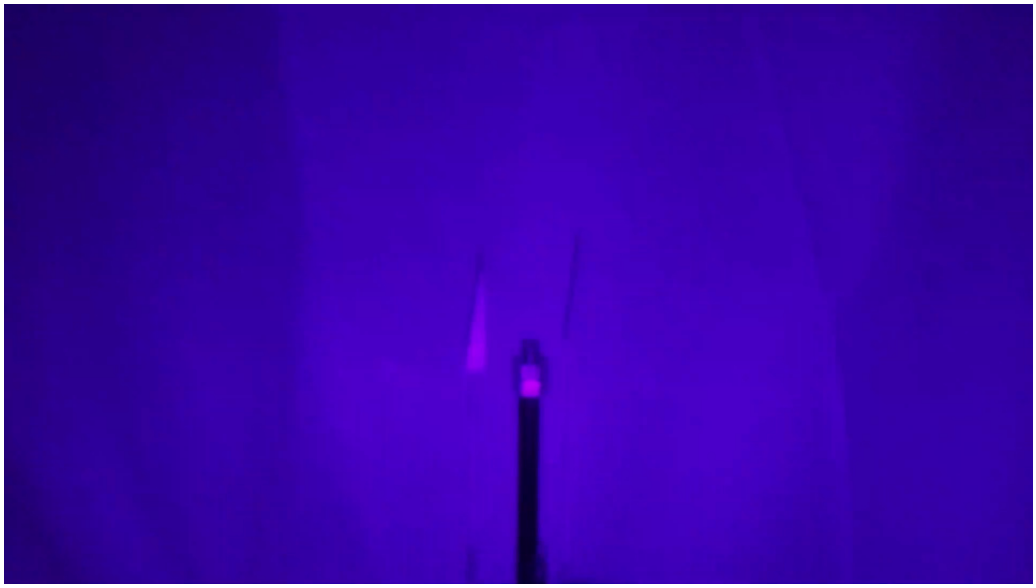

Figure 5.9.: Model birds illuminated by the LED_{12} with $8mA$, and the frame is obtained from video with FPS:60, shutter:1/60s, gain:16. The white model has a considerably better outline than the black model.

5.1.4. Discussion

Isolating the box was effective for removing the external NIR illumination for the experiment, as can be seen in Figure 5.8. This is crucial for determining the required illumination, as any additional light source not accounted for will potentially cause the obtained required illumination to be too low. However, the background is brightly illuminated, while it is expected that the distances in a real scenario will cause the background to remain the same. This can cause the image to appear brighter and the contours of the models to be weakened.

A current of $8mA$ was considered the minimum illumination, where the white model was clear against the background and the black model slightly visible, as can be seen in Figure 5.9. However, a good termination criterion is not developed, and it is challenging to determine whether the outline is sufficient. Further, it is uncertain to what degree the models are representative of the reflective properties of a real bird.

Both the background reflectivity and the uncertainty to what degree the model birds' reflectivity is representative give reason to believe that the model is too simplified. Thus, the $8mA$ current cannot be considered representative before the experimental setup is further validated. To reduce the background reflectivity, a more spacious environment is required such that no light is reflected, and the bird models should be compared to real birds. Further, a termination criterion should be developed to validate the results.

5.1.5. Conclusion

The box test indicates, based on human inspection only, that a current of $8mA$ to the LED_{12} is sufficient for detecting the models. Yet, due to the uncertainties of background- and model birds' reflectivity, a test with real birds in a real scenario needs to be performed. Further, a termination criterion is needed to evaluate the results.

5.2. Iteration 2: Testing with Stuffed Birds

5.2.1. Motivation

To validate the experimental setup from section 5.1, an experiment with real birds was desirable. Due to the ethical and practical implications of using a living bird in experiments, alternatives were investigated. The NTNU University Museum has a collection of stuffed birds, and two were borrowed. The birds provided a reference for comparison with the model birds, enabling assessment of how realistic the model bird is. Properties of interest are the shape, edges, and reflectivity.

Lightsource

As the bird's color is likely to impact the bird's visibility, it was decided to use a black and a white bird. For the black bird, a cormorant was chosen as it is a typical marine species found in most coastal environments[27]. There are many white marine birds to choose from, and a northern fulmar was selected as it was available. The feather coat of the stuffed birds likely has some properties deviating from living birds due to extended exposure to a dry environment. Still, the effects are expected to be negligible. A white and black foamboard was chosen for comparison.

To gain a good impression of the various characteristic reflections of a bird, it is desirable to expose the birds to a full-scale light source. However, a full-scale test can be harmful if the NIR lamp is not adequately verified as safe. Due to the lack of visual stimuli, the natural aversion responses of humans; reduced pupil diameter, blinking, and turning away from the light source, are not activated. In the IEC 60825 standard, the duration of exposure and light intensity are the determining factors for the exposure limit, Equation 2.10. However, the standard only concern the exposure to the eye of an observer looking directly into the source, while the exposure limit includes all incoming light. In an experimental setting, the total exposure to NIR radiation is uncertain due to reflections from walls and nearby objects in an indoor environment. As handling a high-power NIR light source requires extensive knowledge of the hazards and due to time constraints, it was in this report decided to develop an experimental setup that allows safe conditions without the risk of harming humans or animals. This allows for postponing the process and preparations required for handling a high-power NIR source until the solution proves promising. However, any design of the lamp will be constricted to the exposure limits of the IEC 62471 standard to ensure the safe implementation of the solution.

NIR radiation reflects similarly to visible light[28], and it should thus be possible to use visible light in a large-scale test. Cameras are more sensitive to specific

wavelengths of light, so the image brightness will appear differently for a scenery illuminated by visible light and a NIR source. The sensitivity to various wavelengths can be found in the datasheet of the camera, presented as the *spectral response* or *spectral sensitivity*[3]. The spectral sensitivity characteristics of a camera indicate how sensitive the camera is to various wavelengths of light[29].

This suggests that an image depicting a scenery illuminated by a visible light source can indicate the brightness obtained if only exposed to a NIR light source. On this premise, one can find the required illumination of a NIR light source by using the required illumination of a visible light source. By multiplying the required irradiance for visible light, E_{req}^{vis}, with the spectral sensitivity corresponding to the wavelength of the NIR light source, k_{850nm}, we should be able to obtain the required irradiance in the NIR spectrum from Equation 5.3.

$$E_{NIR}^{req} = E_{vis}^{req} * k_{850nm} \tag{5.3}$$

The spectral sensitivity of the IMX 477 sensor does not, however, consider light above 700nm[4]. Albeit, inspecting the spectral sensitivity of other CMOS camera sensors [8, 30], suggests that a spectral sensitivity to 850nm, k_{850nm}, between 15-25% of the peak sensitivity is reasonable.

However, it is desirable to illuminate the birds with a NIR light source, to obtain a reference for evaluating the hypothesis of NIR compensation mentioned previously. As a high power source is considered unsafe until adequately investigated, a smaller NIR light source can be utilized. Lowering the lamp's power reduces its radiance and irradiance, thus moving beneath the IEC limits. Reducing the power also reduces the risk of harmful levels of light reflecting from walls and objects. If a powerful lamp reflects on many surfaces indoors, the total irradiance on the eye will be higher and difficult to account for in the risk-assessment process. If the light is highly directed, meaning there is only a narrow light beam, it is easier to avoid exposure to the eye. In addition, it reduces the potentially harmful reflections from other objects as a smaller area is illuminated. Further, accordign to Equation 2.11, a small source size will yield a large radiance limit due to the α of the apparent source being smaller. Consequently, it is more likely that a small NIR source is within the exempt group of the IEC standards, as it has a lower potential for causing damage to the eye and thus allows for safe, accessible, and adaptable locations for experimentation. However, throughout this thesis, measures were implemented to avoid direct exposure of NIR light to the eye, to remove any uncertainties.

[3]The sensitivity of a camera to various wavelengths will be referred to with the Spectral sensitivity in this report.

[4]Datasheet IMX477: https://www.uctronics.com/download/Image_Sensor/IMX477-DS.pdf

(a) 20W visual light LED lamp.

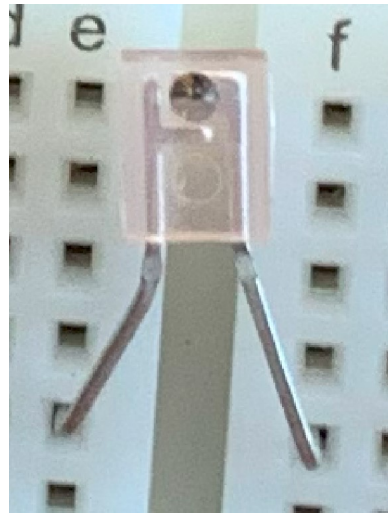

(b) 850nm NIR LED.

Figure 5.10.: The lamps used in the experiments.

5.2.2. Method

To investigate the reflectance of a bird and to find the necessary irradiance, the two stuffed birds, a cormorant and a northern fulmar, Figure 5.11, were placed in a dark room together with the RPi HQ camera and a modified 20W visual light LED lamp and the NIR LED from Figure 5.10. The cormorant was the main focus for testing due to its black feathers, which are here assumed to be more difficult to distinguish from a dark night sky than white feathers. The northern fulmar, with its white feather coat, was added to investigate this assumption. The birds were borrowed from the Trondheim Science Museum, and the tests were performed in their available storage room. Two different tests were performed:

1. Comparing the reflectivity of the birds to the foamcore plates with visual and NIR light.
2. Moving the cormorant away from the rig to find the distance to where the light conditions were too low to detect the birds.

The protective glass and the reflector had been removed in unrelated experiments, so the FOV was approximately 180°.

(a) Stuffed cormorant

(b) Stuffed northern fulmar

Figure 5.11.: Stuffed birds for testing reflectivity and visibility.

Image processing

The bash script `camera_test.sh`[5] ran the `libcamera-vid` command with different configurations and placed each in dedicated folders. A description of the variables used in the script can be found in Appendix B. The second frame for the video in question was obtained and converted to a `.JPG` file by using the `CV2.imwrite()`[6] function, for presentation in subsection 5.2.3. The camera was focused by manual inspection of a live stream from the camera, displayed on an available screen.

Setup

To obtain a benchmark for each test, videos were captured with the cormorant placed 1m away from the rig and the light switched off. Two light sources were present in the room; an exit lamp covered by a thick fabric and light reflecting from a window in the neighboring room. Both rooms had white concrete walls, cardboard boxes, and white metallic shelves.

Test 1

To compare reflectivity in test 1, the birds were subjected to:

- 850nm NIR LED with a voltage of $1.67V$ and $28mA$ from a DC power

[5] https://github.com/BirkHveding/Bird-monitoring-with-NIR-illumination/tree/main
[6] https://docs.opencv.org/3.4/d4/da8/group__imgcodecs.html#gabbc7ef1aa2edfaa87772f1202d67e0ce

source[7]

- White LED with a 20W AC power supply

The birds were placed 0.6m away from the camera and the NIR LED. The two plates were placed on each side of the bids to be compared with the chest feathers of each bird. To compare the NIR and visible light reflectivity, the NIR LED was supposed to be switched with a white LED. However, due to an alarm, the test had to be ended. Thus, the footage from test 2 had to be used instead. The NIR reflectivity test was performed with frame rates of 40, 50, and 60 FPS due to time-saving, as the high frame rates here were of interest.

The birds and plates were placed beside each other for every measurement distance to work as a reference. At a distance of 7m, the hallway's width was too narrow for both the bird and the plates, and the plates were left at 6m.

Test 2
To find the necessary irradiance in test 2, the cormorant was manually moved away from the rig with 1m for every iteration, from 1m to 11m. Each foamcore plate was placed beside the bird to compare reflectivity. A video was taken with 1, 2, 5, 10, 20, 30, 40, 50, and 60 FPS for every measured distance to compare the visibility of the bird. The lamp was placed beside the camera as depicted in Figure 5.12.

Attempts were made to use two object-detecting search engines to determine when the light conditions were too poor: Google Images[8] and Artsorakelet[9]. Google Image is an algorithm comparing uploaded images to their platform, inspecting colors, textures, lines, and points[10]. Artsorakelet is a machine-learning algorithm developed by the Norwegian Biodiversity Information Center and Naturalis Biodiversity Center, and it is trained on publicly available images of wild animals in Norway[31].

The results from each picture were divided into three categories based on their accuracy: Cormorant, Bird, and None. If one of the image searches from the image suggested a cormorant, the image was binned into 'Cormorant'. If the image search indicated any bird, the image was binned as 'Bird'. 'None' indicate there were not enough features for relevant suggestions.

The images were uploaded to the search engines to test whether the light conditions were sufficient for detecting the bird. As the white balance in the image was distorted due to the IR filter removal, the images were uploaded in color and

[7]NIR LED used for testing: https://docs.rs-online.com/ddc9/0900766b808aed9c.pdf
[8]https://images.google.com/
[9]https://orakel.artsdatabanken.no/
[10]https://www.youtube.com/watch?v=keTZaJg0784

(a) Lights tuned ON

(b) Lights tuned of

Figure 5.12.: Setup for camera and 20W visual light source in the storage room where the experiments were performed. The cormorant was placed on the floor and the trolley moved out of the way.

grayscale, converted with the Open CV functions `cvtCOLOR` and `COLOR_BRG2GRAY`. In addition, manually cropped images were uploaded to investigate if the image's complex back- and foreground distracted the search engines from detecting the bird, such that it included the bird only and a minimum of its surroundings. When uploaded to google images, the images were auto scaled. For Artsorakelet, the images were scaled manually to the point where their width was similar to a base frame in the application.

Further, due to the general training of the two search engines, they cannot be compared with specialized algorithms or AI. Thus, a visual inspection of the images was considered to determine whether the images were good enough for the human eye. As it is hard to decide on an objective measurement for when the image is sufficiently illuminated, all photos are added to `Results/Irradainces` in [32] for evaluation by an AI or machine learning engineer.

5.2.3. Result

NIR reflectivity

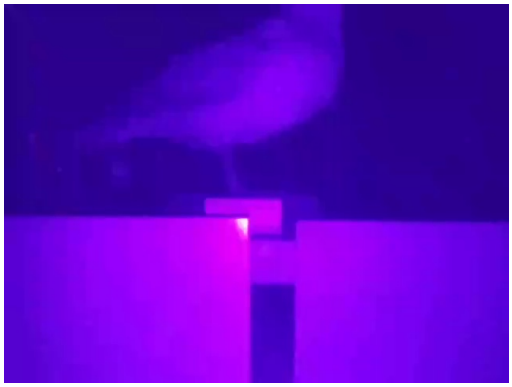

(a) Northern Fulmar, FPS:60, shutter:1/60s, gain:16, distance 0.6m

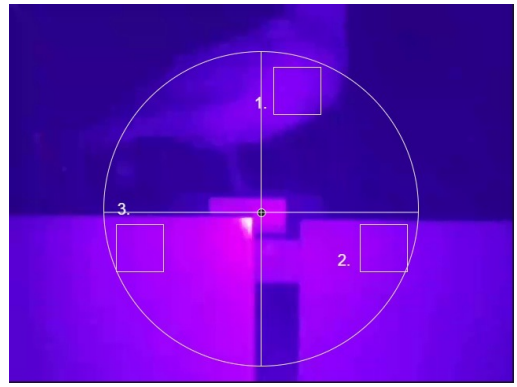

(b) Sections for comparison

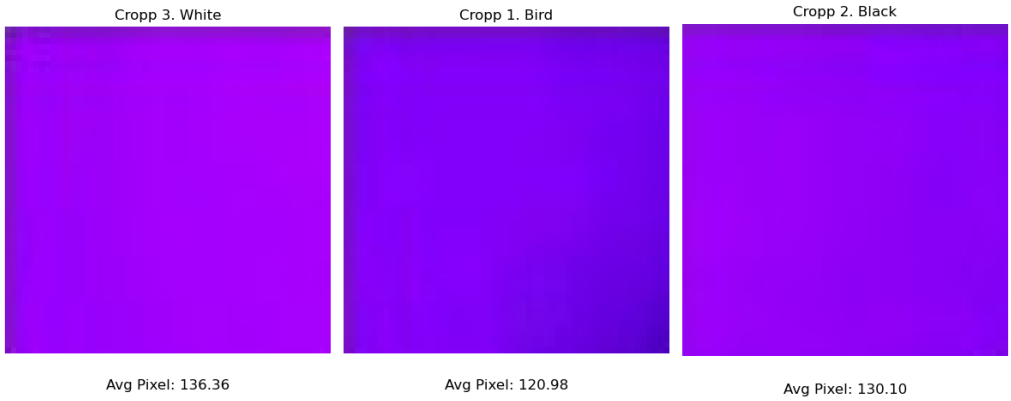

(c) Sections

Figure 5.13.: Northern Fulmar NIR reflection comparison. **(a)** Image captured by the camera with the white plate to the left, the black plate to the right, and the fulmar in the middle. **(b)** Illustration of the location of the sections cut out from the image and their position relative to the center of the resource. The circle is centered at the approximate center of the light source, placed manually in Draw.io[11] **(c)** Comparison of the sections obtained from (b) with the average pixel value from the section.

(a) Cormorant, FPS:60, shutter:1/60s, gain:16, distance 0.6m

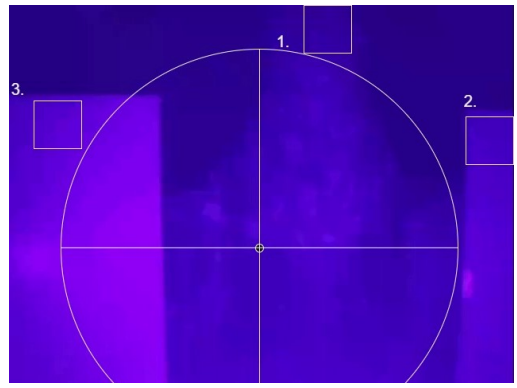

(b) Sections for comparison

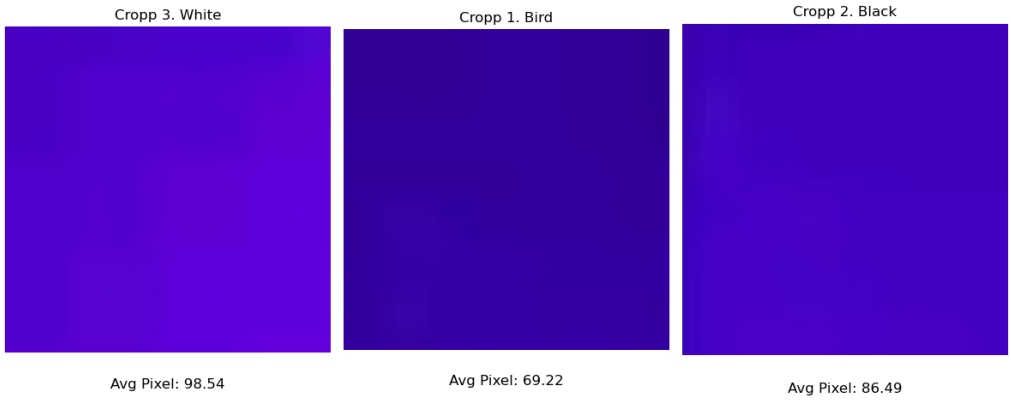

(c) Sections

Figure 5.14.: Cormorant NIR reflection comparison. **(a)** Image captured by the camera with the white plate to the left, the black plate to the right, and the cormorant in the middle. **(b)** Illustration of the location of the sections cut out from the image and their position relative to the center of the light source. The circle is centered at the approximate center of the light source, placed manually in Draw.io[12] **(c)** Comparison of the sections obtained from (b) with the average pixel value from the section.

Flickering in footage

(a) Frame 2 **(b)** Frame 10

Figure 5.15.: LED flickering in 60 FPS video. Comparison of frames 2 and 10 from video with shutter:3s, gain:16, dist:5m. From close inspection of the two frames, one can see that frame 2 has a slight blur compared to frame 10.

(a) Shutter: Default, gain: 16

(b) Shutter: Default, gain: Default

(c) Shutter: 1/40s, gain: 16

Figure 5.16.: Aliasing in 40 FPS video. Comparison of the second frame for different configurations of shutter and gain. One can see that image (a) has clear dark lines with bright regions in between. In (b), slight indications of the bright regions observed in (a) can be seen on the left side wall. In (c), there is no clear indication to light flickering.

(a) Shutter: Default, gain: 16

(b) Shutter: Default, gain: Default

(c) Shutter: 3s, gain: 16

Figure 5.17.: Aliasing in 1 FPS video. Comparison of the second frame for different configurations of shutter and gain.

Later, after the experiment, it was found that the default shutter speed of the IMX477 is dependent on the brightness of the image. Note that the shutter speed is the inverse of the exposure time. The camera was thus placed under a lamp to investigate the behavior and run with different configurations. In Figure 5.18 the results are presented. One can see that the shutter speed is the fastest for the 5.18 (a) while the slowest for (c). Note that these are the same configurations as the images presented in Figure 5.16 and 5.17. **ag** and **dg** represent the analog and digital gains respectively, but the maximum total gain of the camera is 16.

```
#21 (40.21 fps) exp 91.00 ag 16.00 dg 1.00
#22 (40.01 fps) exp 91.00 ag 16.00 dg 1.00
```

(a) Configuration: FPS:40, Shutter: default, gain: 16

```
#115 (40.02 fps) exp 166.00 ag 1.00 dg 1.02
#116 (40.01 fps) exp 182.00 ag 1.00 dg 1.02
```

(b) Configuration: FPS:40, Shutter: default, gain: Default

```
#1 (40.01 fps) exp 24661.00 ag 16.00 dg 1.00
#2 (40.01 fps) exp 24661.00 ag 16.00 dg 1.00
```

(c) Configuration: FPS:40, Shutter: 1/40s, gain: 16

Figure 5.18.: Exposure time of 40 FPS video with the same light conditions and varying configurations. The **exp** value represents the exposure time and is presented in μs. The configurations are in (a): shutter: Default, gain: 16, in (b): shutter: Default, gain: Default, and in (c) shutter: 1/40s, gain:16. Note how configuration (a) gives the shortest exposure time, (b) slightly longer, while (c) significantly longer.

Importance of background

(a) Northern Fulmar

(b) Cormorant

Figure 5.19.: Comparison of the visibility of the Northern Fulmar and the Cormorant. FPS:60, shutter: Default, gain: Default, dist: 11m

Recognition

Distance [m]	**Colored Full size**	**Colored Cropped**	**Gray Full size**	**Gray Cropped**
1	Bird	N/A	Bird	N/A
2	Cormorant	Cormorant	Cormorant	Cormorant
3	Bird	None	Bird	Cormorant
4	None	None	None	None
5	None	None	None	None
6	None	None	None	None
7	None	None	None	None
8	None	None	None	None
9	None	None	None	None
10	None	None	None	None
10 diffused	None	None	None	None
11	None	None	None	None

Table 5.2.: Minimum irradiance for detection and identification - Google Images. The bird fully covered the images at a 1m distance and did not need cropping. Thus the cropped images at 1m are marked N/A.

Distance	Colored Full Size	Colored Cropped	Gray Full Size	Gray Cropped
1	None	N/A	None	
N/A height2	Cormorant	None	Bird	None
3	None	None	None	None
4	None	None	None	None
5	Bird	None	None	None
6	None	Bird	None	None
7	Bird	Bird	None	None
8	Bird	Bird	None	None
9	Bird	None	None	None
10	Bird	Bird	None	None
10 diffused	Bird	Bird	None	None
11	Bird	Bird	None	Bird

Table 5.3.: Minimum irradiance for detection and identification - Artsorakelet. The bird fully covered the images at a 1m distance and did not need cropping. Thus the cropped images at 1m are marked N/A.

Experimentation with the size of the images showed that Artsorakelet was highly sensitive to picture adjustments and scaling. When shrinking the cropped images to about 40-60% of the frame size in Artsorakelet, the AI suggested more birds than for the images with an approximate frame width. However, when repeating the same process, the suggestions varied widely, from both in different species and in confidence.

The image's color highly influenced both search engines. For the colored images with a pink tone, Google Images suggested various pink images. For the grayscale images with visible tiles, suggestions of CCTV footage were more common. For Artsorakelet, grayscale images frequently resulted in whale species and other aquatic animals. For most images, Artsorakelet suggested that the picture contained an otter with 90-100% certainty.

Importance of geometry

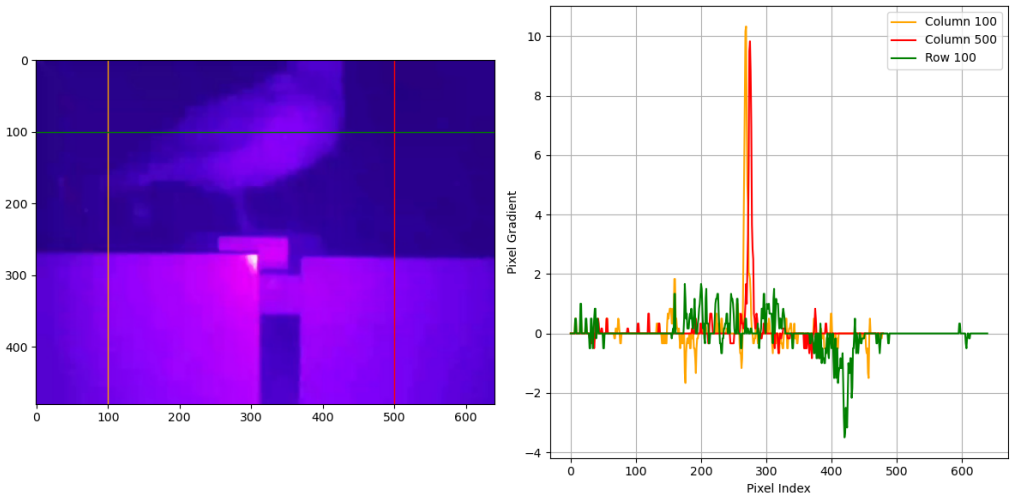

Figure 5.20.: Left: The row and columns in the fulmar image which is evaluated in the plot. **Right:** The gradient corresponding to the pixel values of the row and columns marked by the lines in the left side image. Negative gradient values indicate that the pixel values drop when moving from left to right, and vice versa for positive gradient values. High absolute values indicate a rapid change in pixel intensity.

Pixels per meter

The commands run by the bash script gave videos with the default resolution of 640x480. This gave a projected sensor width of $13.3m$ at the end of the hallway, $11.5m$ from the camera, resulting in a PPM of 48.2. From subsection 2.1.4, we know that a 1920x1080 resolution yields a PPM of 8.3, approximately a fifth of the PPM in this test.

5.2.4. Discussion

This section discusses the findings of the Required Irradiance test, evaluating the applicability of the findings, sources of error, and lessons learned from the test.

Reflectivity

From visual inspection of Figure 5.2.3 and 5.2.3, the reflectivity of the black plate seems the closest proximity to the birds. For both the fulmar and the cormorant, the average pixel values of the black plate yield the closest results. The deviation in pixel values between the black plate and the fulmar is 7.53% and 24.97% for the cormorant, while 12.71% and 42%, respectively, for the white plate. Due to the difference in curvature and variation in distances to the source, the experiment cannot accurately measure the relative differences in reflectivity. However, the experiment provides valuable information about the proximity of the plates to the birds, the importance of curvature for the appearance of a silhouette, and the relative reduction in color information in the image.

As the goal of the small-scale tests is to indicate whether a NIR lamp solution is possible, the black plate will be considered sufficient for indicating the visibility of a bird in further testing. This allows for discarding a NIR lamp solution in an early stage if further testing proves that illumination is not possible with better-than-ideal circumstances. If experiments with the plates as models indicate that NIR illumination is possible, better experiments can be performed to investigate if the solution is still applicable.

The test revealed the importance of curvature for reflections, where a surface curving away from the source is less distinct than a hard edge. In Figure 5.20, the gradient of the pixel values over single lines is presented. The two-pixel columns change rapidly when passing the edge of the boards, while the row passing the fulmar has a smaller change. As edges are important for distinguishing and detecting the silhouette of an object, the curvature should be accounted for.

Medina et al. obtained a measurement of the NIR reflectivity of a selection of birds found in Australia, including the great cormorant with a reflectivity of about 15% on its chest[33]. While the northern fulmar is not evaluated in their research, similarly white marine birds like the pacific gull are. This can be used to generate models with reflectivity closer to the real birds or generate methods that correct any deviations in reflectivity. Due to a lack of equipment or a method with the available equipment for measuring the NIR reflectivity of various materials, this is not performed in this report.

Comparing the colors of the plates in the scenery illuminated by the visible source to the NIR source, one can see a reduction in contrast between the plates in the

NIR-illuminated images. This is likely due to the homogeneous wavelengths of the NIR source and the lack of wavelengths corresponding to red, green, and blue light. The purple color is likely a ratio of how much NIR radiation that is allowed through the various color filters in the Beyer filter. As the ratio remains the same, all colors illuminated by the NIR source appear in various gradients of purple. This will cause any color features on the bird to be lost. As the grayscale image uses the same pixel values as a colored image, a grayscale image of a NIR illuminated scenery will differ from one illuminated by a visible light source. This will likely confuse a species-recognizing algorithm that is trained on colored image data, something which will be discussed further later in this section.

The results indicate that several aspects of the box test were inadequate. The reflections from the walls of the box are likely too high for the assumption of a single light source. Additionally, the edge of the model bird is likely too sharp compared to a bird and the reflectivity of the plates is likely higher than for the real birds. Lastly, the background color has a large impact on the appearance of the bird. Comparing the NIR illuminated images in Figure 5.2.3 and 5.2.3, the background is darker than what it was in the box results. Thus, a more spacious environment than the box is desirable for further testing.

Finding the required irradiance

Due to the narrow hallway and the small size of the storage room causing reflection, the assumption of the 20W lamp being the only light source does not hold. The hallway's width was approximately 2 meters, with one side consisting of reflecting surfaces, sustaining the light more than what can be considered representative of an outdoor setting. This can be considered as additional light sources, and the assumption posed when utilizing Equation 2.7 is not satisfied. In addition, an inspection of the slow shutter speeds of $1 - 2s$ shows that the external light sources were not sufficiently covered. Thus, this test cannot obtain the required irradiance for a visible light source.

Inspecting the image sequence in section A.1 in Appendix A, one can observe significantly greater detail of the cormorant in images (b)-(e) than in the remaining sequence. In images (f)-(i), outline and detail disappears, making distinguishing the bird from its surroundings hard. However, the outline is again distinguishable from the background for images (j)-(l). The reduced detail is likely due to the spatial resolution of the camera, where the projected area of each pixel becomes higher the further away the bird is. With a low spatial resolution, the bird's outline is also harder to distinguish from the background due to its averaging effect. Thus, the camera's spatial resolution limits the detail in the image, both for the characteristics of the bird and, to some degree, its outline.

The reappearing silhouette of the cormorant in images (j)-(l) reveals the importance of background color. In images (f)-(i), the shadow has a perceived color similar to the cormorant, thus blurring its silhouette. In images (b)-(e), the bird's shadow is weak, probably due to reflections from walls and objects, making the edge between the bird more prominent. A similar issue can be seen in Figure 5.2.3 where the fulmar's white feathers are less distinct than the cormorant on the white and beige background.

The search results from the search engines indicate that color has a large impact on the recognition of species. Comparing the search results from Artsorakelet, it recognized the colored images as birds, even though the colors were off. The grayscale images gave no results, likely due to the training data in Artsbanken, where the images are usually colored to ease human interpretation. The scenery where the bird is commonly found will likely cause a database bias in the search results if not carefully managed. This is further supported by the search results from Google Images, where the pink tones in the visible light and the grayscale images resulted in pink image suggestions and CCTV hallway images, respectively. The general application of both search engines makes the surroundings and colors more decisive than desirable. Comparing the colored image search results from the more generally trained Google Images to the more specified training of Artsorakelet, the bird is more often detected. This supports the hypothesis that an algorithm trained solely on bird detection and recognition will find the bird and that a general AI cannot be compared to a specialized AI. Further, as the visual light images were used, the search results may not indicate how well the search engines will recognize a NIR image. However, the findings indicate that a bird's silhouette will be recognizable as a bird and possibly a species with a sufficient spatial resolution.

LED flickering

Due to the previous tests having used a DC power source, an unexpected observation during the experiment was LED flickering. In Figure 5.17 and 5.17, image (a), one can see that the images with the default shutter and gain set to 16 have horizontal dark lines. In the related videos[13], the lines appear to move downwards. A similar shadow pattern can be seen in the videos with the shutter and gain set to default values while being less distinct. Inspecting frames 2 and 10 in Figure 5.15, one can see that frame 10 is slightly sharper than frame 2. In the corresponding video[14], a dark patch moves over the image.

[13] 1 FPS video file: fps1_shutter0s_gain16_time094805_dist2mSharp_lightON_velNO.h264, 40 FPS videofile: fps40_shutter0s_gain16_time094608_dist2mSharp_lightON_velNO.h264
[14] Videofile: fps60_shutter3s_gain16_time102216_dist10m_lightON_velNO.h264

Since the shutter speed is automatically set in the default configuration, the shutter is not known for the frames (a) and (b) in Figure 5.16 and 5.17. However, comparing them to the trend observed in Figure 5.18, it is reasonable to believe that the exposure time is somewhere around the frequency of the LED in the lamp. For the configurations of frames (a), about 3 lines are present, which is likely due to the lamp being shut on and off 3 times in the duration of a single frame. This is a common issue in the field of photography, known as *banding*[34].

For frames (b) in Figure 5.16 and 5.17, the exposure time is likely slightly longer, as indicated by the trend in Figure 5.18, causing the dark lines to be smoothed out. Yet, some indication of the flickering can be seen in the image, indicating that it is not too much longer than the lamp's flickering frequency. In the (c) frames, the exposure time is significantly longer, and the lines are not present at all. In both the (b) and (c) frames, the flickering appears, but the pixels receive values light longer and are thus not visible.

This is an important finding for the design of a lamp system, where the flickering frequency needs to be sufficiently high relative to the frame rate. Alternatively, a method for avoiding a pulsating LED is needed.

Resolution

Another unexpected discovery in this experiment was the high difference in PPM for the close-range experimental setup and the full-scale setup at $200m$. With a PPM of 48.2 in the experiment at $11.5m$ from the camera, it is approximately five times higher than if a bird were $200m$ away and the resolution was 1920x1080. Thus, the real scenario image will have significantly less detail than the ones obtained in this experiment. However, this means that it is likely only the bird's outline, in addition to other parameters such as flight pattern, that is decisive for species recognition at these distances.

5.2.5. Conclusion

This experiment indicates that a white visual light source cannot be used for determining the required NIR irradiance based on the camera's spectral sensitivity alone. Further investigation of the relationship between pixel intensities from an image with NIR illumination and visual light illumination might resolve this issue but is not considered further in this report. The results do, however, indicate that the background illumination and color will be important for the detection of any bird. A background similar to the bird's appearance will make it hard to distinguish from the background. Further, future experiments should be performed in a spacious environment to reduce reflections from nearby objects and walls.

The reflectivity of the plates is likely higher than the birds, based on this experiment. However, as it would be time-consuming to find more suitable materials, they will be considered representative with the intent of determining the relevance of NIR illumination. If a solution proves suitable, further testing can be performed to investigate the precise minimum of illumination. In addition, the geometry of the birds and plates is likely to have a large impact on how strongly their silhouette appears in the background.

The spatial resolution in the test is too high compared to the real-world scenario, but the lack of detail in these results indicates that the spatial resolution of the same camera would yield a less detailed image. Thus it is likely the silhouette that is most important for species recognition, and not smaller details in the feather coat. Thus will the difference in shading from visible light and NIR light source not be crucial for species recognition at large distances.

The results from using general-purpose AI for object detection support the theory that silhouette is a key factor for machine learning to recognize an object as a bird. Further, it indicates that a general-purpose AI is not likely to be suited for detecting a bird or determining the species without proper color information. However, if a general-purpose AI is able to detect the bird in future experiments, it is likely that a specialized AI would do so as well.

At last, the frequency of the light source should be higher than the shutter speed of the camera. Alternatively, the intensity of the light source should be adjusted with a method that avoids flickering in the light.

5.3. Iteration 3: Small scale in spacious room

Based on the conclusion from section 5.1, the box was discarded. A large storage room without light sources became available, where the last iteration of the camera rig was developed. This section will discuss the method used to investigate the performance of a 20W NIR lamp at a $200m$ distance. In addition, the procedure to finding the required irradiance of the bird.

5.3.1. Motivation and Method

As the results from the section 5.1 indicated that the black plate compared better to the birds' reflectivity, an additional model bird in black was cut out. To remove the sharp edges of cut-out bird models, the cardboard of the same plates was cut out and rolled into cones of a similar size to the original models.

The camera rig from iteration 2. was moved to a storage room as seen in Figure 5.22 (a). The were several objects with reflective surfaces in the room, but at distances equal to or larger than the distance between the model bird and the camera.

A *secure shell* (SSH) connection to an external computer was used to modify the bash script `camera_model.sh`[15]. To detect any discrepancies in the videos at an early stage, the video was streamed onto a monitor. Two variable power supplies were used for controlling the power to the LED and the DC motor moving the bird.

To minimize the light pollution from the screens, their screen intensity was reduced to the minimum, and a wall of plates was placed between the screens and the test rig as illustrated in Figure 5.22 (b). The only light sources causing light pollution in the room were the screens and a small LED on the RPi. To function as a reference, footage was taken with the ceiling-light and the NIR LED turned off.

Sufficiency of a 20W lamp:
To investigate if a $20W$ NIR lamp was sufficient for detecting a bird at $200m$, the LED_{12} served as a light source, and both bird models were placed at a distance of $0.5m$ away as illustrated in Figure 5.21 (a). The procedure was performed twice, once with the sharp-edge bird models and once with the rounded-edge models presented in Figure 5.21 (b). The bird models did not move, as the goal of the test was to determine if the irradiance was sufficient and not the motion blur for the different frame rates.

[15]Script can be found in https://github.com/BirkHveding/Bird-monitoring-with-NIR-illumination/new/main

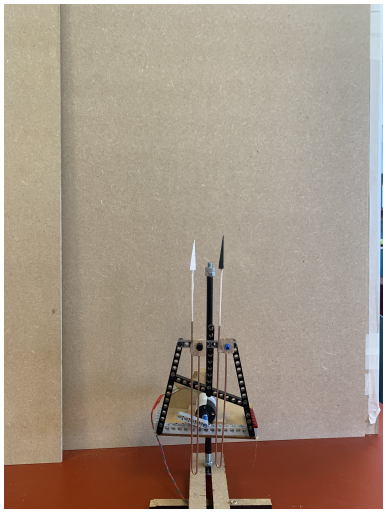

(a) Two model birds attached to the camera rig.

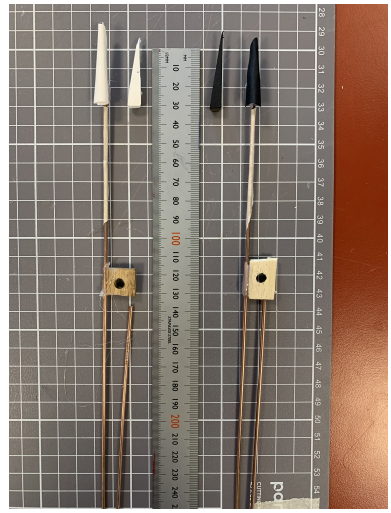

(b) Model birds attached to lever

Figure 5.21.: Bird models and the setup

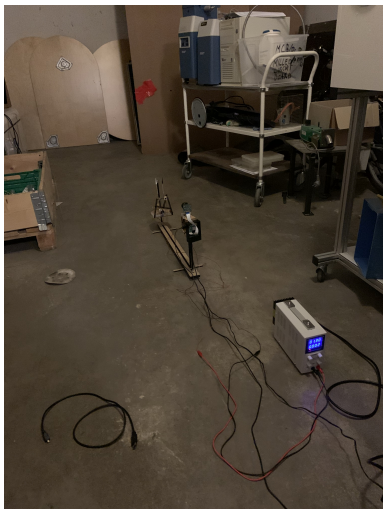

(a) Rig placed in the storage room with surrounding objects.

(b) Blocking the light from the screens and power sources.

Figure 5.22.: Setup for testing the suitability of a 20W lamp with LED_{12} - Storage room.

The focus area of the LED was adjusted to cover both bird models at the same time. This was done by observing the hot-spot of the light through the camera before the light was turned off and adjusted. This procedure continued until the distance from the bird models to the periphery of the hot spot was identical.

The radiant intensity, I, includes both the power and FOV of the lamp, and was thus chosen for obtaining the required specifications of a full-size lamp. From 2.5, and knowing that the source power is 20W and assuming the horizontal and vertical FOV of the lamp is 40°, the radiant intensity of the lamp,I^{lamp}, can be calculated to $41W/sr$. By using the inverse square law, the radiant intensity of the LED, I^{LED}, with Equation 5.4, giving a I^{LED} of $0.26mW/sr$. Since $I^{LED} << I^{40°}_{min}$, $LED_{40°}$ could not be used. However, LED_{12} was within the limit, which will be proven in the following section, and was thus further used.

$$\begin{aligned} I^{LED} &= I^{lamp} \cdot \frac{0.5^2\mathrm{m}^2}{200^2\mathrm{m}^2} \\ &= \frac{20\mathrm{W}}{(40° \cdot \frac{\pi}{180})^2} \cdot \frac{0.5^2\mathrm{m}^2}{200^2\mathrm{m}^2} \\ &= 0.26 \cdot 10^-3 \quad \mathrm{W\,sr^{-1}} \end{aligned} \tag{5.4}$$

Unknown current, I_{I_F} known:
In the LED_{12} documentation, Figure 5.23 illustrates the change in radiant distribution, presented as I_e, for different input currents, I_F.

Note: The input current to the LED_{12} will only be denoted with I_F or the actual current value. This was chosen for the continuity between the LED_{12} data sheet and the report. For any radiant intensity for a given current, the current is presented as the subscript, i.e for a current I_F of $20mA$, its radiant intensity is denoted as I_{20mA}. For an arbitrary current I_F, the corresponding radiant intensity is denoted as I_{IF}.

To find the radiant intensity for the LED_{12}, we need to develop an expression for the Y-axis of Figure 5.23, which is presented as I_{I_F}/I_{100mA}. Since $I_{min/max}$ for LED_{12} is known to be in the range $[6.5, 50]$ at $20mA$, we can find an expression for I_{100mA}. By substituting I_{100mA} with the expression found in Equation 5.5, we get an expression for $I_{min/max}/I_{100mA}$. For a desired radiant intensity, I_{I_F}, the required input current to the LED, I_F, was found by using the $I_{min/max}/I_{100mA}$ calculated with Equation 5.6, drawing a line down to the X-axis of Figure 5.23.

$$\frac{I_{20mA}}{I_{100mA}} = 0.17$$
$$I_{100mA} = \frac{I_{20mA}}{0.17} \tag{5.5}$$

$$\frac{I_{I_F}}{I_{100mA}} = \frac{I_{I_F} \cdot 0.17}{I_{20mA}} \tag{5.6}$$

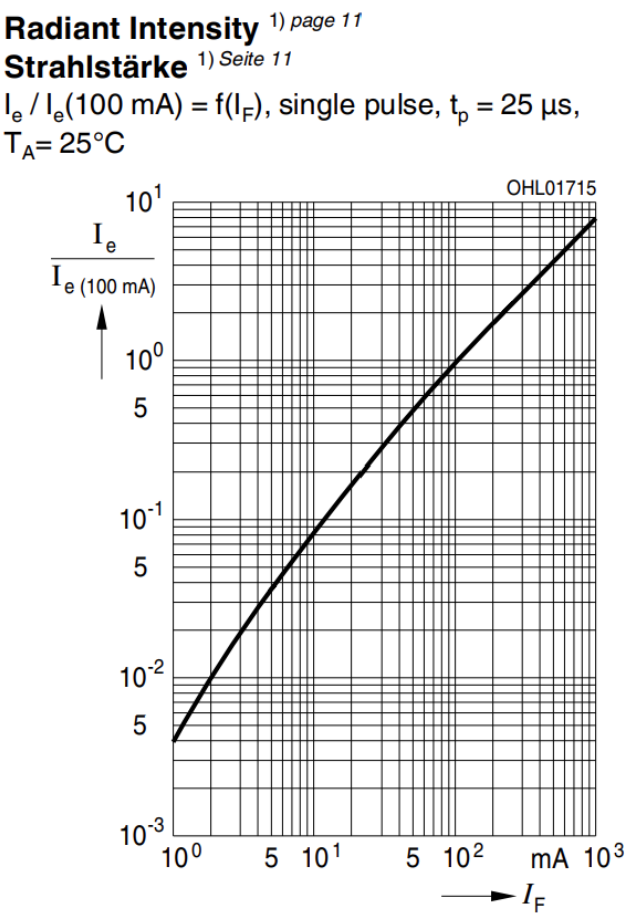

Figure 5.23.: Radiant intensity behavior for LED_{12} for varying input current I_F

Finding minimum requirements to the light source:
To find the minimum required radiant intensity of the lamp, I_{req}^{lamp}, the light source

was adjusted until the outline of the bird model was distinguishable from the background. An attempt was made to use Open CV `findContours()`[16], directly on the RPi, which caused lagging in the video stream. It was thus decided to use human inspection of the live stream as a termination criterion instead. A video stream was generated using the function `libcamera-vid`, and the desired frame rate was presented on a screen. To capture video, only the lines related to 120, 60, and 40 FPS from `Camera_model.sh` were run. While monitoring the video stream, the current was increased until the outline of the black bird model was clearly distinguishable from its background. Additional footage was taken with lower and higher I_F for comparison when a limit was found.

On the evaluated footage, Ostu's tresholding[17] was applied before applying Canny edge detection. Further, a gradient evaluation was performed on 3 to 4 rows over the image to investigate the effect of increased radiant intensity. The rows were placed manually, separated by 50 pixels, to investigate the trend in contrast from the top of the bird models to the bottom. The images were cropped with `Microsoft Picture Manager` for better presentation while maintaining the pixel density in the image to avoid altering the gradient in the image.

To find the full-scale radiant intensity corresponding to a given current I_F, Equation 5.6 was solved for I_{I_F}, resulting in Equation 5.7. Here, r_{I_F} is the value corresponding value to I_F, obtained from Figure 5.23.

$$I_{I_F} = r_{I_F} \cdot \frac{I_{20mA}}{0.17} \tag{5.7}$$

With I_{I_F}, the full-scale radiant intensity was obtained by using the inverse-square law, 2.7 and the conservation of radiance, then solve for I_{req} to obtain Equation 5.8

$$I_{req} = I_{I_F} \cdot \frac{200^2\mathrm{m}^2}{0.5^2\mathrm{m}^2} \tag{5.8}$$

Evaluating bird model in motion

The model bird was set to a swiping, translational motion in a plane parallel to the camera lens to evaluate the adequacy of various camera setting configurations. Due to inaccurate angles in the lever and the mechanism's nature, the model bird's velocity varied through each swiping sequence. Thus, the frames of each evaluated video were iterated manually to obtain frames from the same sequence. This way, the velocity of the model bird was approximately the same in all the frames presented in the result. The models' velocity was measured by placing a ruler close behind the model while swiping, while a timer was displayed on a screen in

[16] https://docs.opencv.org/3.4/df/d0d/tutorial_find_contours.html?loclr=blogmap
[17] https://docs.opencv.org/4.x/d7/d4d/tutorial_py_thresholding.html

the background. A slow-motion video was then captured with a phone to measure the distance and time the bird traveled over the area captured by the frames. The slow-motion video captured three swiping sequences, yielding $0.38m/s$, $0.27m/s$, and $0.29m/s$, with a mean of $0.31m/s$. Using the angular velocity, we obtain an expression for the actual velocity of the model bird at a range of distances away from the camera, Equation 5.9. In Figure 5.24, we can see that the velocity of a bird at $200m$ away from the camera needs to be $124m/s$ for it to appear as the same velocity as the bird model, which is unlikely even at high winds. However, for birds flying up to 40m from the camera, the velocity is equal to or lower than $25m/s$. This is a typical cutoff wind speed for wind turbines, and a bird flying with the wind is likely to achieve this velocity. As a bird with a high velocity, flying close to the camera will have the highest possible perceived velocity, and it is desirable to design the camera and lamp specifications for this speed. This ensures that the camera and light conditions are adequate for birds flying at high speeds at all distances.

$$\begin{aligned} \omega_{0.5m} &= \omega_d \\ \frac{v_{0.5m}}{0.5\text{m}} &= \frac{v_d}{d} \\ v_d &= v_{0.5m} \cdot \frac{d}{0.5\text{m}} \end{aligned} \tag{5.9}$$

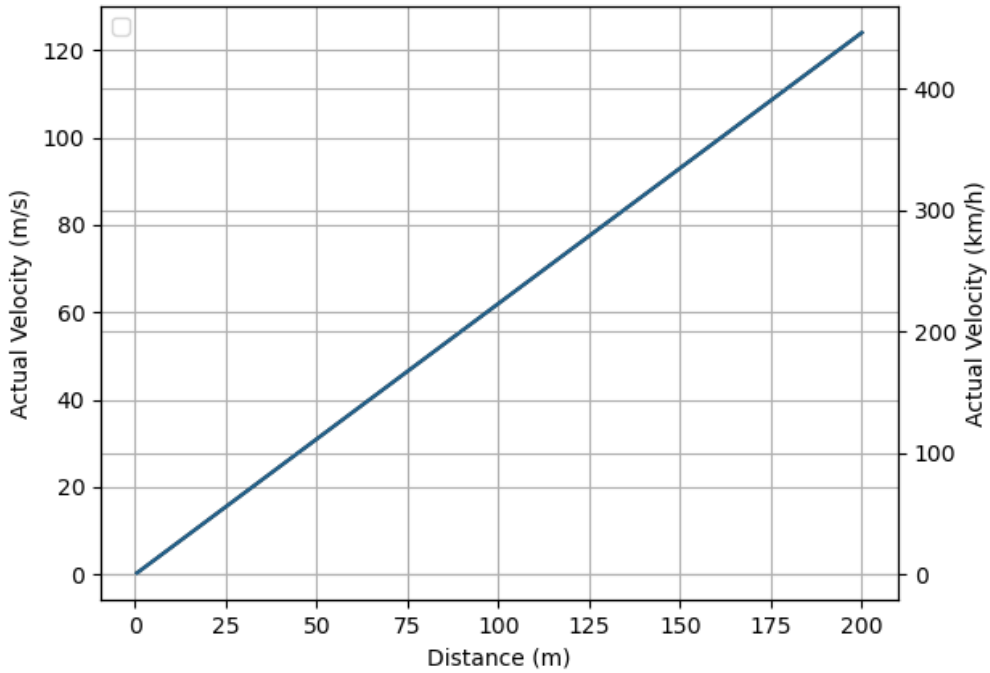

Figure 5.24.: Plot of the actual velocity of a bird at various distances from the camera, corresponding to the velocity of the model bird.

5.3.2. Results

Due to a high number of images, only some of the results are presented here while the reminding results can be found in section A.2.

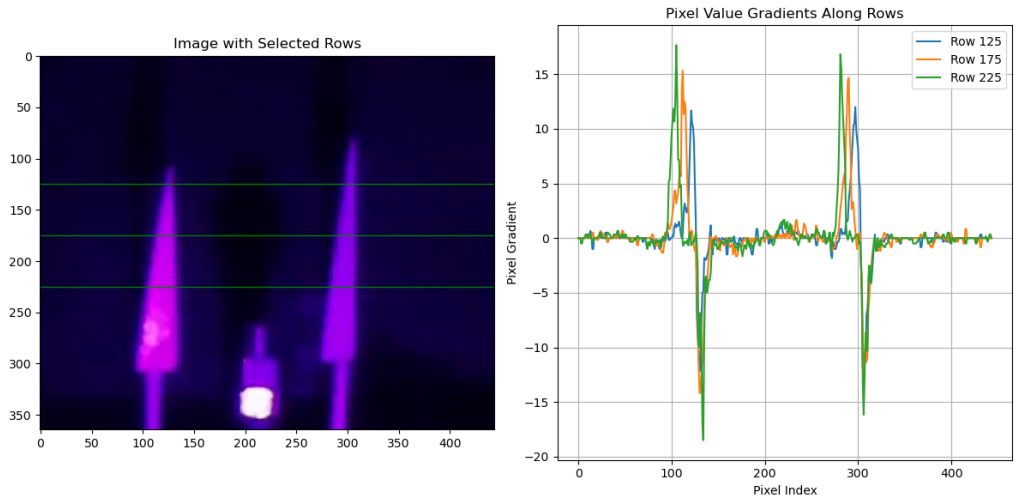

Figure 5.25.: Gradient measurement over sharp-edge bird models, with I_F set to 28mA. 3 pixel rows are evaluated to investigate the trend in gradient values over the triangles as the width increase. Pixel rows spaced with 50 pixels.

The gradient illustrates the changes in pixel intensity. This does not consider color but the mean of the three color channels from the camera. A spike in the gradient describes a rapid change in pixel intensity. Small spikes indicate that the changes in value are low, while high values describe high pixel-value changes. As the index of each row is counted from left to right, a positive spike indicates that the left side is dark and the right side is white, and vice versa for the negative spikes. If the index of each row were counted from the right to the left, the gradient plots would be inverse, with the negative spikes being positive and so on. In Figure 5.25 one can see that there is a trend in the gradients when moving from the top of the triangles to the bottom, with higher contrasts at the bottom.

Importance of edge geometry

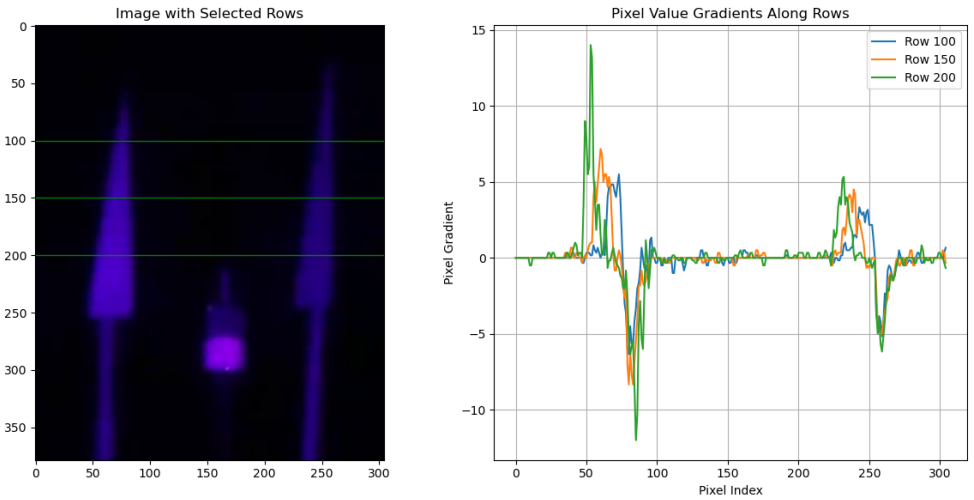

Figure 5.26.: Gradient measurement over sharp-edge bird models, with I_F set to 4 mA and videosetings FPS:60, shutter:1/60s, gain:16. 3 pixel rows are evaluated to investigate the trend in gradient values over the triangles as the width increase. Pixel rows spaced with 50 pixels.

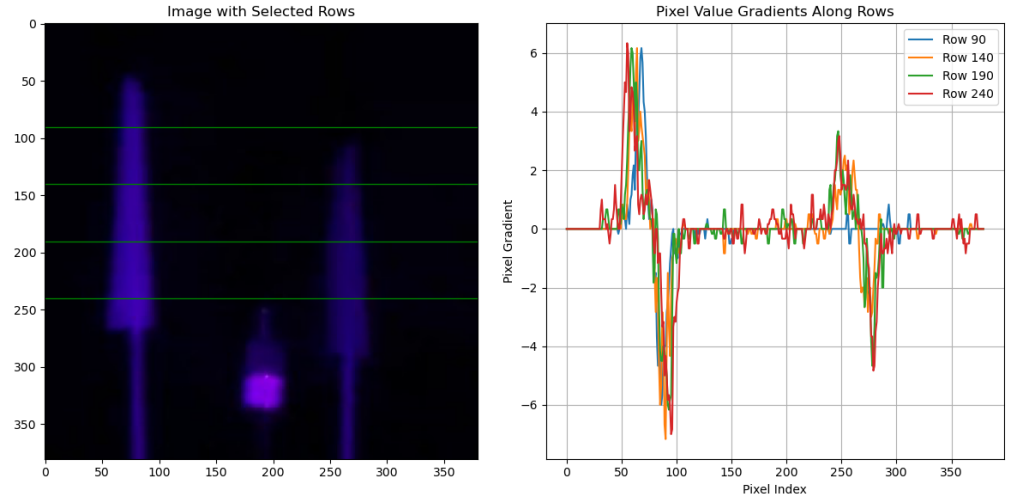

Figure 5.27.: Gradient measurement over round-edge bird models, with I_F set to 4 mA and videosetings FPS:60, shutter:1/60s, gain:16. 4 pixel rows are evaluated to investigate the trend in gradient values over the triangles as the width increase. Pixel rows spaced with 50 pixels.

	White model	Black model
Sharp edge	6-14 (-6) - (-12)	3-5 (-5)
Rounded edge	6 (-5) - (-7)	2-3 (-2)-(-5)

Table 5.4.: Maximum values for the gradient of the sharp edge image in Figure 5.26, higher in absolute value than the round edge image in 5.27. In each cell, the maximum value is presented on the top and the minimum value on the bottom. Note that the max/min values indicate only if the pixels from left to right are going from dark to brighter or vice versa. The values are presented here in ranges to include all measuring lines from the plots. A difference between the maximum and minimum values indicates that one side of the model has a sharper edge.

Note that 3 rows were evaluated for the sharp edge image, while 4 for the rounded edge image. This is due to a length difference between the rounded bird models and their levers.

Motion blur and outline

Figure 5.28.: Motion blur for the video-configuration FPS:20, shutter:1/20s, gain:16. **Left:** Grayscale image cropped out of the original frame. **Middle:** Otsu thresholded version of the left image.**Right:** Edge of the thresholded image, obtained with Canny edge detection.

Figure 5.29.: Motion blur for the video-configuration FPS:20, shutter:1/602, gain:16

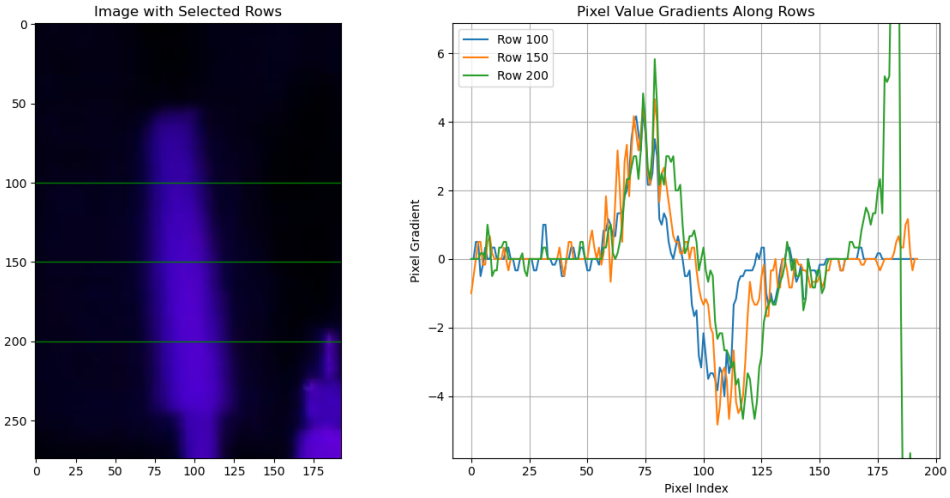

Figure 5.30.: Gradient over moving, round black bird model with I_F:12mA, fps:60, shutter:1/60s, gain:16.

Applying I_F

Assuming that Figure 5.30 with I_F of 12mA is sufficient for a human or computer to determine species, the radiant intensity of the full-scale lamp lies close to the range 19.5 to 149.6 W/sr. For lamps with a FOV of 40 degrees, this is equivalent to a 59.2W to 455.7W lamp. For a 20W lamp with adjustable, symmetrical FOV, the FOV must be in the range 21° to 58.1°.

5.3.3. Discussion

By comparison of the images taken with I_F at $28mA$ in Figure 5.25, and the $4mA$ in Figure 5.26, the gradients of the black model bird are approximately 3

times larger for the $28mA$ light intensity than the $4mA$. An indication of which of the light conditions bears proximity to the real-world conditions can be obtained by comparison to the experience of Verhoef et al[3]. In their field experiment, the light condition with a 14W lamp was insufficient for the low-light camera to obtain a sharp image of the flying bird with low shutter speeds. In the nighttime observations provided in their report[18], the bird's path is beneath the turbine hub and, thus, likely closer than 200m. From this, we can deduce that their bird footage is brighter than how a bird would appear at 200m, which is the distance considered in this model. Assuming the low-light camera they used is as sensitive or more than the IMX 477, and considering that the light intensity in this experiment was higher and the model bird likely more reflective than their observed bird, the $4mA$ footage will likely be closer to the real world. This should, however, be verified by a more accurate LED or an EMR measuring instrument, allowing for a more accurate model.

The gradient curve in the figure has more noise than expected. The similarity in the noise frequencies, where all the curves drop and increase in the same pixel indices, indicates that an image compression algorithm or the demosaicing process causes the noise. Binning is a method used to reduce the video stream's bit rate by combining neighboring pixels into one larger pixel. According to the documentation of the RPi HQ camera, 2x2 pixels are binned when recording with high frame rates and resolutions[25].

Comparing the slightly lower gradient of the sharp-edged, Figure 5.26 and rounded bird models, Figure 5.27, the rounded edge shows a decrease in appearance. The curvature of the bird will probably vary, as the wings will provide a large flat surface area with sharp edges, similar to the short-edge model, while the bird's body will be of closer resemblance to the rounded model. For the detection of an object in the night sky, this indicates that the bird's wings will be more easily detected than its body. However, for species recognition, an outline of the entire body will likely increase confidence in the observations. Thus, the rounded models will be used for further evaluation.

The issue of motion blur is discussed by Verhoef et al., proposing a shutter speed of 0.1s or 0.2s in future experiments[3]. However, the motion blur in Figure 5.28 shows that the image will still be smeared significantly. This makes it hard or impossible for humans to determine the species based on the outline alone. Methods for extracting a sharp image with AI have shown promising results[35, 36, 37]. However, the images presented in the obtained papers have significantly less motion blur than what can be seen in the Figure 5.28. Thus, a lower shutter speed is beneficial for both human interpretation of the image and for the possibility of using image enhancement. Comparing the gradients over 40 and 60 FPS with

[18]Figure4.7 [3]

default shutter speed in Figure A.12 and A.11 to their maximum shutter speeds in Figure A.6 and A.13 respectively, one can see a slight increase in gradient values for the long shutter speeds, as expected. Comparing 40 to 60 FPS shots, the contrast is slightly higher for 40 FPS. However, inspecting the images shows an extended smear of the model bird for 40 compared to 60 FPS. Yet, the bird models do not have much detail, and it is difficult to determine which configuration can be considered satisfactory. Thus, an experiment should be performed with greater detail in the bird models, such that an evaluation of the camera settings should be performed.

While Otsu's thresholding method can capture an outline of the model bird, the size of the bird model can be misleading. Since the model bird is uniform, we do not know if a smaller object with a low gradient over the whole surface would be detected. The whole triangle may be thresholded together, thus giving false confidence in how accurately small surfaces are detected. Details of smaller objects whose pixel intensity is low appear as detected in this image but would have been removed if not connected to the larger body.

An array of bird models separated and increasing in size will give a better ground for determining the suitable camera specifications for both detection and recognition in a full-scale setting. Adding a colored pattern on the model, similar to a lens testing chart, will further add to the measurable complexity of the bird. Knowing the exact speed and size of each model can allow for an analytical basis for comparing various frame rates and shutter speeds, where the illuminated area captured by the image can be compared to the still image. This would allow for obtaining the optimal camera configuration for capturing a sharp image in low-light conditions.

Due to the large uncertainty in the radiant intensity delivered by the LED, and a lack of a method for evaluating the minimum illumination, it was not possible to determine the minimum radiant intensity of the lamp. The experiment indicates that a 20W light source with av vertical and horizontal FOV of 40°, but due to the uncertainties in the experiment, it is insufficient for giving a definitive limit. Nevertheless, it suggests that a high frame rate be used to detect the presence of a bird and possibly its outline. Further, the presence of light opens up for using image enhancements through traditional methods such as histogram equalization and deep learning-based methods such as super-resolution [38] and low-light image enhancement [39, 40].

5.3.4. Conclusion

The experiment fails to obtain a minimum radiant intensity but shows promising results for detecting birds with NIR illumination. The NIR-modified camera

managed to detect the slight contrast of a small moving object with relatively little illumination. This indicates that the required amount of light is in a realistic order of magnitude, and it should be possible to obtain interpretable footage. The footage quality should also be possible to improve with traditional image-enhancing techniques. This will be considered further in the following chapter. While birds both have round and sharp edges, round-edged models will be evaluated further as their contrast is the hardest to distinguish from the background of the two. Using Otsu's method, an outline of the model bird is easily detectable. However, it is uncertain if smaller details in a silhouette will be detected or not.

Chapter 6.

Narrow swiping lamp

6.1. Motivation

As the issue of a continuous lamp is the low irradiance caused by the inverse square-distance law, a method for increasing energy per frame was investigated. A reduction in the distance between the lamp and the bird would allow for a higher irradiance, but due to the short range of the lamps, it would require placing lamps on the tower or nacelle. This would be in conflict with the requirement specifications, which state that placing lamps anywhere on the turbine tower or nacelle is undesirable, found in Appendix C. Thus, a solution for increasing the irradiance of a rail-mounted source is desirable. A way of achieving this is by reducing the lamp's FOV. Changing the FOV of a light source from α to β as illustrated in Figure 6.1, will cause the radiant intensity to increase with the relation of Equation 6.1.

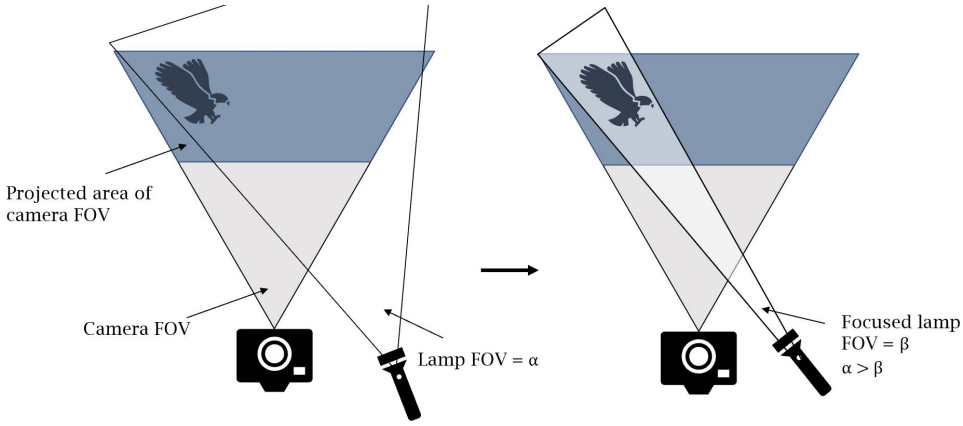

Figure 6.1.: Focused FOV of a lamp to increase radiant intensity. Illustrative icons are provided by PowerPoint.

$$\begin{aligned} \frac{I_\beta}{I_\alpha} &= \frac{(\frac{P}{\Omega_\beta})}{(\frac{P}{\Omega_\alpha})} \\ &= \frac{\Omega_\alpha}{\Omega_\beta} \end{aligned} \tag{6.1}$$

Inserting the expression for Ω of a light beam with a squared cross section, Equation 2.15, the ratio becomes:

$$\frac{I_\beta}{I_\alpha} = \frac{\alpha^2}{\beta^2} \tag{6.2}$$

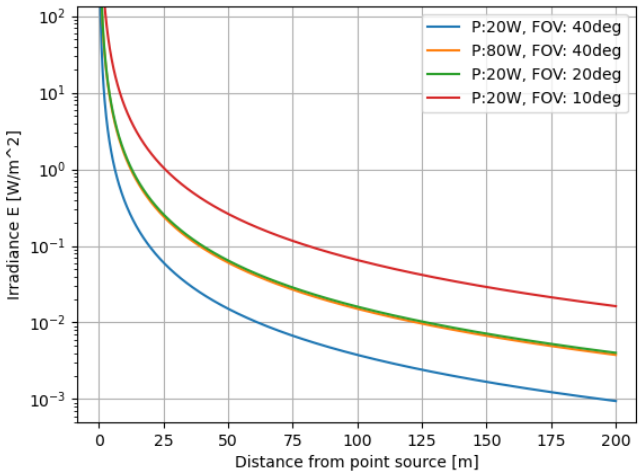

Figure 6.2.: Comparison of irradiance reduction for a single lamp with P:20W, symmetrical FOV:10°, 20°, and 40°. In addition, a lamp with power P:80W and symmetrical FOV:40°. One can see that the 80W lamp is about identical to the 20W lamp when the FOV is focused to 20°.

One can see from Figure 6.2 that a reduction of FOV has a significantly higher impact than adding more lamps.

However, reducing the area will cause the light beam to cover a smaller area. Reducing the FOV too much will result in the illuminated area to less than the projected camera area, thus generating blind spots. One can see from Figure 6.3 that reducing the FOV of a lamp from 40 to 20 degrees will reduce the illuminated

area from $21.2 \cdot 10^4 m^2$ to $5 \cdot 10^4 m^2$ at 200m away from the source.

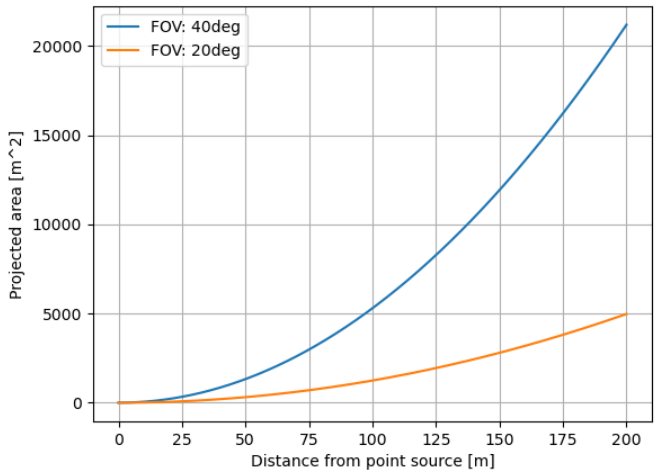

Figure 6.3.: The projected area of a point source at a distance 0-200m away when the FOV of the lamp's FOV is 40° and 20°. The plot assumes the horizontal and vertical FOV is identical.

To resolve this issue, the narrow lamp can be steered to cover the same area as the original. For instance, consider the lamp of Figure 6.4 (b), who's cross-section of the lamp's solid angle is reduced from being identical to that of the camera to being narrower in width but equal in height. This way, the light source only needs to be rotated, such that it, over a time period Δt_{swipe}, has illuminated the whole projected area of the camera.

However, due to the conservation of radiance, subsection 2.2.6, we know that the output radiance can only be equal to or lower than the input radiance of a geometrical optical system. Hence, more light is not present, it is only consecrated to a smaller area. What we are looking to do is increase the amount of energy reflected by the bird. Further, since a camera frame only depicts the energy gathered by each frame, we want to consider the amount of energy reflected to the camera in the duration of the camera's exposure time.

This can be evaluated by investigating the radiant exposure, H, the bird is subjected to. It describes the energy received by a surface over a duration of time. A higher H means that more light befell the bird, and thus more light was reflected back, hence yielding a brighter image of the bird. Assuming the irradiance is constant over the exposure time Δt, we get the following expression for radiant exposure:

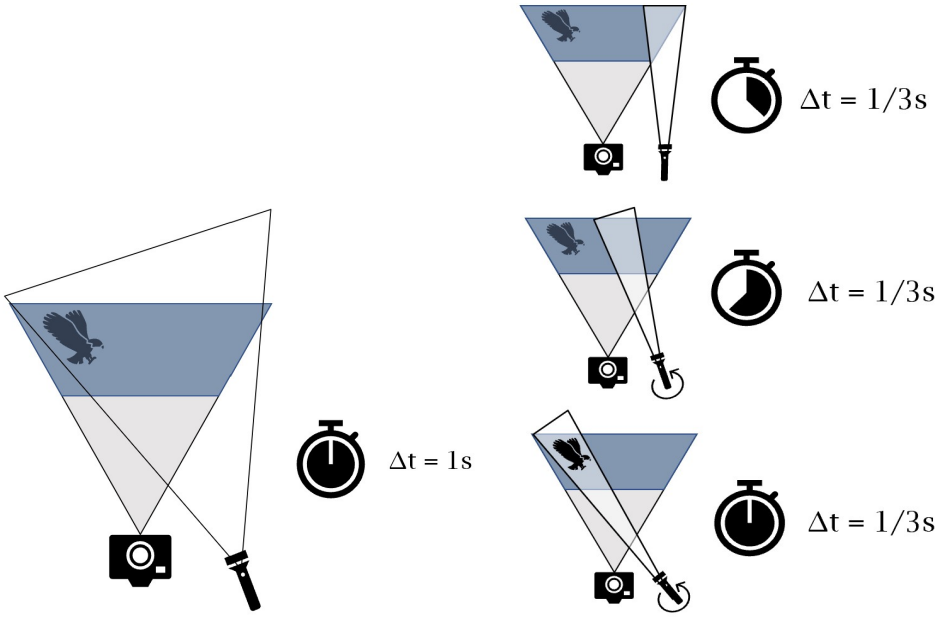

(a) Stationary wide lamp **(b)** Rotating narrow lamp

Figure 6.4.: (a) A stationary lamp illuminating the whole projected area of the camera. **(b)** A rotating lamp covering one-third of the camera's projected area, illuminating each section one-third of a second. Both lamps cover the full area in the same amount of time.

$$\begin{aligned} H &= E \cdot \Delta t \\ H &= \frac{P}{A} \cdot \Delta t \end{aligned} \tag{6.3}$$

Consider a lamp illumination an area, A, for the duration Δt, this would give a radiant exposure of H. Now assume the projected area of the lamp is reduced to $\frac{A}{3}$. As we want to illuminate the same area as before in the same amount of time, the swiping lamp will need move three times faster. This will cause the exposure time per unit area to be reduced, and for a constant swiping motion, it will cover each unit area in one third of the original time. Thus, H remains the same:

$$H = \frac{3 \cdot P}{A} \cdot \frac{\Delta t}{3} \tag{6.4}$$

Consequently, the bird will not appear brighter in the image, even though the irradiance is higher. The only option for increasing H is thus to increase the power of the lamp of increase the exposure time Δt. As the available power is limited, the most interesting alternative is to increase Δt.

Δt can be divided into two; the time the bird is illuminated, Δt_{lamp}, and the shutter speed of the camera, $\Delta t_{shutter}$. The shortest of the two will determine the number of photons reaching the pixels in a frame. For instance, if the shutter speed is set to 1 second and the bird is lit up for 0.5 seconds, no more photons than those reflected in the 0.5 seconds will return to the image sensor. If the shutter speed is set to 0.5 seconds and the bird is lit up for 1 second, the reflected photons reaching the sensor after 0.5 seconds will not be captured in one frame. To avoid motion blur in the image, having a short Δt is desirable as it reduces the distance a moving bird can travel. This can be achieved by moving the light at a speed significantly higher than the bird's velocity or by illuminating the bird enough for a high shutter speed to detect it.

With a slow shutter speed and a swiping period more than half of $\Delta t_{shutter}$, the resulting image will depict the bird several times, as the bird will be illuminated several times over a single frame. This can, in turn, be used to interpolate its trajectory based on each observed position. However, it poses a risk of overlapping images if a bird has too low of a velocity, flies back to the same area, or several birds are present. Additionally, since most videos use high frame rates where the objects appear only once in every frame, it is reasonable to assume that most computer vision algorithms are designed to find the object only once in every frame. For instance, a single frame depicting the same bird several times resembles an image of two birds flying through at a higher speed. In addition

will low-resolution images have few features, making it challenging to distinguish birds. Thus, a low frame rate poses specially designed algorithms. Δt_{lamp} will also be determined by the width of the light beam and its translational velocity. Due to the scattering of light and the distances considered, some light leakage out of the beam will occur, causing a wider beam, and thus, its velocity would need to be high.

For the case of a fast shutter speed, Δt_{lamp} can be equivalent to or longer than the shutter speed. Setting the shutter speed equivalent to the camera's frame rate will maximize H. For a swiping lamp, a long Δt_{lamp} is achieved by reducing the light beam's translational speed over the camera's projected area. This will cause different sections in each frame to be illuminated, as illustrated in Figure 6.5. The bird will then only appear in some images, and if the bird is flying through a blind spot before the lamp return to that section, it will not be detected. Thus, a sufficiently high velocity of the light beam is required.

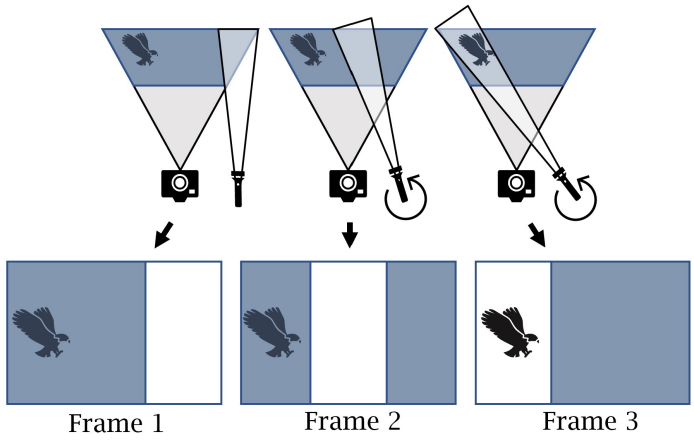

Figure 6.5.: The swiping motion of the lamp's light beam illuminates different areas of the camera's FOV. The blue region represents the projected area of the camera at a given distance, and the white cone from the torch illustrates the narrow light beam. The frames illustrate the image captured by the camera, where one can see the white section illuminated by the narrow lamp.

6.1.1. Functional limits

Knowing the projected area ratio, r_A^d, between the projected area of the lamp, A_l^d, and the camera, A_c^d at a distance d from the source, we can develop an expression for the minimum number of frames required before the whole projected area of the camera is covered. This assumes an ideal ratio, where a new section of the projected area is illuminated in every frame and does not overlap, thus covering

the camera's entire projected area in a complete swiping cycle. For a lamp with smaller horizontal and vertical FOV than the camera, the ratio will decrease as the distance increase. Thus, the minimum ratio will be evaluated at the furthest evaluated distance of 200m:

$$r_A^{200m} = \frac{A_l^{200m}}{A_c^{200m}} \tag{6.5}$$

If the swiping lamp covers a new section in each video frame, this would be equivalent to several cameras covering different areas with a lower frame rate. For instance, if the lamp needs 3 video frames to cover the projected area of the camera at a distance of 200m, then each frame will monitor different sections. Assuming the swiping cycle of the lamp is repeated each second, each section will have a video stream, or *channel*, with a 1/3 of the original frame rate as seen in Figure 6.6. In this report, a channel will refer to the video stream capturing a specific illuminated area in the camera frame.

For a given frame rate of the camera, FPS_{camera}, and with the number of channels, $N_{channels}$, the frame rate of each channel, $FPS_{channel}$, is described by Equation 6.6. For an ideal r_A^d, the number of channels in the video stream, $N_{channels}$, is identical. Thus, for a low r_A^d, the frame rate of each channel will be low.

$$FPS_{channel} = \frac{FPS_{camera}}{N_{channels}} \tag{6.6}$$

While the frame rate is not essential for the sharpness, except by limiting the possible duration for exposure, it is important for the continuity of the video. A low frame rate will make it harder to determine the path of a fast-moving object but can be significantly lower than the exposure time.

To avoid the possibility of a bird flying through all the blind spots, thus being hidden from the camera, it is desirable with a high $FPS_{channel}$. To find a limit to how fast a bird can move through the image frame, we can develop an expression for the time it takes before A_c^d is covered, t_{cycle}. For an ideal r_A^d, this can be expressed as the inverse product of the number of channels times the camera frame rate:

$$t_{cycle} = \frac{1}{N_{channels} \cdot FPS_{camera}} \tag{6.7}$$

With t_{cycle} and the shortest width of A_c^d ,w_A^{min}, we can develop an expression for the bird's maximum velocity, $V_{bird}^{cycle,max}$, to be in the frame through a whole

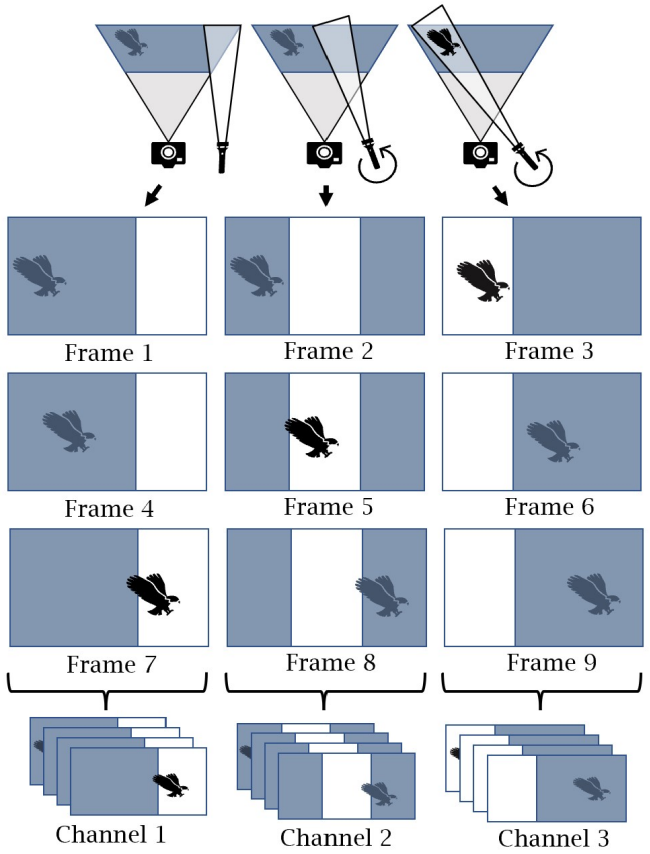

Figure 6.6.: Illustration of channels. For a system where the frame rate and cycle of the swiping lamp are synchronized, a pattern in the frames will arise. Here the lamp swipes such that every n'th video frame will be illuminated on the right side, every n+1 frame in the middle, and every n+3 frame will be illuminated on the left side. Each illuminated sector will be referred to as a channel in this report.

swiping cycle:

$$V_{bird}^{cycle,max} = \frac{w_A^{min}}{t_{cycle}} \tag{6.8}$$

However, it is generally desirable to obtain more than one image of the bird so that its path can be evaluated. Further, the system must be able to detect all birds flying through for it to be a reliable data source. Thus, the swiping of the lamp should be significantly faster than $V_{bird}^{cycle,max}$, such that the bird is illuminated several times. One way of achieving this is to require that the bird's maximum velocity V_{bird}^{max} is a fraction, p, of $V_{bird}^{cycle,max}$:

$$V_{bird}^{max} = \frac{1}{p} \cdot V_{bird}^{cycle,max} \tag{6.9}$$

6.1.2. Swiping motion

Another limitation is how fast the light cone can be moved, which depends on how the swiping motion is achieved. One method is to move the whole light source. However, for a large lamp, this will require a powerful actuator, and the rapid motion will stress the components and cause fatigue. Another option is to move the lens relative to the light source. This is known as *beam steering*, and is used for laser steering and solar tracking[41, 42]. This method allows fewer components to be moved and, consequently, less maintenance. However, with the procedure used by Flood et al., the light cone can only be moved $\pm 10°$[42]. However, for a light cone with a width w_{cone} significantly lass than the maximum width of the camera w_A^{max}, the required angular displacement form the center axis, $\Delta\theta$, will be higher than $\pm 10°$. Thus, further research will be required to find a solution for moving the light cone.

6.1.3. Radiometric exposure limits

To minimize the required power of the NIR light source, the light can be directed with a combination of reflectors and lenses. This is a common practice for lamp systems, such as flashlights and car headlights. However, it poses extra attention for design limitations, where in addition to the standards for lamps, IEC 62471, the standard for projectors, IEC 62471-5, must be minded.

The IEC 62471 standard concerning the photobiological safety of lamps and lamp systems presents limitations to a lamp's exitance/irradiance and radiance. Lamps are categorized into 4 risk groups: exempt group, risk group 1, 2, and 3. It is

desirable that the lamp can be categorized as the exempt group, which is considered to be harmless for all exposure times. As a bird might hover over the lamp or sit in a position exposed to the light beam, the possible exposure time is assumed to be over several minutes. A lamp within the exempt group will allow for the safe implementation of the lamp for humans. Based on the common usage of NIR sources for wildlife monitoring and the general increase in strictness for human safety limits compared to animals, it is assumed in this report that the safety limits apply to birds as well. However, according to Verhoef et al. there is uncertainty about how sensitive birds are to NIR light, so further investigation is required before this system can be put to use[3].

In IEC 62471, requirement 4.3.6 considers the retinal thermal hazard exposure limit for a source with weak visual stimuli. It states that the radiance of the lamp in the exempt group must be less than $6000/\alpha\ W/m^2sr$ for exposure times longer than 10s. Here, α is the angular subtense of the apparent source and is calculated as presented in Equation 2.13, where further information can be found in section 2.3. Note that it is the *apparent* source and not the full source that is considered. For instance, for a lamp with a flat surface area of $50cm^2$ covered by a plate with an opening of $20cm^2$, it is the $20cm^2$ opening that is to be considered. However, if the lamp's light is concentrated with either reflectors or lenses, the system will be considered a projector, and the IEC 62471-5 standard applies. As with a lamp, the radiance limit of a projector is dependent on the angular subtense of the apparent source. Here, the apparent source is the area cross-section of the light beam at the outer surface of the projector's outer lens.

From Equation 2.13, we can see that α is determined by the apparent source area, and the distance from the light source to the observer. For the lamp standard, the length is dependent on the shortest distance to where an observer can look directly into the light source. For the projector standard, a distance of $1m$ from the observer to the outermost lens, plus the distance from the outer lens to the exit pupil of the projector. As a narrow beam system is dependent on a reflector and lens system, the IEC 62471-5 should be applied. However, it does not consider sources with low visual stimuli, and thus, the radiance limit of IEC 62471-5 is less strict than IEC 62471:

- IEC 62471: $L_{IR} \leq \frac{6000}{\alpha} \mathrm{W\,m^{-2}\,sr^{-1}}$
- IEC 62471-5: $L_R \leq \frac{28000}{\alpha} \mathrm{W\,m^{-2}\,sr^{-1}}$

Therefore, the IEC 62471 standard for lamp systems should be the reference point for designing the swiping lamp system. Due to the limitations of the eye and its natural movement, a minimum and maximum angular subtense are presented. The minimum, α_{min}, is set to 0.017 radians, and the maximum, α_{max} set to 0.1 radian. As illustrated in Figure 6.7, for an angular subtense of the apparent source

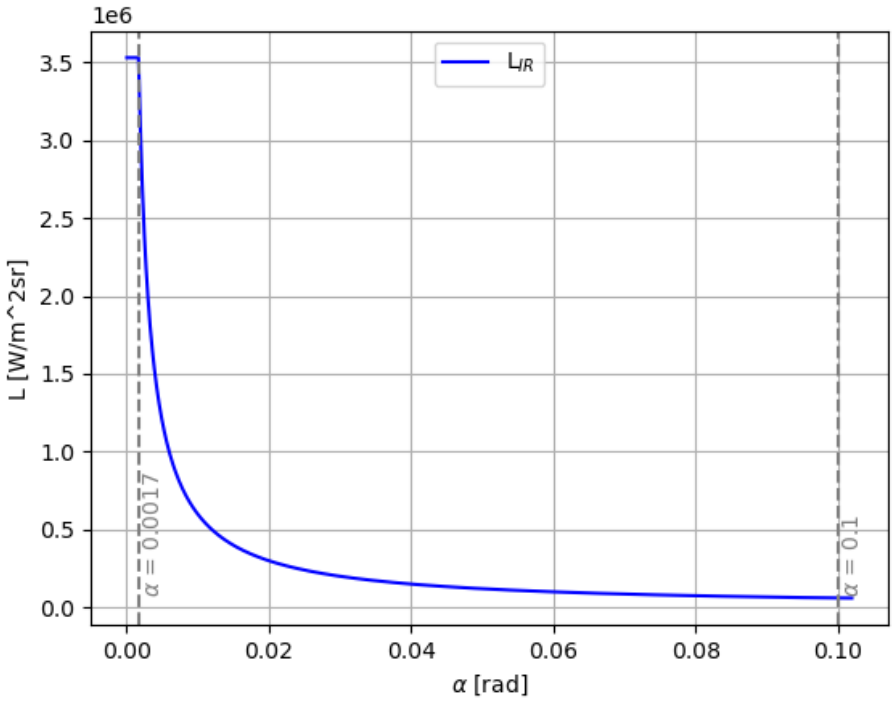

Figure 6.7.: The radiance limit for light sources with low stimuli, L_{IR}, for various apparent source sizes, α. For α below α_{min}= 0.0017 or above α_{max}=0.1, then the $\alpha_{min/max}$ value applies.

larger or smaller than these, the limited α applies. If α is between α_{min} and α_{max}, then Equation 2.11 applies.

In both standards, the irradiance limit, E_{IR}, is set to $100W/m^2$ for the exempt group. Also here the measurement methods differ. In IEC 62471, the limit is measured at $200mm$ from the source, while in the IEC 62471-5 standard, the measurement is performed at $1m$ from the outer surface of the lens. However, in both standards, the phrasing of the measurement procedures indicates that these distances are determined with regard to the measuring equipment and its limitations. Thus, the irradiance of the lamp should be calculated with the apparent source's surface area on the lens's outer surface.

When designing the swiping lamp, it is desirable with a small source size to ease its implementation, whereas a large lamp will take up room on the platform. In addition, a low solid angle of the lamp is desirable for increasing the radiant intensity to illuminate a bird sufficiently. However, the irradiance and radiance

limit constricts the minimum size of the lamp, and for a given irradiance, the solid angle is limited by the radiance limit. By inserting the definition of irradiance, Equation 2.3, into the limit,2.9, and solving for the area, we obtain an expression for the minimum area of the lamp:

$$\begin{aligned} \frac{P}{A_{min}} &\leq 100\mathrm{W\,m^{-2}} \\ A_{min} &\geq \frac{P}{100\mathrm{W\,m^{-2}}} \end{aligned} \tag{6.10}$$

To evaluate if this satisfies the radiance, it is necessary to find α. For a $20W$ power source, A_{min} becomes $0.2m^2$, and if the apparent source is square, its width becomes $0.44m$. By using Equation 2.13, we find that the maximum and minimum values of α equal $2.2 \cdot 10^{-}3rad$ at $200m$ and $2.2rad$ at $200mm$. As $2.2 > \alpha_{max}$ $2.2 \cdot 10^{-}3 < \alpha_{min}$, we will use the $\alpha_{min/max}$ values for calculations of the radiance. As the radiance of the system must be lower than the limit, it is the lowest value of L_{IR} that needs to be considered, obtained with α_{max}. Inserting α_{max} in Equation 2.11 gives the limit:

$$\begin{aligned} L &\leq L_{IR} \\ &\leq \frac{6000}{0.1}\mathrm{W\,m^{-2}\,sr^{-1}} \\ &\leq 6 \cdot 10^{4}\mathrm{W\,m^{-2}\,sr^{-1}} \end{aligned} \tag{6.11}$$

By inserting Equation 2.3 in 6.11 we can develop an expression for the minimum solid angle of the lamp's beam:

$$\begin{aligned} \frac{E}{\Omega} &\leq 6 \cdot 1045\mathrm{W\,m^{-2}\,sr^{-1}} \\ \Omega &\geq \frac{E}{6 \cdot 10^{4}\mathrm{W\,m^{-2}\,sr^{-1}}} \end{aligned} \tag{6.12}$$

This procedure can be performed for a range of possible power sources. Figure 6.8 and Figure 6.9 give the minimum area of the apparent source and its corresponding minimum solid angle of the beam. This can function as a guide for further design processes.

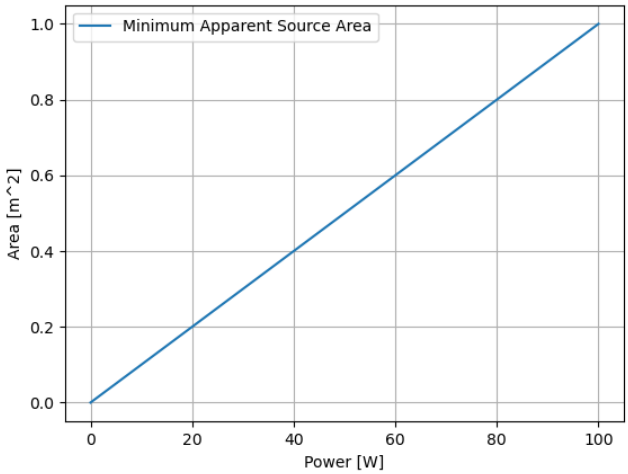

Figure 6.8.: The minimum area for the apparent source to satisfy the irradiance limit, given various power outputs. The line represents the irradiance limit of $100W/m^2$, where only the configuration below the line satisfies the criterion.

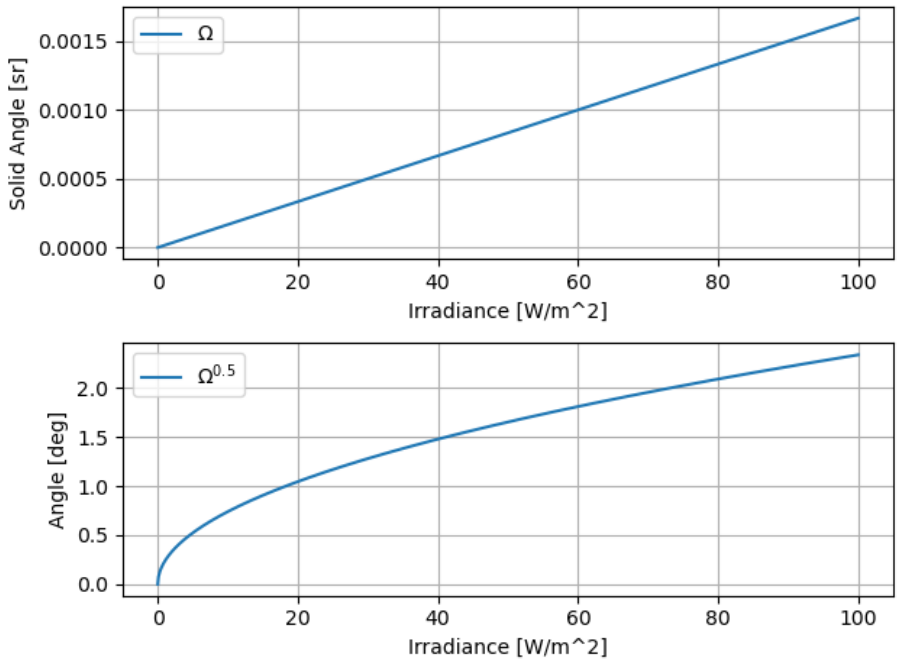

Figure 6.9.: Top: The minimum solid angle of a lamp to satisfy the radiance limit for weak visual stimuli. **Lower:** The minimum FOV for a lamp with symmetrical FOV to satisfy the irradiance limit. In both cases, the configuration must be above the graph to be satisfactory.

6.1.4. Reducing the distance

As a last resort, if the ratio between the projected area of the camera and the lamp is too large requiring an undesirable channel frame rate, the distance between the lamp and the bird can be reduced. The range of the rail-mounted lamp can be reduced by placing an additional lamp on top of the turbine. Additionally, the top-mounted lamp can cover the monitored area of several cameras, effectively reducing the installation cost. It is common with a platform for instrumentation on the roof of a wind turbine nacelle. Due to safety requirements, accessing this platform is not as easy as the rail. Additionally, more work is required to maintain and fix installations.

6.2. Method

To function as a proof of concept for a swiping lamp, the $LED'_{12}s$ light was concentrated with an available magnifying lens. A slider-crank mechanism was

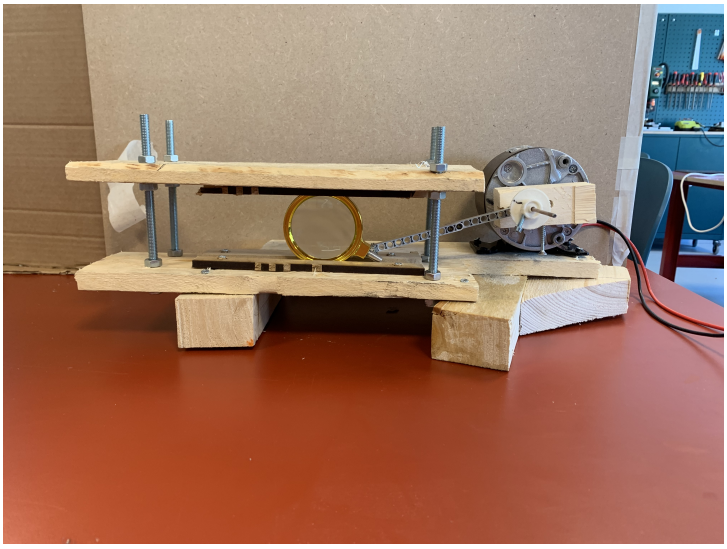

Figure 6.10.: Slider crank mechanism for obtaining light cone and generating a swiping motion as proof of concept. A top and bottom track forced the lens to move perpendicular to the axis of the DC motor.

manufactured to convert the rotating motion of a DC motor to a linear motion of the lens, generating the swiping motion of the light cone. The magnifying lens was attached to the slider, forced to move along a track. The mechanism can be found in Figure 6.10, and a schematic drawing of the crankshaft mechanism in Figure 6.11. The velocity of the lens was adjusted with the angular velocity of the motor, which again was regulated with a variable DC power supply.

To illustrate the theoretical placement of the light beam for each frame, the position of the lens at a given time t was plotted together with markings of the frame rate. This will represent the theoretical channels produced by the system. To illustrate the theoretical placement of the lens, the expression for a crankshaft mechanism with a displaced axis was utilized:

$$\text{pos} = -\sqrt{(r+l)^2 - e^2} + r \cdot \left(\cos(\theta) + \frac{l}{r} \cdot \sqrt{1 - \left(\left(\frac{e}{l} - \sin(\theta) \right) \cdot \frac{r}{l} \right)^2} \right) \tag{6.13}$$

Where θ can be found with:

$$\theta = \omega \cdot t \tag{6.14}$$

e	5.7cm
l	14.2cm
r	2.3cm

Table 6.1.: Dimensions of slider-crank mechanism.

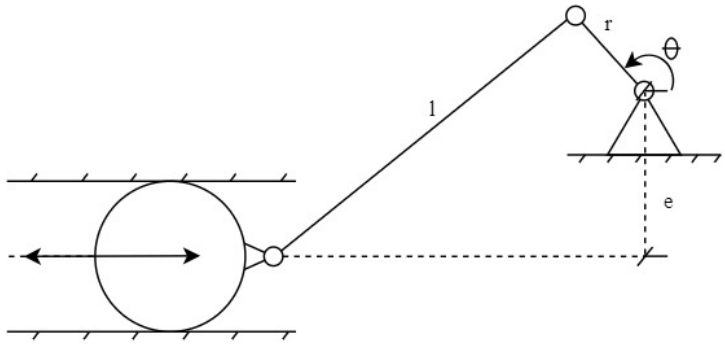

Figure 6.11.: Schematic figure of the crankshaft mechanism with dimensions and variable names. The link r rotates with an angular velocity ω, from which the position θ can be derived by the relationship $\theta = \omega \cdot t$. r connected to l, thus driving the slider connected to the lens. The axis of the slider is offset to the rotating axis with a distance e.

The dimensions of e, l, and r can be found in Table 6.1:

The angular velocity, ω, was obtained by video during the experiment, counting rotations per second which were found to be approximately 5Hz. ω was then calculated with Equation 6.15, where f is the frequency of the motor. This was later tested with the same power output to the motor, confirming the obtained frequency and ω. For validating footage, a Fourier transform was performed on the position of the light beam center in frames of the obtained video over a 2-second interval. The ω corresponding to the obtained frequency was then used to compare the measurements to compare the physical and theoretical models.

$$\omega = f \cdot 2\pi \tag{6.15}$$

The diameter of the lens was measured to $5.6cm$, and its distance from the LED_{12} was $9.3cm$. The approximate focal length of the lens was $16.2cm$, measured by the distance from a point where the projected image was reversed.

The mechanism was placed between the LED and the model bird of the camera rig. Due to the height of the light steering mechanism, it blocked the camera's

(a) Topside view of the camera rig with the lens moving mechanism placed between the LED_{12} and the bird model.

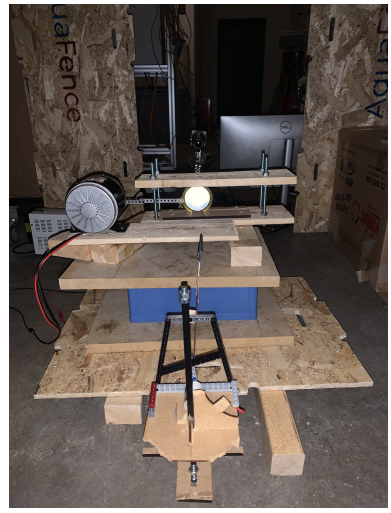

(b) Backside view of the camera rig with the lens moving mechanism in front of LED_{12}. The rig was elevated with available material.

Figure 6.12.: Placement of the lens moving mechanism on the camera rig. The lens moved within the FOV of the LED_{12}.

view, and the camera had to be elevated. The lens metrics were unknown, so the distance between the light source and beam steering mechanism was adjusted by hand to obtain illustrative light beam focus and velocity. To ease the process of placing the mechanism, the NIR LED was replaced with a visual light LED, such that the irradiance caused by the beam could be evaluated. An illustration of the setup can be seen in Figure 6.12.

The experiment was performed directly after the experiment performed in section 5.3 iteration 3. Thus, the modifications suggested in the respective conclusion were not implemented in this experiment. The velocity of the model bird remained at $0.31m/s$, and the distance to the camera was approximately $0.5m$. Other than the light steering mechanism and an elevation of the camera, the location and setup of the experiment are thus identical to the experiment in 5.3, where a detailed description can be found in subsection 5.3.1.

The main goal of the experiment was to observe if illuminated channels could be observed in the video footage, in addition to revealing unknown factors. Thus the width of the light beam had to be lower than the width covered by the swiping motion of the model bird. A flat surface was placed behind the bird model to observe the beam's width before beginning the experiment. While this did not give a direct measure of the beam's width at the location of the model bird, it gave

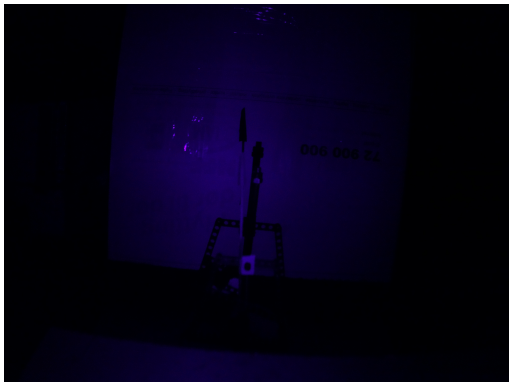

(a) Light beam from LED_{12} before inserting the focusing lens.

(b) Light beam from LED_{12} after inserting the focusing lens.

Figure 6.13.: Illustration of the light intensity with and without the focusing lens.

a sufficient indication for determining if it was too broad. When the beam's width was satisfactory, the LED_{12} was placed back into the breadboard. The LED_{12} beam was inspected with a live stream provided by the camera and turned off before minor adjustments were performed to maintain eye safety. An illustration of the illumination with and without the lens is presented in Figure 6.13

6.3. Results

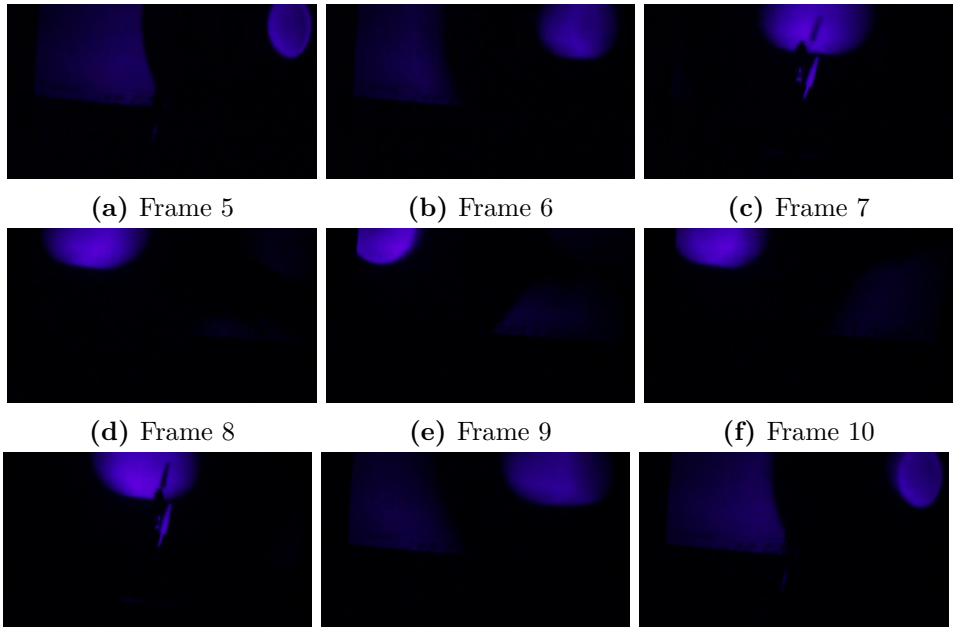

(a) Frame 5 **(b)** Frame 6 **(c)** Frame 7

(d) Frame 8 **(e)** Frame 9 **(f)** Frame 10

(g) Frame 11 **(h)** Frame 12 **(i)** Frame 13

Figure 6.14.: 9 frames of lens swipe from video with configuration: FPS:60, shutter:1/60s, gain:16. One can see the irradiance of the light beam on the back plate as a bright purple area. In frames 3, 7, and 12, the model bird is illuminated by the light beam. A faint glow of light can be seen in the periphery of the lens' shadow, which is the light not captured by the lens.

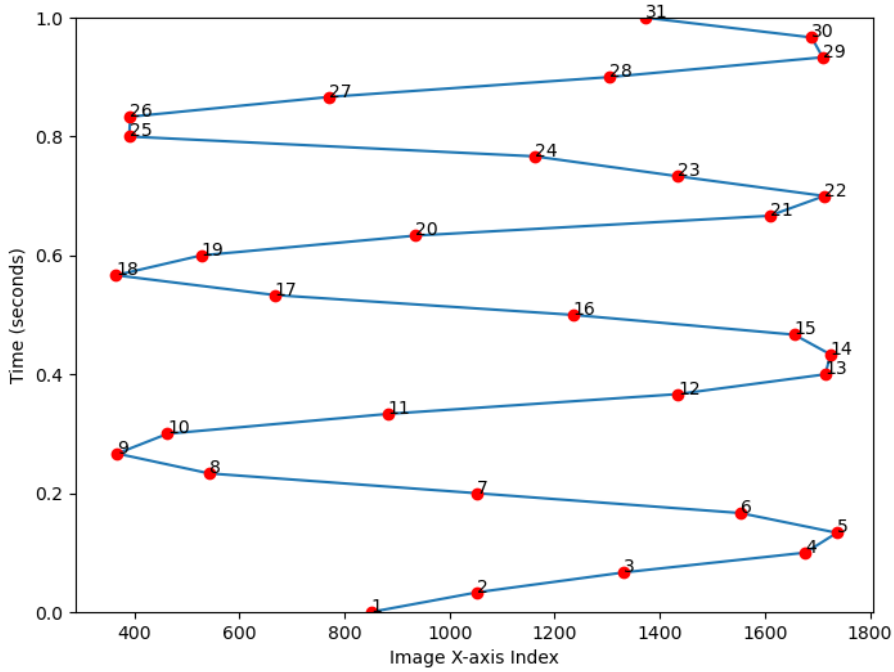

Figure 6.15.: Measured swiping cycles over 1 second from video with FPS:60, shutter:1/60s, gain:16. Each frame is presented as red dots with their corresponding frame number in the plot.

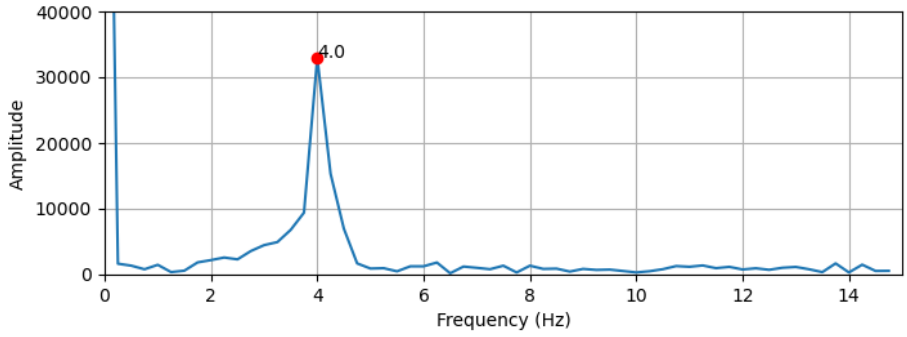

Figure 6.16.: Fourier transform of the sample, illustrating a swiping frequency of the light beam is $4Hz$.

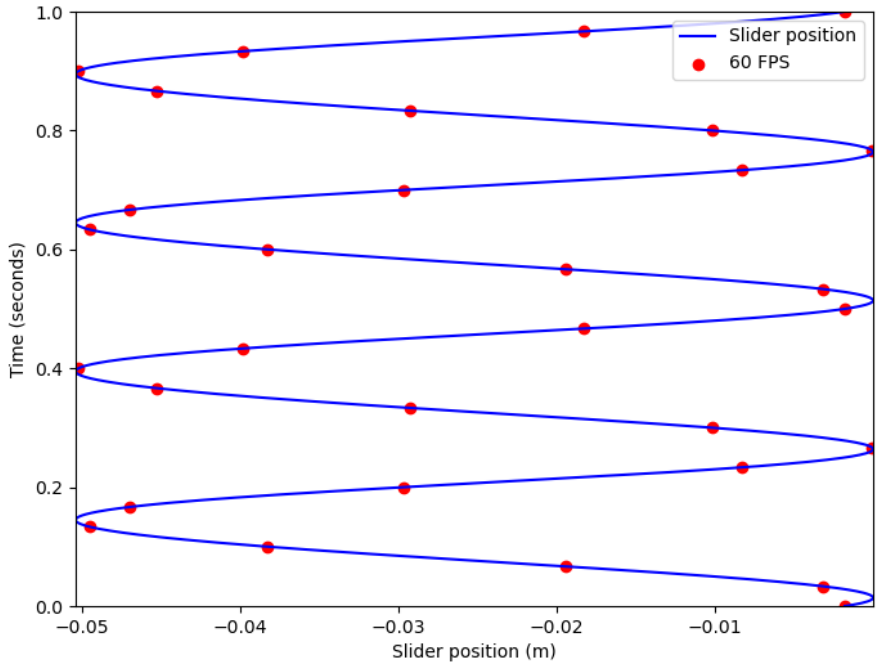

Figure 6.17.: Theoretical position (blue line) of the lens over a 1s sequence, together with the camera frame rate (red dots) of 60 FPS. Following the lens path for one cycle, moving from one side to the other and back.

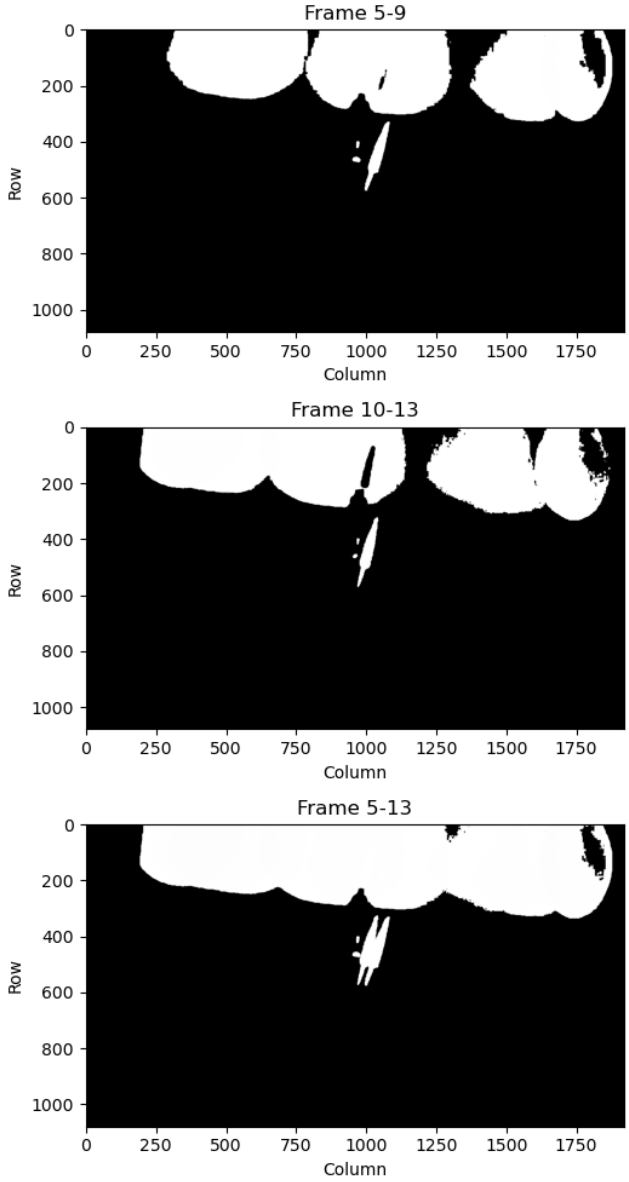

Figure 6.18.: Total illumination over the first half cycle (Top), the second half (Middle), and the combined illumination over one cycle (Bottom). The illuminated area from each frame is combined to illustrate the total coverage over and potential blind spots. The sharp white spots beneath the illuminated area of the top and middle figures are frames where the light beam illuminated the model bird. In the full cycle image (Bottom), one can see the distance traveled by the model between each exposure.

6.4. Discussion

An initial mismatch in the frequencies of the obtained footage at $8Hz$ and the measured $5Hz$ revealed a flaw in the experiment. Comparing the theoretical model of the lens position and the position of the light beam in the footage revealed that the sampling rate was also twice as large. This was likely caused by *frame dropping* during the video, where every second frame is discarded. Inspecting the documentation of the camera, the maximum frame rate for the 1920x1080 resolution utilized in the experiment, the frame rate is capped at 50 FPS for mode 2. The high bit rate of the video stream can thus have caused the dropping of frames to reduce the load. This can cause a de facto frame rate of 30 FPS with a shutter speed equivalent to a 60 FPS frame rate. Comparing the expected sampling of the theoretical model in Figure 6.17 and the obtained samples, 6.15, supports this theory. The de facto frame rate of 60fps for the high-resolution images does not have an impact on the experiments performed in chapter 4 and 5, as they were testing light conditions for stationary targets.

The lens swipe frequency of $4Hz$ still deviates from the model, which can be an accumulated result of imprecise measurements of sizes and velocities. Further, due to the shape of the lens, the slider mechanism was allowed to rotate and move vertically when stopping at the right side of the track. This caused the lens to stagnate longer on the right side than what is considered in the model.

Inspecting Figure 6.15, the channels do not appear clearly. This is to be expected due to the accumulation of small model deviations and camera delays. However, inspecting a pattern can be found where every in-cycle in the $1s$ sequence begins 7-9 frames after the previous one.

The experiment illustrates how the swiping lamp can cover the entire projected area of the camera over several frames. Inspecting the total illuminated area from frame 5-9 in Figure 6.18, close to the entire width is illuminated. To illuminate the entire frame height, a suitable lens could generate an oblong shape. One can also see how the blind spots of each half-cycle are covered by the other, resulting in a near-total illumination of the beam path from frames 5-13. Observing the oblong contour of the model bird, one can see how far it traveled between each frame.

Further, the combined 5-13 frame in Figure 6.5 also illustrates the repeated imaging issue of a configuration where the shutter speed $\Delta t_{shutter}$ is longer than Δt_{lamp}. Imaging of the bird should, in theory, be identical to the combined 5-13 image. The bird is here depicted on top of itself, which can confuse both human and computer interpretation. With the experiment's configuration of a $\Delta t_{shutter}$ shorter than the Δt_{lamp}, the bird can be observed only once in each frame.

The distance between the light source and the lens is not representable to the real world, nor is the size of the lens. Thus the experiment can only function as a proof of concept for the swiping motion and expose unknown issues. For further development, the development of a lens and reflector design is needed. For guidance, the limitations developed in this chapter can be an initial starting point for the design process.

6.5. Conclusion

In this chapter, a method for increasing the visibility of a bird by increasing the radiant intensity of the lamp is suggested. Further, an investigation of requirements and limitations is discussed, suggesting a framework for determining the solution's suitability when given a minimum irradiance. The swiping light beam illustrates a promising ability to cover the projected area of the camera. The experiment performed in this chapter cannot be considered representable for a full-scale light-swiping system due to unrealistic dimensions. Nevertheless, the experiment illustrates that a high swiping velocity of the light beam is obtainable with the movement of a lens. Additionally, it demonstrates the limitation of angular displacement of the light beam with a single-lens system. Further experiments should be performed with a lens- and light-source setup similar to what can be expected of a full-scale system.

Chapter 7.

Summary discussion

In this summary discussion, the findings of the experiments presented in this thesis will be evaluated. Further, the sources of error are presented, and suggestions to further work are presented.

The use of a NIR light source in combination with a NIR modified RGB camera appears promising for monitoring bird activity at night. A combination of illumination and image processing is likely to enable the detection of nearby birds of all sizes and large birds with good reflectivity at greater distances. It is not clear at what level it is possible to determine species. There is reason to believe that a swiping lamp with high radiant intensity will provide better footage illumination of the bird, thus increasing the distance at which it can be detected. However, due to the uncertainties of the experiments performed in this study, further research is required before deciding whether the solution is satisfactory. This entails examining the sweeping mechanism, the maximum swiping velocity, and the lamp's ability to cover the full projected area of the camera. Further, a value of the required illumination for detection and identification is required to determine the solution's applicability.

Even in the worst-case scenario, the results obtained section 5.3 indicate that an outline of the bird should be possible to obtain at close distances. Contrast enhancements with traditional methods, such as histogram equalization, should improve the footage for human inspection. It is unclear whether Verhoef et al. performed any image enhancement on their results. Assuming no contrast enhancement was performed, their result depicting the motion blur of a bird or bat flying past the entire frame[1] indicates that enough information should have been available for a higher frame rate to be utilized. However, as the altitude and velocity of the animal are not known, one can not determine the minimum frame rate of the camera in the given circumstance. Further, one cannot determine whether

[1] Figure 4.7[3]

the light source was sufficient for detecting birds at higher altitudes. Thus, it is necessary to obtain the required irradiance on a bird for both the detection and recognition of species. Suggestions for future experimental setups will be presented in section 7.1. While a large-scale experiment should be able to determine the required irradiance, the small-scale camera rig developed in this thesis provides a good base for rapid development.

For determining the required illumination, a suitable evaluation criterion is needed. The termination criteria investigated in this thesis have primarily been based on visual inspection of a model with little detail, with some quantitative parameters. The evaluation has been grounded in the theory of general object detection, where edge detection has been the main focus. With this approach, the resulting solution will produce footage that can detect the presence of a bird with simple image-enhancing techniques. While the findings in this thesis indicate that detection can be possible with high frame rates, the test has not been performed at full scale. Further, it does not consider the level of detail and colors which can be expected in a real-world scenario.

The IMX477 image sensor illustrates a satisfactory ability to detect NIR radiation, which indicates that it can be used for monitoring in combination with a NIR light source. For the camera specifications, only the NIR sensitivity has been considered in the research, as the remaining specifications, such as required resolution and focal length, are case-dependent. However, the uncertainty of its spectral sensitivity makes it difficult to compare with other cameras. Further, as the warranty of the camera is violated when removing the IR cutoff filter, it itself is not ideal for implementation in the final product. For companies already using cameras for monitoring, a method for comparing their camera to the test camera is desirable.

The presented NIR light system relies on the invisibility of NIR radiation to humans and animals. Yet, as pointed out by Verhoef et al., there is some uncertainty regarding this assumption. This could cause the bird to change behavior and thus invalidating the data and possibly, endangering the bird if it is enticed to fly close to the rotating turbine. In addition, albeit a light source is considered safe for human vision, a review of the safety of birds is needed before experimentation with live animals is acceptable.

The experiments performed in this thesis are not validated with statistical evaluations. Instead, iterations of low-resolution prototyping have been conducted with the goal to verify whether an iteration should be evaluated further. This was a deliberate choice, which, as described by Steiner & Leifer concerning the Wayfaring approach[1], allows for postponing the resource-heavy tasks until a promising solution is detected. However, it became clear that a lack of sufficient background knowledge of advanced image processing and radiometry caused issues along the

way. This deviates from their description of the method, where they state that the required tools are necessary. Thus, there might be promising solutions not investigated, and issues like frame dropping could have been detected in an early stage. Nevertheless, the wayfaring approach has allowed for the development of a new approach to nighttime bird monitoring with limited time and background knowledge.

The camera was not color balanced after removing the IR cutoff filter, as it was assumed that the gray-scale images would be sufficient. This was based on the wide use of grayscale image processing methods. However, the results from chapter 5 illustrate the importance of colors for detection and recognition with machine learning algorithms trained on colored images. Thus, the degree of recognition by using generally trained AI can not be considered representative of how well they would detect the actual bird or recognize the species.

7.1. Further work

Termination criteria
For companies and institutions of research who may be interested in adopting the method outlined in this thesis, the termination criterion should be developed based on their method for recording bird activity. That is, if humans evaluate the footage, the degree of illumination required should be determined based on human interpretability. If an AI is utilized, its response to various images of birds illuminated by NIR in full scale should be the termination criterion.

Small scale model
Unless actual birds are available, models with various sizes and details should be utilized. For the camera test rig developed in this thesis, the model birds can be partitioned into smaller sizes and added details. To obtain analytical parameters on which camera configurations should be used, the model's outline and illumination can be obtained in good lighting conditions and used as a benchmark for the experiments. Thus the detected outline can give a relative measure of motion blur and illumination.

Determining NIR sensitivity
Unless a camera with data on its spectral sensitivity in the NIR region is available, experimental measurements of the IMX477 can be performed. This does, however, require specialized equipment and is not necessarily available. Thus, if the cameras available to a company are available, the experiments should be performed with them. Otherwise, an industrial camera should be investigated.

Swiping mechanism
The use of lenses and reflectors for focusing and directing the light beam is crucial

for the swiping lamp concept. It is desirable with a narrow beam with little leakage as this might be necessary for satisfactory illumination at $200m$ away from the source. Further, the use of beam steering with lens arrays should be investigated for obtaining a satisfactory displacement of the light beam. This can, in addition, allow for higher frequencies, as less mass is moved, which again can allow for detecting birds flying in high velocities.

Chapter 8.

Summary conclusion

In this study, the possibility of using a consumer RGB camera in combination with a NIR light source for nighttime monitoring of bird activity is investigated. The study suggests that commercial RGB cameras without IR cutoff filters can be used to detect the presence of birds at close distances if a directed 850nm (NIR) light source is present. Further, contrast-enhancing image processing techniques are recommended for improving the footage. A requirement for the minimum required illumination is not obtained, but the approach for obtaining it with full-scale testing is presented. Further, it is considered likely that the required illumination is too high for a single lamp, and a method for increasing the illumination without adding lamps, nor attaching them to the wind tribune itself, is presented.

It entails increasing the focus of the light source and generating a swiping motion of the light beam to cover the area of the camera's field of view. An approach for generating the swiping motion with the translation of one or mere lenses is suggested, and a proof of function is performed. It illustrates promising results and is suggested for further development. However, several issues are yet to be investigated before the solution can be considered for implementation. This entails the safety of birds and their sensitivity to NIR radiation, in addition to the practical issues of focusing and swiping the lamp.

The probing approach to the task allows for some degree of confidence that the proposed method is suitable for implementation. However, potentially promising solutions may have been bypassed, and investigation of untested pathways is encouraged. This thesis fails to develop a plug-and-play solution for enabling bird monitoring with RGB cameras. However, valuable information and guidelines for further work are obtained and presented, including the practical and safety limitations of the proposed solution.

References

[1] Martin Steinert and Larry Leifer. "'Finding One's Way': Re-Discovering a Hunter-Gatherer Model based on Wayfaring". In: *International Journal of Engineering Education* 28 (Jan. 2012), pp. 251–252.

[2] Ivan Savitsky. "ORJIP Offshore Wind: Review of seabird monitoring technologies for offshore wind farms". en. In: (), p. 127. URL: https://www.carbontrust.com/our-work-and-impact/guides-reports-and-tools/review-of-seabird-monitoring-technologies-for-offshore-wind-farms.

[3] J P Verhoef, P J Eecen, R J Nijdam, H Korterink, and H H Scholtens. "WT-Bird A Low Cost Solution for Detecting Bird Collisions". en. In: (). URL: https://tethys.pnnl.gov/publications/wt-bird-low-cost-solution-detecting-bird-collisions.

[4] Achim Gerstenberg, Heikki Sjöman, Thov Reime, Pekka Abrahamsson, and Martin Steinert. "A Simultaneous, Multidisciplinary Development and Design Journey – Reflections on Prototyping". en. In: *Entertainment Computing - ICEC 2015*. Ed. by Konstantinos Chorianopoulos, Monica Divitini, Jannicke Baalsrud Hauge, Letizia Jaccheri, and Rainer Malaka. Lecture Notes in Computer Science. Cham: Springer International Publishing, 2015, pp. 409–416. ISBN: 978-3-319-24589-8. DOI: 10.1007/978-3-319-24589-8_33.

[5] *CCTV Camera Resolution | CCTV Resolution Chart for Cameras*. en-US. URL: https://optiviewusa.com/cctv-video-resolutions/ (visited on 07/10/2023).

[6] *Imaging Electronics 101: Understanding Camera Sensors for Machine Vision Applications*. en. URL: https://www.edmundoptics.com/knowledge-center/application-notes/imaging/understanding-camera-sensors-for-machine-vision-applications/ (visited on 07/10/2023).

[7] *IMX477/IMX477R: Datasheet PDF, Specs, Use & Buy (2022)*. en-US. URL: https://www.arducam.com/sony/imx477/ (visited on 07/08/2023).

[8] Wenjin Wang and Albertus C. Den Brinker. "Modified RGB Cameras for Infrared Remote-PPG". en. In: *IEEE Transactions on Biomedical Engineering* 67.10 (Oct. 2020), pp. 2893–2904. ISSN: 0018-9294, 1558-2531. DOI: 10.1109/TBME.2020.2973313. URL: https://ieeexplore.ieee.org/document/8993753/ (visited on 06/17/2023).

[9] Ross McCluney. *Introduction to Radiometry and Photometry*. English. Vol. Second edition. Artech House Applied Photonics Series. Boston: Artech House, 2014. ISBN: 978-1-60807-833-2. URL: https://search.ebscohost.com/login.aspx?direct=true&db=nlebk&AN=1155196&site=ehost-live&scope=site (visited on 06/29/2023).

[10] Egil Lillestørm, Ola Hunderi, and Jan R. Lien. *Generell fysikk for universiteter og høyskoler*. Norwegian. Vol. 2. Universitetsforlaget, 2021. ISBN: 978-82-15-00006-0. (Visited on 06/20/2023).

[11] *Inverse-square law*. en. Page Version ID: 1160542884. June 2023. URL: https://en.wikipedia.org/w/index.php?title=Inverse-square_law&oldid=1160542884 (visited on 06/29/2023).

[12] *Radiance*. en. Page Version ID: 1158212614. June 2023. URL: https://en.wikipedia.org/w/index.php?title=Radiance&oldid=1158212614 (visited on 06/29/2023).

[13] Germain Chartier. *Introduction to Optics*. 1997. ISBN: 0-387-40346-9.

[14] Hyuk-Ju Kwon and Sung-Hak Lee. "Visible and Near-Infrared Image Acquisition and Fusion for Night Surveillance". en. In: *Chemosensors* 9.4 (Apr. 2021). Number: 4 Publisher: Multidisciplinary Digital Publishing Institute, p. 75. ISSN: 2227-9040. DOI: 10.3390/chemosensors9040075. URL: https://www.mdpi.com/2227-9040/9/4/75 (visited on 03/09/2023).

[15] Yuqian Ma, Jin Bao, Yuanwei Zhang, Zhanjun Li, Xiangyu Zhou, Changlin Wan, Ling Huang, Yang Zhao, Gang Han, and Tian Xue. "Mammalian Near-Infrared Image Vision through Injectable and Self-Powered Retinal Nanoantennae". English. In: *Cell* 177.2 (Apr. 2019). Publisher: Elsevier, 243–255.e15. ISSN: 0092-8674, 1097-4172. DOI: 10.1016/j.cell.2019.01.038. URL: https://www.cell.com/cell/abstract/S0092-8674(19)30101-1 (visited on 07/10/2023).

[16] *NEK IEC 62471:2006*. URL: https://handle.standard.no/no/Nettbutikk/produktkatalogen/Produktpresentasjon/?ProductID=264644 (visited on 07/06/2023).

[17] *NEK IEC 62471-5:2015*. URL: https://handle.standard.no/no/Nettbutikk/produktkatalogen/Produktpresentasjon/?ProductID=758793 (visited on 07/06/2023).

[18] Birk Hveding Ersdal. *Technology for Biodiversity: A Prestudy for the Development of Autonomous Measurement of Collisions Between Birds and Offshore Wind Turbines*. Not published. Dec. 2022.

[19] R. Tjørnløv, H. Skov, M. Armitage, M. Maker, J. Jørgensen, K. Thomas, and T. Uhrenholdt. "Resolving Key Uncertainties of Seabird Flight and Avoidance Behaviours at Offshore Wind Farms: Final Report for the study period 2020-2021." en. In: *2023-20-02* (). URL: https://tethys.pnnl.gov/publications/resolving-key-uncertainties-seabird-flight-avoidance-behaviours-offshore-wind-farms.

[20] Fabio Falchi, Pierantonio Cinzano, Dan Duriscoe, Christopher C. M. Kyba, Christopher D. Elvidge, Kimberly Baugh, Boris A. Portnov, Nataliya A. Rybnikova, and Riccardo Furgoni. "The new world atlas of artificial night sky brightness". In: *Science Advances* 2.6 (June 2016). Publisher: American Association for the Advancement of Science, e1600377. DOI: 10.1126/sciadv.1600377. URL: https://www.science.org/doi/full/10.1126/sciadv.1600377 (visited on 04/18/2023).

[21] Andreas Hänel, Thomas Posch, Salvador J. Ribas, Martin Aubé, Dan Duriscoe, Andreas Jechow, Zoltán Kollath, Dorien E. Lolkema, Chadwick Moore, Norbert Schmidt, Henk Spoelstra, Günther Wuchterl, and Christopher C. M. Kyba. "Measuring night sky brightness: methods and challenges". en. In: *Journal of Quantitative Spectroscopy and Radiative Transfer* 205 (Jan. 2018), pp. 278–290. ISSN: 0022-4073. DOI: 10.1016/j.jqsrt.2017.09.008. URL: https://www.sciencedirect.com/science/article/pii/S0022407317304442 (visited on 04/19/2023).

[22] Richard H. Vollmerhausen, Ronald G. Driggers, and Van A. Hodgkin. "Night illumination in the near- and short-wave infrared spectral bands and the potential for silicon and indium-gallium-arsenide imagers to perform night targeting". In: *Optical Engineering* 52.4 (Apr. 2013). Publisher: SPIE, p. 043202. ISSN: 0091-3286, 1560-2303. DOI: 10.1117/1.OE.52.4.043202. URL: https://www.spiedigitallibrary.org/journals/optical-engineering/volume-52/issue-4/043202/Night-illumination-in-the-near--and-short-wave-infrared/10.1117/1.OE.52.4.043202.full (visited on 03/30/2023).

[23] Phillip A. Mlsna and Jeffrey J. Rodríguez. "Chapter 19 - Gradient and Laplacian Edge Detection". en. In: *The Essential Guide to Image Processing*. Ed. by Al Bovik. Boston: Academic Press, Jan. 2009, pp. 495–524. ISBN: 978-0-12-374457-9. DOI: 10.1016/B978-0-12-374457-9.00019-6. URL: https://www.sciencedirect.com/science/article/pii/B9780123744579000196 (visited on 07/10/2023).

[24] Richard H. Vollmerhausen and Tana Maurer. "Night illumination in the visible, NIR, and SWIR spectral bands". In: *Infrared Imaging Systems: Design, Analysis, Modeling, and Testing XIV*. Vol. 5076. SPIE, Aug. 2003, pp. 60–69. DOI: 10.1117/12.487189. URL: https://www.spiedigitallibrary.org/conference-proceedings-of-spie/5076/0000/Night-illumination-in-the-visible-NIR-and-SWIR-spectral-bands/10.1117/12.487189.full (visited on 07/10/2023).

[25] *Raspberry Pi Documentation*. URL: https://www.raspberrypi.com/documentation/computers/camera_software.html#still-command-line-options.

[26] John S. Shenk, Jerome J. Workman, Jr, and and Mark O. Westerhaus. "Application of NIR Spectroscopy to Agricultural Products". In: *Handbook of Near-Infrared Analysis*. 3rd ed. Num Pages: 40. CRC Press, 2007. ISBN: 978-0-429-12301-6.

[27] *Storskarv*. nb. May 2015. URL: https://www.artsdatabanken.no/Pages/186784/Storskarv (visited on 06/18/2023).

[28] *NIR (Near-Infrared) Imaging (Fog/Haze Filter)*. en. URL: https://www.infinitioptics.com/technology/nir-near-infrared (visited on 07/12/2023).

[29] Mikko E. Toivonen and Arto Klami. "Practical Camera Sensor Spectral Response and Uncertainty Estimation". en. In: *Journal of Imaging* 6.8 (Aug. 2020). Number: 8 Publisher: Multidisciplinary Digital Publishing Institute, p. 79. ISSN: 2313-433X. DOI: 10.3390/jimaging6080079. URL: https://www.mdpi.com/2313-433X/6/8/79 (visited on 06/17/2023).

[30] Jonathan Crowther. "Monochrome Camera Conversion: Effect on Sensitivity for Multispectral Imaging (Ultraviolet, Visible, and Infrared)". en. In: *Journal of Imaging* 8.3 (Mar. 2022). Number: 3 Publisher: Multidisciplinary Digital Publishing Institute, p. 54. ISSN: 2313-433X. DOI: 10.3390/jimaging8030054. URL: https://www.mdpi.com/2313-433X/8/3/54 (visited on 06/17/2023).

[31] *Artsorakel*. URL: https://orakel.artsdatabanken.no/ (visited on 06/18/2023).

[32] Birk Hveding Ersdal. *Thesis*. original-date: 2023-03-17T08:37:59Z. June 2023. URL: https://github.com/BirkHveding/Bird-monitoring-with-NIR-illumination (visited on 06/18/2023).

[33] Iliana Medina, Elizabeth Newton, Michael R. Kearney, Raoul A. Mulder, Warren P. Porter, and Devi Stuart-Fox. "Reflection of near-infrared light confers thermal protection in birds". en. In: *Nature Communications* 9.1 (Sept. 2018). Number: 1 Publisher: Nature Publishing Group, p. 3610. ISSN: 2041-1723. DOI: 10.1038/s41467-018-05898-8. URL: https://www.nature.com/articles/s41467-018-05898-8 (visited on 03/01/2023).

[34] *An Introduction to Flicker Free LED Strip Dimming | Waveform Lighting*. URL: https://www.waveformlighting.com/film-photography/an-introduction-to-flicker-free-led-strip-dimming (visited on 07/04/2023).

[35] Diksha Adke, Atharva Karnik, Honey Berman, and Shyamala Mathi. "Detection and Blur-Removal of Single Motion Blurred Image using Deep Convolutional Neural Network". In: *2021 International Conference on Artificial Intelligence and Computer Science Technology (ICAICST)*. June 2021, pp. 79–83. DOI: 10.1109/ICAICST53116.2021.9497841.

[36] Sunghyun Cho, Yasuyuki Matsushita, and Seungyong Lee. "Removing Non-Uniform Motion Blur from Images". In: *2007 IEEE 11th International Conference on Computer Vision*. ISSN: 2380-7504. Oct. 2007, pp. 1–8. DOI: 10.1109/ICCV.2007.4408904.

[37] Yunpeng Li, Sing Bing Kang, Neel Joshi, Steve M. Seitz, and Daniel P. Huttenlocher. "Generating sharp panoramas from motion-blurred videos". In: *2010 IEEE Computer Society Conference on Computer Vision and Pattern Recognition*. ISSN: 1063-6919. June 2010, pp. 2424–2431. DOI: 10.1109/CVPR.2010.5539938.

[38] Jingyun Liang, Jiezhang Cao, Yuchen Fan, Kai Zhang, Rakesh Ranjan, Yawei Li, Radu Timofte, and Luc Van Gool. *VRT: A Video Restoration Transformer*. arXiv:2201.12288 [cs, eess] version: 2. June 2022. URL: http://arxiv.org/abs/2201.12288 (visited on 06/23/2023).

[39] Sophy Ai and Jangwoo Kwon. "Extreme Low-Light Image Enhancement for Surveillance Cameras Using Attention U-Net". en. In: *Sensors* 20.2 (Jan. 2020). Number: 2 Publisher: Multidisciplinary Digital Publishing Institute, p. 495. ISSN: 1424-8220. DOI: 10.3390/s20020495. URL: https://www.mdpi.com/1424-8220/20/2/495 (visited on 06/23/2023).

[40] Liang Shen, Zihan Yue, Fan Feng, Quan Chen, Shihao Liu, and Jie Ma. *MSR-net:Low-light Image Enhancement Using Deep Convolutional Network*. arXiv:1711.02488 [cs]. Nov. 2017. DOI: 10.48550/arXiv.1711.02488. URL: http://arxiv.org/abs/1711.02488 (visited on 06/23/2023).

[41] Håkon Jarand Dugstad Johnsen, Astrid Aksnes, and Jan Torgersen. "Solar tracking using beam-steering lens arrays". en. In: *Nonimaging Optics: Efficient Design for Illumination and Solar Concentration XV*. Ed. by Roland Winston and Eli Yablonovitch. San Diego, United States: SPIE, Sept. 2018, p. 4. ISBN: 978-1-5106-2087-2 978-1-5106-2088-9. DOI: 10.1117/12.2320046. URL: https://www.spiedigitallibrary.org/conference-proceedings-of-spie/10758/2320046/Solar-tracking-using-beam-steering-lens-arrays/10.1117/12.2320046.full (visited on 07/10/2023).

[42] Kevin M. Flood, William J. Cassarly, Christina Sigg, and J. Michael Finlan. “Continuous wide-angle beam steering using translation of binary microlens arrays and a liquid-crystal phased array”. In: *Computer and Optically Formed Holographic Optics*. Vol. 1211. SPIE, May 1990, pp. 296–304. DOI: 10.1117/12.17959. URL: https://www.spiedigitallibrary.org/conference-proceedings-of-spie/1211/0000/Continuous-wide-angle-beam-steering-using-translation-of-binary-microlens/10.1117/12.17959.full (visited on 07/10/2023).

Appendix A.

Test results

A.1. Required irradiance

(a) Benchmark image, lamp of and 1m distance to bird

(b) Lamp ON, 1m distance to bird

(c) Lamp ON, 2m distance to bird

(d) Lamp ON, 3m distance to bird

Figure A.1.: Finding required irradiance. Frame: 2, FPS:60, Shutter:1/60s, Gain:16, stationary bird and lamp. - Page 1/3

(e) Lamp ON, 4m distance to bird

(f) Lamp ON, 5m distance to bird

(g) Lamp ON, 6m distance to bird

(h) Lamp ON, 7m distance to bird

(i) Lamp ON, 8m distance to bird

(j) Lamp ON, 9m distance to bird

Figure A.1.: Finding required irradiance. Frame: 2, FPS:60, Shutter:1/60s, Gain:16, stationary bird and lamp. - Page 2/3

(a) Lamp ON, 10m distance to bird **(b)** Lamp ON, 11m distance to bird

Figure A.2.: Finding required irradiance. Frame: 2, FPS:60, Shutter:1/60s, Gain:16, stationary bird and lamp. - Page 3/3

A.2. Small-scale test rig

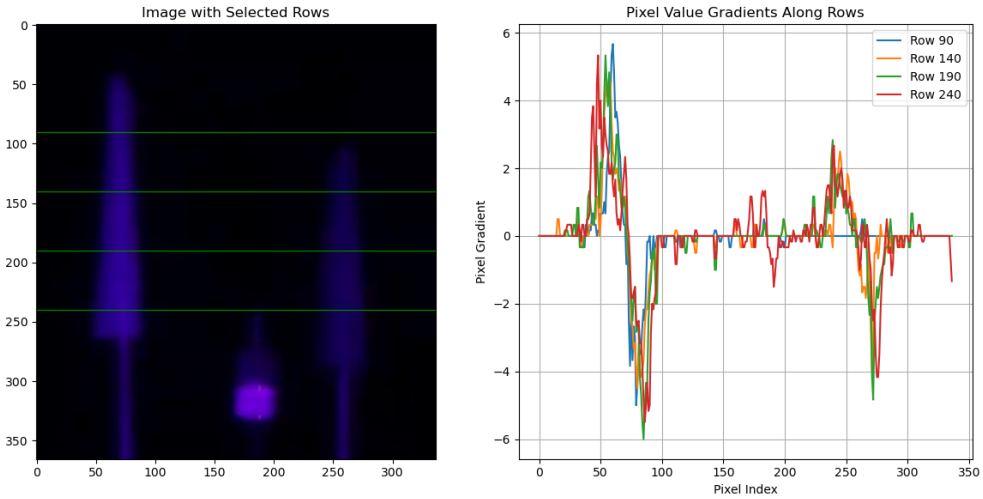

Figure A.3.: 20W small scale test with rounded bird model, I_F:3mA

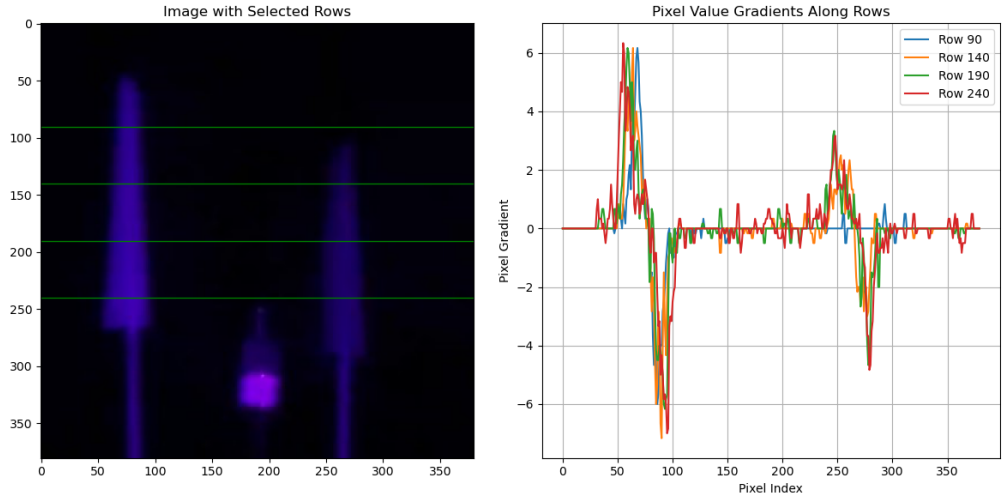

Figure A.4.: 20W small scale test with rounded bird model, I_F:4mA

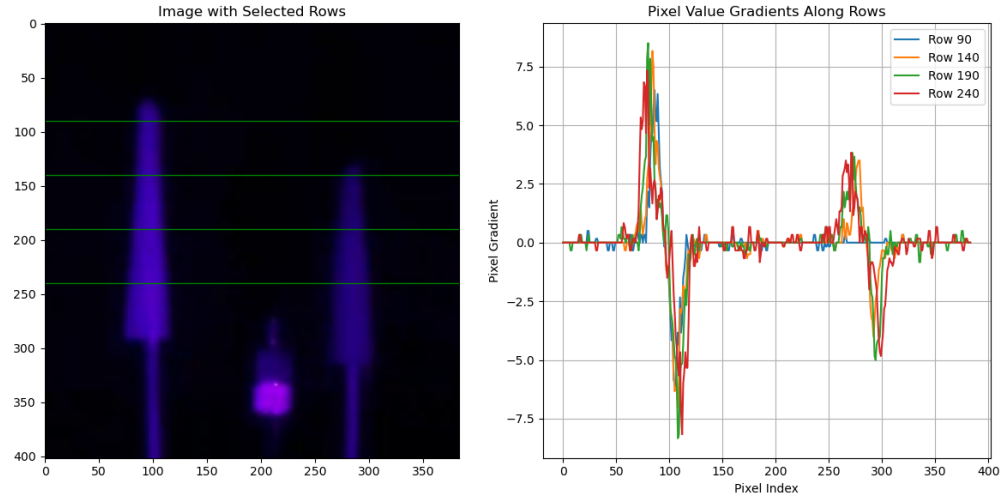

Figure A.5.: 20W small scale test with rounded bird model, I_F:5mA

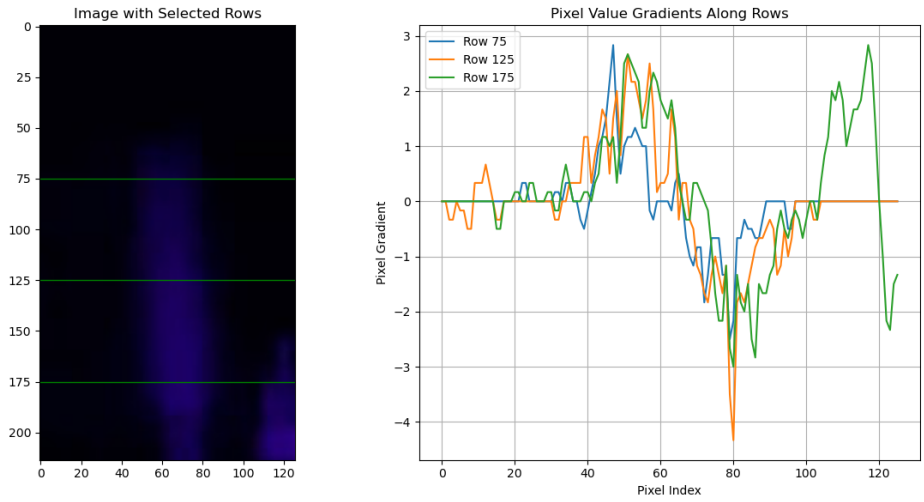

Figure A.6.: Gradient over moving round black bird model with I_F:3mA, fps:40, Shutter:1/40s, gain:16.

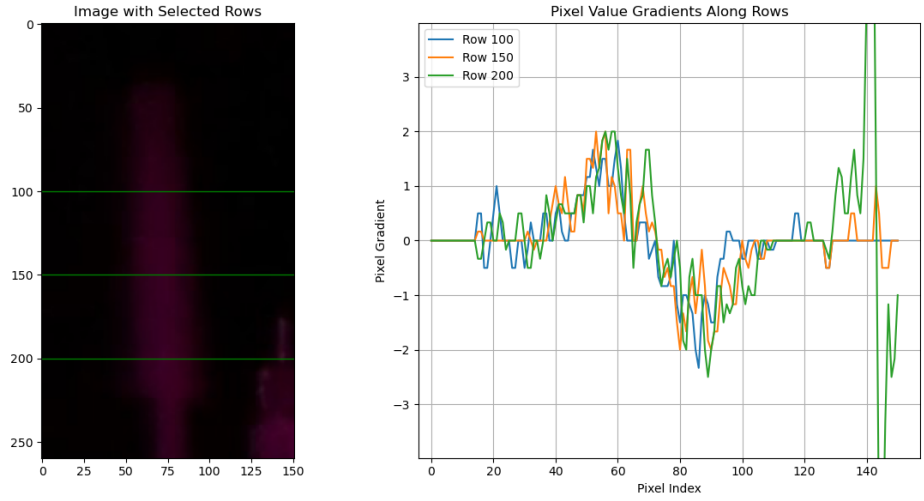

Figure A.7.: Gradient over moving round black bird model with I_F:3mA, fps:60, Shutter:Default, gain:16.

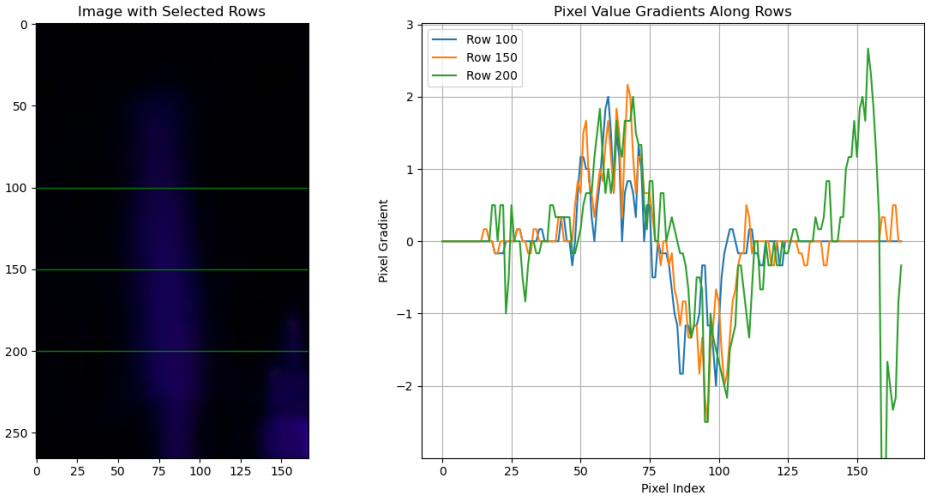

Figure A.8.: Gradient over moving round black bird model with I_F:3mA, fps:60, shutter:1/60s, gain:16.

Figure A.9.: FPS:40, Shutter:Default, gain:16

Figure A.10.: FPS:40, Shutter:1/40s, gain:16

Figure A.11.: FPS:60, Shutter:Default, gain:16

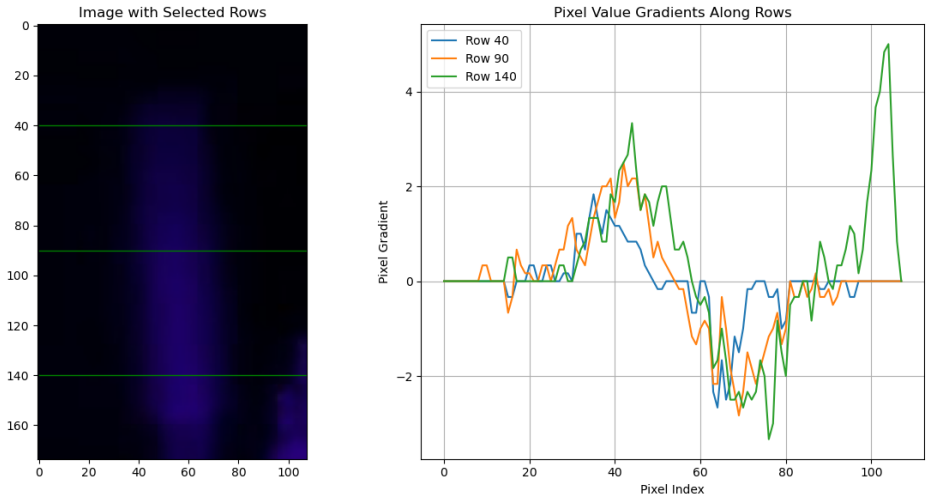

Figure A.12.: Gradient over moving round black bird model with I_F:3mA, fps:40, Shutter:Default, gain:16.

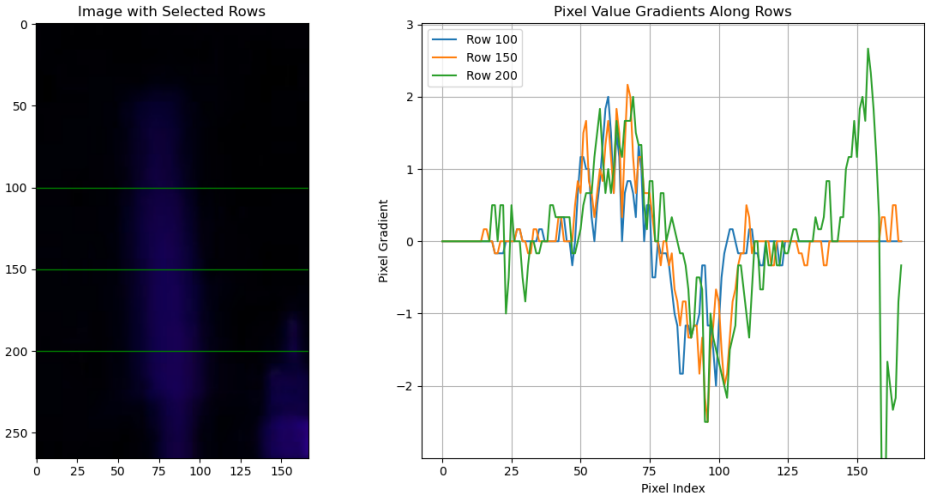

Figure A.13.: Gradient over moving round black bird model with I_F:3mA, fps:60, shutter:1/60s, gain:16.

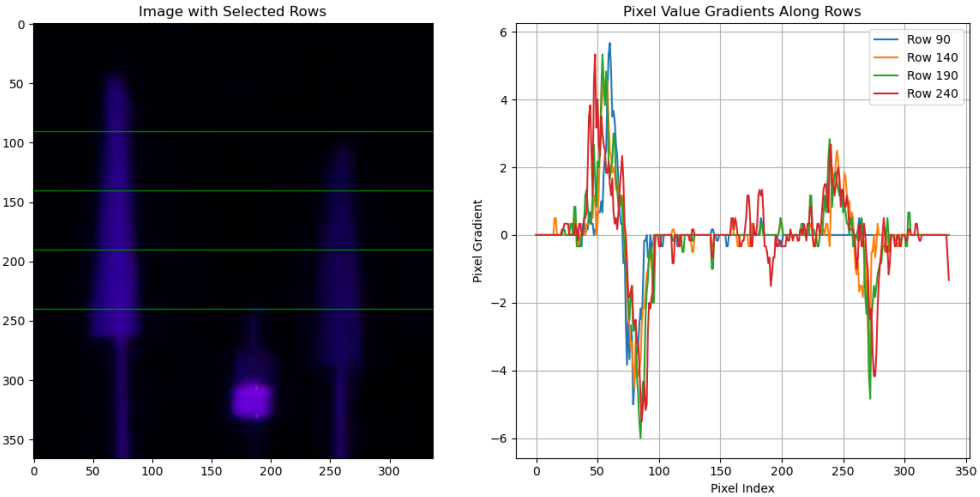

Figure A.14.: Approximate 14W test, for comparison with the results obtained by Verhoef et al.[3]

Appendix B.

Background

B.1. Requirement specifications

This section will give the requirement specifications upon which this paper is built upon. The preceding work of this report considered the design of a full monitoring system, while this report aims to enable existing systems to work at night. Thus, the requirement specifications obtained in the preceding work are comprehensive, where some are irrelevant to this work. This section will introduce only the requirement specifications relevant to this paper. The requirement specifications are divided into three categories; Institutions of science and nature, industry, and circumstances.

Institutes of nature and science

- Shall be able to identify bird species
- Shall be able to count how many birds died/got injured
- Shall have continuous 24/7 monitoring in operational conditions
- Should be accurate
- Plus if bird activity is registered

Industry

- Shall be robust
- Shall be easy to implement
- Shall be easy to maintain
- Shall avoid compromising warranties
- Shall avoid sensitive data

- Shall avoid compromising HSSE
- Shall avoid damaging other components of the rig
- Shall not come in the way of service boats
- Should be cheap
- Should not be of hinder to maintenance workers on the offshore wind turbine rig
- Should avoid downtime (non-operational time) of the turbine

Circumstances

- Shall be able to operate in wind speeds up to $25m/s$
- Shall handle wind gusts up to $30m/s$ when non-operable
- Shall work in all reasonable wave and current conditions
- Should work in fog, snow and rainy conditions
- Should not rely on a separate bottom fixed mooring
- Shall cover the turbine-swept area of the turbine
- Should take the movement of turbines into account
- Should be applicable for large offshore wind turbine parks
- Shall detect birds of sizes between 0.41m - 1.8m
- Shall be able to detect birds colored white, black, gray, brown, or a combination of these
- Should avoid false positives and negatives such as water foam and rain

Appendix C.

File naming

Filename variable	**Function variable**	**Description**
fps	frame rate	Determines the frame rate of the camera.
shutter#s	shutter	In the tests, # = 3 indicates that the shutter speed was set to 3 seconds, while # = 0 indicates that the `--shutter` function was removed and default shutter used instead.
gain	gain	Sets the analog gain to the pixel values.
time	now	Automatically saves the timestamp before the video is captured. Added to avoid file overwriting in the case of faulty variable changes. Time format: HHMMSS in 24h clock cycle.
dist	dist	Manually changed variable describing the distance between the bird and the camera rig.
lightON/OFF/NIR_close_plate	light	Manually changed variable indicating whether the lamp is on or off for the irradiance range test. Changed to NIR for the reflectivity comparison test.

velNO	vel	Variable added to indicate whether a test with a moving bird. However, due to time limitations, no such test was performed.
NorthFulmar	N/A	Added to denote in which videos the cormorant was replaced by the northern fulmar.
DifusedByPlate	N/A	Added to denote the test where the black plate was placed behind the cormorant to diffuse the background.

Table C.1.: A description of how to interpret the naming-variables in the video and image files, together with the corresponding variables in the bash script.

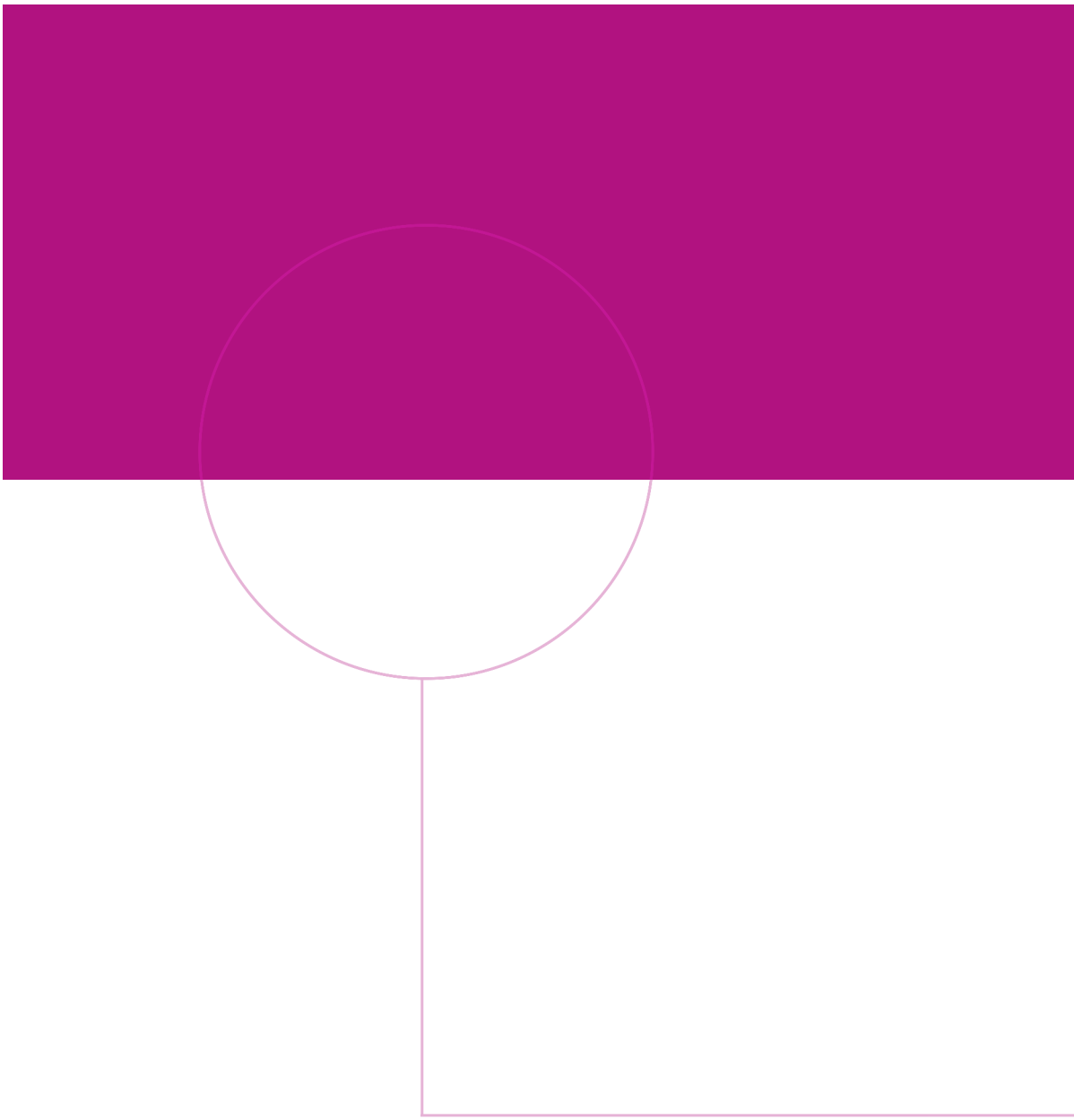

NTNU

Norwegian University of
Science and Technology